Acoustic Emission as a Structural Health Monitoring (SHM) method for stay cables

Master's Thesis

R.J. Diender

January 2019, Delft

(blank page)

Acoustic emission (AE) as a structural health monitoring (SHM) method for stay cables

Research into the possibilities of AE for stay cables of cable stayed bridges

By

R. J. Diender

in partial fulfilment of the requirements for the degree of

Master of Science
in Civil Engineering

Structural Engineering – Steel, hybrid and composite structures

at the faculty of Civil Engineering and Geosciences at Delft University of Technology

30 January 2019, Delft

Thesis committee	Prof. dr. ir. M. Veljkovic	TU Delft
	Dr. Ir. L. Pahlavan	TU Delft
	Dr. Ir. Y. Yang	TU Delft
Daily supervisors	Dr. H. Xin	TU Delft
	MSEng O. Joostensz	Rijkswaterstaat

TU Delft

Rijkswaterstaat
Ministry of Infrastructure and Water Management

(blank page)

ABSTRACT

The stay cables of the north bridge of the Galecopperbrug are reaching the end of their life span. Rijkswaterstaat, which is responsible for the bridges, needs a reliable Structural Health Monitoring (SHM) method to monitor the current state of the stay cables. At the moment, Rijkswaterstaat experiences issues with defining the state and the residual life span of the stay cables of the Galecopperbrug. This study focuses on the technique of Acoustic Emission (AE) for monitoring the stay cables of the Galecopperbrug.

The main research question of this study was: "Is the AE-system used in a fracture-based assessment suitable for structural health monitoring of the stay cables of the Galecopperbrug?".

In this study the following methods were used to investigate the AE behaviour of stay cables: a literature study on previous research and the current knowledge of AE and the structural behaviour of cables was done, a full-scale and two verification experiments were performed to investigate the AE behaviour related to wire breaks and to investigate the accuracy of linear source location techniques, an analytical model of the stay cables was made to investigate the influence of different parameters to the capacity of the stay cables and to predict the stress distribution in the wires during the experiment and finally, a SCIA model of the Galecopperbrug was used to investigate the load bearing distribution of the Galecopperbrug.

In this study, it was found that wire breaks inside (stay) cables will generate elastic stress waves which can be captured and recorded by AE sensors. Based on an experiment where multiple wire breaks occurred, it was shown that wire breaks can be identified with the help of AE techniques. However, the identification of wire breaks is mainly depending on the correct choice of sensor type. Based on the experiments and assumptions that were made in this study the R6I-AST type of sensors are more suitable for wire break detection and the R3I-AST sensors are more suitable for AE signals due to impacts. Based on the assumptions and the experiments performed in this study it can be concluded that AE can be used in a fracture-based assessment for SHM of the stay cables of the Galecopperbrug.

(blank page)

PREFACE

In front of you lies the research "Acoustic emission as a structural health monitoring (SHM) method for stay cables". This research is part of the requirements to obtain the Master's degree in Civil Engineering at the Delft University of Technology. This Master's degree is obtained for the Structural Engineering track with the Steel, hybrid and composite structures specialisation. This research was performed from March 2018 to January 2019. This research is carried out together with Rijkswaterstaat which is the executing body of the Dutch Ministry for Infrastructure and Water Management.

First of all, I would like to thank Rijkswaterstaat for the possibility to carry out this research and helping me through this process. Without the permission to participate in the ongoing experiments from Allseas, an offshore installation company, it was not possible to carry out any experiments in the lab. So, I would like to thank Allseas for letting me participate in the ongoing experiments.

I also would like to thank my graduation committee, consisting of prof. dr. ir. M. Veljkovic, dr. ir. L. Pahlavan, dr. ir. Y. Yang, dr. H. Xin and MSEng. O. Joostensz for their guidance and support during this research. I would like to thank ir. F. Zhang for helping me with the AE equipment during the experiments.

Furthermore, I would like to thank Hristo Ivanov, who was involved in the ongoing experiments from Allseas, for helping me with the experiments and for all the grateful work he did on the preparation of the experiments before I was involved in the experiments. Also, many thanks go out to all the people working in Stevin Lab II, which were involved in the experiments by helping during the preparation and/or during the execution of the experiment. Last but not least, I want to thank everybody in my direct environment who helped and supported me during this process.

I hope you will enjoy reading this research.

R.J. (Robin) Diender
Delft, January 2019

(blank page)

TABLE OF CONTENT

LIST OF FIGURES

LIST OF TABLES

ABBREVIATIONS

AE	Acoustic Emission
AI	Artificial Intelligence
ARK	Amsterdam-Rijnkanaal
CBS	Centraal Bureau voor de Statistiek
CFRP	Carbon Fiber Reinforced Polymers
CNN	Convolutional Neural Networks
DL	Deep Learning
DWT	Direct Wavelet Transform
GCB	Galecopperbrug
HSC	High Strength Concrete
IWRC	Independent Wire Rope Core
MBL	Minimum breakage load
ML	Machining Learning
RBK	Richtlijnen Beoordeling Kunstwerken
ROK	Richtlijnen Ontwerpen Kunstwerken
RWS	Rijkwaterstaat
SLS	Serviceability Limit State
SHM	Structural Health Monitoring
TDOA	Time Difference Of Arrival
ULS	Ultimate Limit State
WS	Warrington-Seale

SYMBOLS

$\alpha/\alpha_{kl}/\alpha_{ij}$	lay angle of the wires
$\beta/\beta_l/\beta_j$	lay angle of the strands
β	reliability index
$v/v_l/v_j/v_{kl}/v_{ij}$	Poisson's ratio
A	amplitude
$A/A_{kl}/A_{ij}$	area of specific wire
d	distance between sensor and source location
D	spacing sensors
E	modulus of elasticity
f_{max}	maximum allowable stress in SLS
f_{uk}	minimum breakage stress
F_i	tension force in wire
h_w	lay length
n_s	number of strands
n_w	number of wires
N_{max}	maximum allowable load in SLS
N_{uk}	minimum breakage load
Q_i	shear force
r_w	wire winding radius
s	left direction of the wires
S	left direction of the strands
S_i	tension force in cable
Δt	time difference
T_1	time of arrival 1
T_2	time of arrival 2
U_i	torque force
V	wave speed
V_p	peak voltage
V_{ref}	reference voltage
z	right direction of the wires
z_{ij}	number of wires in i wire layer and j strand layer
z_j	number of strands in j strand layer
Z	right direction of the strands

1 INTRODUCTION

This chapter provides a general introduction to the problem. The problem definition is formulated in paragraph 1.1. In paragraph 1.2 and 1.3 the objectives and the research questions of this research are presented. The methodology is given in paragraph 1.4 and an overview of the report is given in paragraph 1.5.

In the Netherlands there are many waterways and highways. To overcome the problem of crossing waterways by highways is quite simple, namely building bridges. Most of the highway bridges were built in the years between 1969 and 1985, which was the result of an enormously increase in (Van Dooren, Gration, Den Blanken, Nagtegaal, Ashurst & Kunst, 2010). Bridges are designed with a specific life span; according to Rijkswaterstaat (2013) new bridges are designed with an expected life span, or design reference period, of 100 years. All those bridges which are built between 1969 and 1985 are reaching half of their life span. Individual parts of the bridge can have lower life spans. For instance, the stay cables of a bridge can have lower life spans. This depends on which type of cable is used, assumptions which are made and on other environmental conditions. The original life span of a bridge is determined based on assumptions made in the design phase of the bridge. For example, assumptions for the expected traffic increase in the future. The real amount of traffic increase can be different compared to the assumptions made several years ago. Next to this, other issues during the life span of the bridge can influence the remaining life span of the bridge. For example, corrosion problems, crack initiation, ship or car collisions can influence the state of the bridge. Rijkswaterstaat, which is the executing body of the Dutch Ministry of Infrastructure and Water Management, is responsible for those bridges and guarantees the safety of those bridges during the life span of the bridges. During the residual life span of the bridge, Rijkswaterstaat guarantees enough safety for the users. This residual life span amongst others can be determined by the help of recalculations or regular inspections of the bridge. In exceptional situations, Rijkswaterstaat experience some issues to guarantee a residual life span. For instance, they have problems with defining the state of the bridge due to unreachable places. This is the case for, monitoring the status of the stay cables of the Galecopperbrug. The Galecopperbrug is a cable stayed bridge which carries the A12 highway and local roads over the Amsterdam Rijnkanaal (ARK). The Galecopperbrug is located in the southern part of Utrecht in the Netherlands. The bridge is a part of the ring of Utrecht and it plays an important role in the highway infrastructure of the Netherlands. In the cases where Rijkswaterstaat experience problems with defining the state of the bridge, Rijkswaterstaat is searching for alternatives to guarantee a residual life span. Rijkswaterstaat is investigating the possibilities of Acoustic Emission (AE) as a Structural Health Monitoring (SHM) method to monitor the stay cables of the Galecopperbrug.

To ensure durability, sustainability, serviceability and safety of structures SHM methods can be used (Li & Ou, 2016). The objective of SHM is to monitor the behaviour of a structure in an efficient and accurate way (Bakht & Mufti, 2008) by implementing a damage detection system and characterization (Zhang, 2017). SHM is needed for a good assessment of the performances of a structure under different service loads, but also under environmental conditions. SHM methods allows to detect damage in a structure or examine the current health of the structure (Li & Ou, 2016).

One of the techniques for SHM is AE. According to Grosse & Ohtsu (2008), AE is a passive non-destructive technique (NDT). The passive property of AE is related to the fact that only defects which are developed during the monitoring period are identified. AE sensors record elastic waves, which are generated due to wire breaks, crack initiation and propagation or background noises. The sensors convert these elastic waves into electrical signals. By processing of those signals the crack process can be evaluated. Those signals can be recorded and processed continuously without interrupting the loading conditions (Grosse & Ohtsu, 2008). The technique of AE is used in many steel and concrete bridges to monitor steel or concrete elements.

1.1 Problem Definition

The stay cables of the north bridge of the Galecopperbrug, which is built in 1976 (ARUP, 2009), are reaching the end of their life span. Rijkswaterstaat, which is responsible for the bridges, needs a reliable SHM method to monitor the current state of the stay cables. At the moment Rijkswaterstaat experience issues with defining the state and the residual life span of the stay cables of the Galecopperbrug. The technique of AE for monitoring the stay cables of the Galecopperbrug is investigated in this research.

The AE signals which are received by the sensors can have different sources. Background noises can be divided into signals due to traffic, impact or weather conditions. For assessing the current state of the stay cables, the signals due to wire breaks are of great importance. Wire breaks inside a stay cable can influence the capacity of the stay cables and this can influence the safety level of the bridge. It is important to distinguish AE signals related to wire breaks from the other sources. With the help of the characteristics of AE signals due to wire breaks, the distinguishing of AE signals can be made.

According to Verreet (2005) the capacity of a stay cable decreases if multiple wire breaks occur within a segment of cable with limited length. Next to the number, also the locations of the wire breaks influence the capacity of the stay cables. By using a linear source location technique, the location of the source of the AE signal, in this case the signal due to a wire break, can be determined. According to Zhou, Zhou, Dong, Cai, Rui and Ke (2017) and Holford and Lark (2005), several source location techniques are available for determining the location. These techniques require the time difference of arrival (TDOA) between the sensors. These TDOAs can be obtained by three different methods: (1) first threshold passing, (2) P-wave analysis and (3) wavelet analysis.

1.2 Objectives

The objectives of this research are as follows:

- Investigation of the performance of the AE-system, which is available at TUD, for better assessment of the stay cables of the Galecopperbrug.
- Investigation to the contribution of different structural components to the load bearing system of the Galecopperbrug.
- Investigate the influence of a wire break inside a stay cable and a complete failure of the cable to the Galecopperbrug.

1.3 Research Questions

The problem definition and the objectives of this research resulted in the following main research question:

> "Is the AE-system used in a fracture-based assessment suitable for structural health monitoring of the stay cables of the Galecopperbrug?"

Answering of the main research questions is possible after answering the sub-questions:

- Is it possible to predict the expected stress distribution in the wires of a stay cable based on an analytical model?
- What is the effect of a wire break inside a stay cable to the load bearing resistance of the stay cable?
- Is it possible to detect wire breaks inside a stay cable?
- What is the accuracy of a linear source location technique based on different obtained arrival times?

1.4 Methodology

To give answers to the research questions, this report will be divided into the following four main parts: state of the art, performance of AE systems, analytical model of cable behaviour and load bearing distribution of the bridge.

State of the art

A review is made on the past research and literature related to this report. The aim of the state of the art is to investigate the knowledge and identify the knowledge gaps. In the state-of-the-art issues like AE experiments, 1D linear source location techniques, recovery length and the influence of wire breaks and an analytical model of the stay cables are investigated.

Performance of AE systems

The main principles and equipment used during the experiments are described. The experiments were performed in Stevin Lab II at the Delft University of Technology. In total three experiments were carried out. The first test subjected the stay cable to pure tension and load it until failure to investigate the capacity and the AE behaviour of the cable. The other two experiment where verification experiments to investigate the accuracy of different methods for a 1D linear source location technique and to investigate the suitability of different types of sensors.

Analytical model

Building an analytical model increase the insight on wire level. This model is built under appropriate assumptions to investigate the stresses in the wires and to investigate the influence of different parameters (lay angles and Poisson's ratio) to the stress distribution in the wires.

Load bearing distributions

A SCIA model of the Galecopperbrug, which is built by Rijkswaterstaat, is used to improve the engineering skills. Next to this, this model is used to investigate the structural behaviour of the Galecopperbrug and to perform a case study related to the load bearing distribution of the Galecopperbrug.

1.5 Overview of the Report

An overview of the chapters in this report is given below:

- Chapter 1 – An introduction followed by the problem definition, the objectives, the research questions and the methodology.
- Chapter 2 – Description of the state of the art on AE, 1D linear source location techniques, recovery length and the behaviour of a stay cable under axial loading.
- Chapter 3 – The performance of AE systems is described with the help of experiments that are performed.
- Chapter 4 – The types of stay cables and the behaviour under axial loading are described. The analytical model is made and various case studies are performed.
- Chapter 5 – The design philosophy of Rijkswaterstaat and the current design of the Galecopperbrug is given. The SCIA model that is used is explained and a case study is performed. Finally, the application of AE for the Galecopperbrug is described.
- Chapter 6 – A summary of all the conclusions is given.
- Chapter 7 – Recommendations are given.

2 STATE OF THE ART

This chapter contains the state of the art. This chapter is divided into four paragraphs: Paragraph 2.1 deals with the current knowledge of AE, the propagation of waves (2.1.1) and source type identification (2.1.2). In paragraph 2.2 different (linear) source location techniques (2.2.1) and the different methods to obtain the TDOA (2.2.2) are described. The research to the recovery length of wires in a cable is given in paragraph 2.3 and finally the analytical model is described in paragraph 2.4. This paragraph deals with the behaviour of the wires under axial loading (2.4.1) and the analytical model (2.4.2).

2.1 ACOUSTIC EMISSION

The sound that is generated by the fracture of materials is quite known in the world. Earthquakes and rock bursts are examples of both the audible and noticeable phenomena which are generated by elastic waves in materials. In earthquakes the generation of elastic waves will result in vibrations of the ground that can be seen by the human eye. During an earthquake also noise can be heard, this is due to the fracture of materials deep in the ground. AE is a SHM method which is based on the generation of elastic waves in materials. These elastic waves will be generated by the rapid release of energy from a source in a material (Nair & Cai, 2010). AE originates at a certain point, this is called the source of an AE signal. The elastic waves propagate with different modes (explained in paragraph 2.1.1) as mechanical waves and hit the transducer in the sensors (Drummond et al., 2006). This source can be a crack initiation, crack propagation or failure of an element.

Kishinoue delivered in 1933 the first report on a scientifically planned experiment based on the AE phenomena of cracking of timber before fracture. In 1950, with the publication of Kaiser's dissertation, it is quite stated that the history of AE started. Kaiser recorded AE signals during tensile testing of materials which consisted of different types of metals. During these tests Kaiser discovered a phenomenon which is nowadays a quite know and important phenomena called the Kaiser effect (Grosse & Ohtsu, 2008). The Kaiser effect is an irreversible phenomenon for AE applications. A certain amount of signals correspond to an initial load that is applied on the specimen. These signals are generated by the stabilisation of the material to bear the stresses in the material. The Kaiser effect stated that no more AE signal will occur until the initial stress in the material will be exceeded (Drummond, Watson & Acarnley, 2006). In figure 1 a visual representation of the Kaiser effect is given. According to Drummond et al. (2006) the presence of the Kaiser effect looks a disadvantage for AE compared to other testing methods, because every AE signal will occur once.

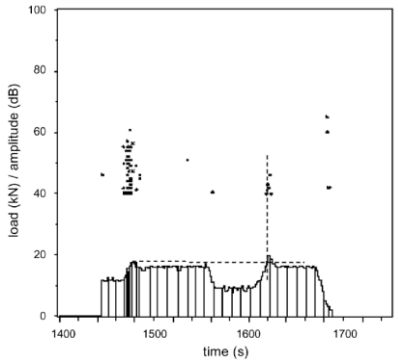

Figure 1 – Kaiser effect (Drummond et al., 2006)

Researchers during the 1950s and 1960s developed AE sensors, investigated the fundamentals of AE and started to characterize the behaviour of many materials. At the end of the 1960's AE started to be recognized as a non-destructive testing method for the purpose of monitoring of fracture processes. The popularity of the use of AE as a non-destructive testing method increases during the 1970s. The introduction of the computer during the 1980s made the computer a basic instrument in the use of AE. In the 1990s less attention was paid to research and more attention was paid to the application of AE in practice.

Drouillard (1996) published a review of the history of AE. After these years many investigations were carried out. For instance, investigations on the discrimination techniques of signals to make AE more reliable. But also, other investigations to make AE a technology that could be used to evaluate several bridges in a more reliable way. Casey and Laura (1996) performed a review of AE monitoring on cables. Casey and Laura (1996) concluded that the detection and the location of wire breaks are the most realistic applications of AE, but the successfulness of this depend on the cable configuration. The length, diameter and the total number of wires play an important aspect in the successfulness of the detection and location of wire breaks. Rizzo and di Scalea (2001) monitored the damage initiation and progression in stay cables made of Carbon Fiber Reinforced Polymers (CFRP). This paper concluded that the CFRP cables are excellent acoustic wave guides and experience low attenuation. The results of this study show some promising results for the future use of in situ SHM of components with AE.

Drummond et al. (2006) carried out an investigation for cables with proof and fatigue loading both with AE sensors. According to Drummond et al. (2006) the "Dunegan Corollary" states that "The acoustic emission experienced during proof testing reveals damage incurred during the preceding operational period". Drummond et al. (2006) carried out experiments to investigate the Dunegan Corollary. In those experiments' cables with different amounts of diameter reductions were tested. In figure 2 the results of those experiments are shown. A linear relation between the percentage of diameter reduction and the total energy is indicated in this figure. The observations of those experiments supported the Dunegan corollary. The level of AE, during proof loading, indicates the level of damage in the cable.

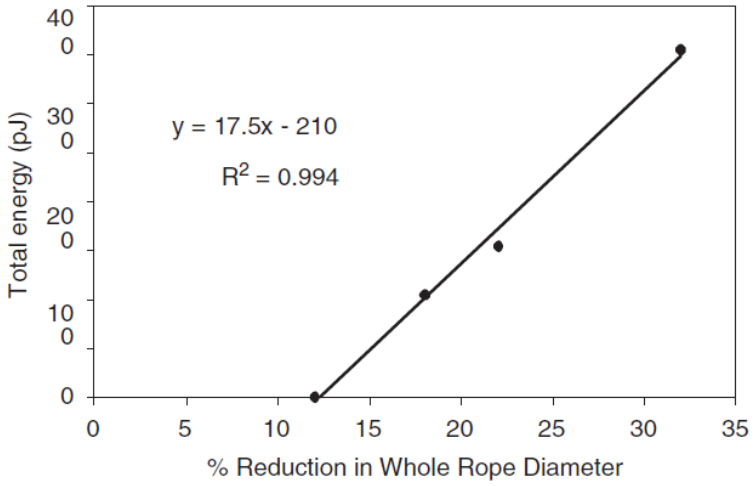

Figure 2 – Energy versus reduction cable diameter (Drummond et al., 2006)

A brief review on AE and the application of AE to SHM of bridges is given by Nair and Cai (2010). Sun and Qian (2011) compared the stress wave propagation due to impact and wire break sources. They concluded that the energy release due to wire break sources is faster compared to impact sources. The main peak frequency for impact source was less than 20 kHz while the main peak frequency for wire break sources was around 150 kHz. Another finding of Sun and Qian (2011) was that the amplitude attenuation is higher for high frequency waves. The amplitude attenuation is higher for frequencies around 150 kHz compared to lower frequencies. Finally, they concluded that the energy release due to an impact source is much smaller compared to energy releases due to a wire break source and that it is possible to identify wire breaks by comparing the energy values of different sources.

Zejli, Gaillet, Laksimi, and Benmedakhene (2012) and Gaillet, Zejli, Laksimi and Tessier (2009) studied the detection and the location of broken wires in anchorage areas. Interwire fretting in a damaged cable is the origin of AE signals. Next to interwire fretting, other sources of AE signals are investigated. Both studies are concluding that the total number of counts and the cumulated energy are the main parameters for AE signals due to interwire fretting. The slip between healthy wires and broken wires is also observed. The conclusion stated that, if the data processing is efficient the presence of broken wires can be detected. The authors found that the reasons why interwire fretting results in AE signals is due to the quality of the surface, the roughness change, interwire contact strength and the state of oiling of the cable. The main conclusion of this study was that this technique can be used to assess the degradation state and the presence of broken wires in cables, but the technique needs further investigation and validation for on-site inspections and bigger cables.

The development of computers makes AE as a non-destructive testing method more efficient. In the last years the monitoring of complete bridges becomes more popular due to all developments in this field. In work of Webb, Vardanega, Fidler, and Middleton (2014), Carrión, Quintana, and Crespo (2017), Zhang, Zhang, and Fischer (2007) and Niroula (2014) the principle of AE is used to evaluate and monitor some complete civil structures. The technology to measure AE signals, collect all the data and analyse this data is nowadays quite known. The biggest challenge of the AE technology nowadays is to filter the big amount of data in data which is important for making decisions. In other words, filter the useful information from the background noise that occurs during the monitoring of real-life structure with the help of AE (Niroula, 2014).

2.1.1 Propagation of waves

The rapid release of energy will generate elastic waves in steel structures. The propagation of these waves influence the acquired signals. Therefore, the wave propagation is an important aspect in the understanding of AE signals. Wave propagation is the basis of AE signals. The propagation of acoustic waves can be categorized into three main modes. The different waves are characterized by the way of oscillation. The following modes can be categorized (Holford & Lark, 2005):

- Body waves
  - Primary waves (P-waves) ~ Longitudinal waves (compression)
  - Secondary waves (S-waves) ~ Transverse waves (shear)
- Surface waves
- Plate waves

The primary waves are also called longitudinal waves. The particles in this type of wave are moving in the same direction as the wave propagates. The secondary waves are also called transverse waves. In this type of waves, the particles move in the transverse direction of the wave propagation (Zhang, 2017). Surface waves originate due to the introduction of boundaries and/or surfaces. The combination of longitudinal and transverse waves close to the surface, result in surface waves. The surface wave is always a combination of longitudinal and transverse waves. This type of wave is also called a Rayleigh wave. If more than two boundaries are introduced more complex wave propagation modes occur, namely plate waves. All these waves can occur in a material. The different types of modes depend on the boundary conditions, shape of the material and material properties (Holford & Lark, 2005). Acoustic wave propagation is a rather complex theory. The best way to understand AE is that a source generates a wave, this wave propagates to the sensor and the sensor is measuring the wave. The wave is reflected and dies away. This happens all in some hundredth of seconds, this process is quite fast. For this research, only the primary waves (P-wave) are of importance. Attenuation, signal shaping and the speeds are other elements regarding to wave propagation, these elements are briefly described below.

Attenuation

Attenuation is the process that during the propagation of an AE signal the amplitude will reduce. This reduction according to Niroula (2014) is due to internal friction, geometrical spreading of the wave, dispersion of some components and the dissipation of the wave. In the near field, the region close to the source, the geometrical spreading of the wave is the dominating factor that influences attenuation. In the far field, the region far away from the source, the absorption is dominant (Holford & Lark, 2005). The energy in the wave is absorbed by the materials and partly converted into heat. For the range of frequencies in which steel is tested with AE, steel absorbs a little amount of energy compared to other materials. Geometrical spreading in cables is limited due to the shape of the cables. Attenuation of the signal is dependent for the sensor spacing. To help with the sensor spacing, attenuation curves can be made. In these curves it is easy to read and determine the sensor spacing. These curves can be made by carrying out a pencil lead break test or an impact test.

Signal shaping

The shaping of signals is important to determine the duration and the rise time of the AE signals. A source can emit a simple wave, but this wave can be transformed into a more complex wave at the sensors. In figure 3 an example of this process is given. A really simple wave at the location of the source, but a complex wave near the sensors (Niroula, 2014).

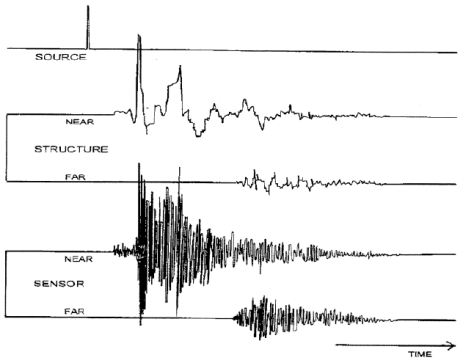

Figure 3 – Signal shaping (Niroula, 2014)

Wave speed

For linear source location techniques, the wave speed is an unknown parameter. This parameter can be determined based on theory or based on experiments. According to Sun and Qian (2011) and Zhang (2017) the fastest wave is the longitudinal wave (P-wave). The transverse waves (S-wave) and the surface waves are slower waves compared to the longitudinal waves. For further processing the longitudinal wave speed is of importance to determine the source location. Sun and Qian (2011) calculated the wave speed according to the Pochhammer dispersion equation. Their results shown a no-dispersion wave speed (C_0) of 5114 m/s and calculations based on the experiments show wave speeds in the range of 5078 – 5155 m/s. They concluded that the wave speed was close to the wave speed with no dispersion (C_0). Because the maximum deviation is only 0.8%, the dispersion of the wave can be neglected. The wave speed without diffusion can be calculated in the following way (Sun and Qian, 2011):

$$C_0 = \sqrt{E/\rho}$$

2.1.2 Source type identification

One of the biggest challenge in the AE technology for SHM methods is the discrimination of sources which are not of interest. It is known that different micro- and macroscopic mechanisms generate different forms of AE. AE can be classified into two different categories. Primary emissions are the emissions which are internally originated from the material, these primary emissions are related to (fatigue) crack developing and the dislocation of movements. These types are associated with microstructural mechanisms (Holford & Lark, 2005). All the emissions which originate from external sources are classified as secondary emissions. Frictional activities are an example of a secondary emission. The characteristics of stress waves, like wave mode, attenuation, source location and effect of multiple paths are related to the detection of AE events (Nair & Cai, 2010).

Next to both categories the term "noise" is used as well. This definition of noise which is widely used in the field of AE describes "emissions which are not of interest for the specific study that is carried out" (Holford & Lark, 2005). Impact by environmental factors and friction are two of the biggest factors which result in noise. According to Niroula (2014) these issues can be addressed in different ways:

- Prevent noise sources in the monitoring of bridges on site;
- Make use of good test set ups and testing material;
- Filtering out of the noise data if the noise source is known;
- An educated set for the threshold level.

Source type identification techniques are used to identify the origin of a source. Generally, there are two approaches to determine the origin of the source. The statistical (or stochastic) approach describes empirical correlations with measured behaviour and properties of the source. On this measured data several distribution and correlation analyse are carried out. The other approach, the deterministic or fundamental approach, tries to develop relations between the measurements and the parameters of the source. The information which is given by this approach is used to characterize the AE data of the unknown sources. This characterisation of the AE signal can be done by easy filtering methods or by the use of complex computer techniques (Holford & Lark, 2005). This research study focusses on the deterministic approach.

2.2 Source Location Techniques

After the source of the primary emissions are identified, the location of the source is of importance too. The localization of sources can be done by source location techniques. These techniques can determine the location of an AE source. Sun and Qian (2011) did research into the wave velocity in high strength steel wires. They concluded that the wave speed and the wavelength are depending on the frequency of the wave, a higher frequency will result in a lower wave speed and wavelength. They also stated that the wave speed is close to the wave speed without any diffusion if the wavelength is much higher compared to the wire radius. Zhou et al. (2017) did research into a new source location technique which is based on the old source location technique but included the refraction of AE signals in different media. They concluded that this new source location technique has for both the same medium and different media advantages over the old source location technique. The accuracy and the stability of the location can be approved by this new technique.

Multiple source location techniques are available for the determination of the location of the AE source. According to Zhou et al. (2017) the methods can be divided into linear, planar and 3D source location techniques. All above mentioned methods are based on the wave speed, distances between the sensors and the TDOA. In figure 4 the three different methods are shown. The linear source location technique is the most suitable for cases where the length over width ratio are high and where the sensor spacing is large compared to the material depth (Holford & Lark, 2005).

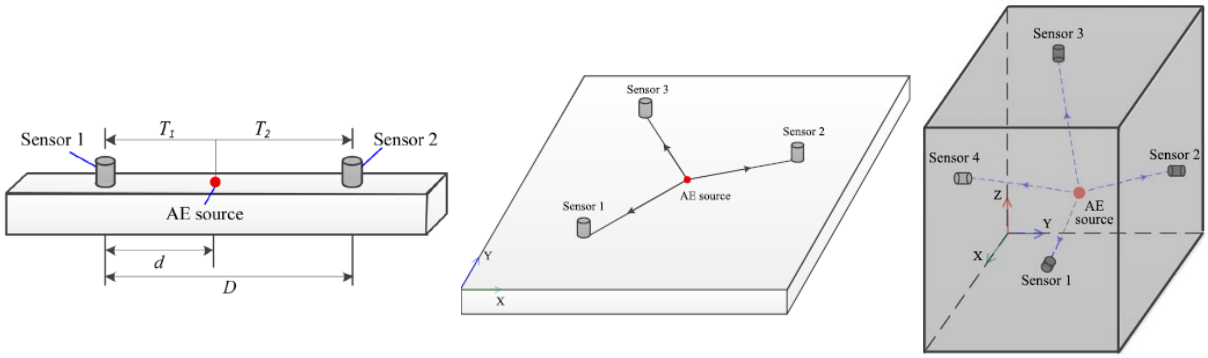

Figure 4 – Linear (l), planar (m) and 3D (r) location techniques (Zhou et al., 2017)

2.2.1 Linear Source Location Technique

In the coming experiments the specimen is a 3-meter-long cable with a diameter of 77 mm. The planar and 3D location techniques are not suitable for these experiments, so more attention is paid to the linear source location technique. The example in figure 4 (left) uses only two sensors and the example in figure 5 uses three sensors. It is necessary to have the sequence of hits for more than two sensors. This sequence can be determined based on the time of arrivals. The main principle for both examples is the same and the variables which are unknown are the wave speed, distance between the sensors and the TDOA.

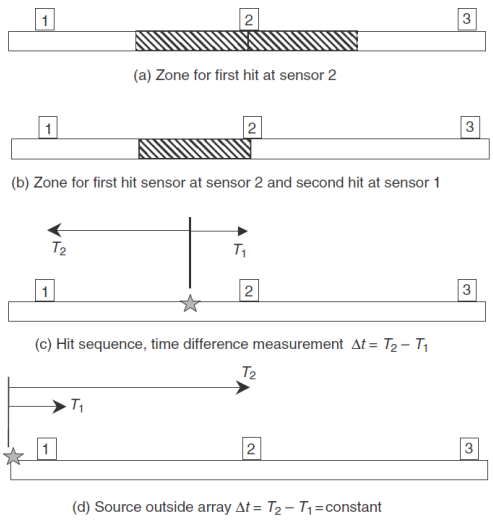

Figure 5 – Linear source location technique (Holford & Lark, 2005)

Under the following two assumptions an equation can be made to determine the location of the source. The wave speed for longitudinal waves is used (1) and the waves propagate along straight lines (2). The distance from the source to the sensors can be determined according to equation 1.

$$d = \frac{1}{2} * (D - \Delta t * V) \qquad (1)$$

In equation 1, d is the distance from the first hit sensor, the spacing of the sensors is given by D, Δt is the TDOAs and V represents the wave speed. A verification of this techniques can be made by the use of a pencil lead break test or an impact test (Niroula, 2014).

2.2.2 Time Difference Of Arrival (TDOA)

One of the unknown variables is the TDOA. This TDOA can be determined in three different ways. The accuracy of those three different ways will be investigated later on in this report. The TDOA will be determined by the help of three different methods (1) first threshold passing, (2) P-wave analysis and (3) wavelet analysis. In method 1 the arrival times are the output data from the sensors. The sensors record the arrival times when the signals reaching the sensors. This point is equal to point 1 in figure 6. For method 2 the arrival time is the first P-wave hit to the sensors. The first P-wave is point 2 in figure 6. To calculate this arrival time Δt will be added to the arrival time from method 1. This Δt can be calculated by multiplying the number of measurement points by the time interval of the data acquisition system. This interval is equal to 0.4 µs.

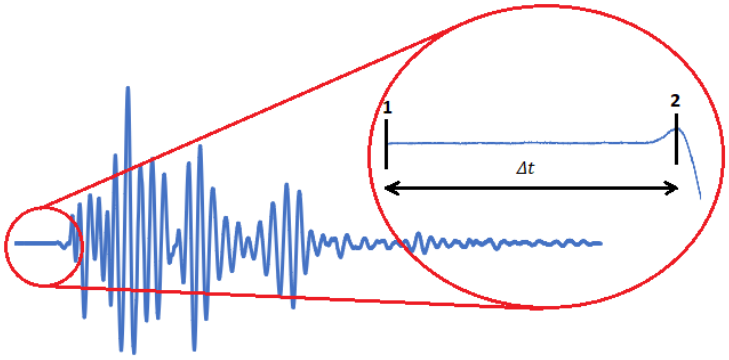

Figure 6 – Determination of the arrival times

In method 3, the TDOA obtained from the wavelet analysis is obtained by a 1D wavelet decomposition. This method is also called the Discrete Wavelet Transform (DWT). This method is used for quick wavelet transformation calculations. The DWT can be implemented in an easy way and another benefit is the reduction in computational time. With the help of filter techniques, a time scale representation of the original digital signal is made. DWT analyses the signal with filters. According to Gokhale & Khanduja (2010) filter techniques are mostly used for signal processing. These filters have at different levels different cut off frequencies. The signals passing through the filters are split into two bands. Two filters, low pass filter and high pass filter, are used for the DWT. The low pass filter filters the raw information of the signal while the high pass filter filters the detailed information of the signal. The number of decomposition levels depends on the length of the signal. At each level the bands spanning only half of the frequency range. The result of this is the decrease of uncertainty due to a doubling of the frequency resolution. The low pass filter removes half of the frequencies. This process is repeated until the decomposition level is reached. In figure 7 a typical level 3 DWT process is shown. This can be called a Mallat-tree decomposition or a Mallat algorithm (Gokhale & Khanduja, 2010). In this decomposition the signal (S) will be decomposed with filters to A_1 and D_1. The next step is the decomposition of A_1 to A_2 and D_2. This process is continued till the level of the decomposition is reached.

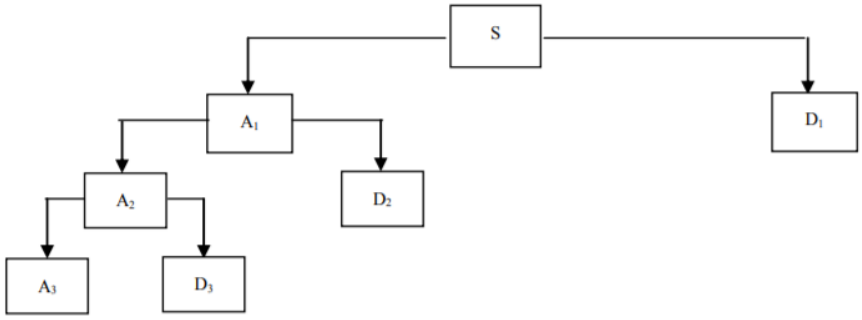

Figure 7 – Level 3 wavelet decomposition (Gokhale & Khanduja, 2010)

2.3 Recovery Length

With the help of source identification, it is possible to identify AE signals due to wire breaks. The localization of those wire breaks can be done with the help of linear source location techniques. The influence of (multiple) wire breaks to the load bearing capacity of the stay cables is important for SHM methods. During the service life of stay cables, it is possible that multiple wires fail. A lot of research is done related to the recovery length in cables. Chien & Costello (1985) did research in an analytical model for the estimation of the recovery length in a six-strand rope and in the centre wire of a seven-wire strand. They based the estimation of the recovery length on the Coulomb friction, Saint-Venant's principle and the contact loads between the wires. Raoof (1991) reported an analytical model to determine the recovery length in a multi-layered strand and concluded that the recovery length is a function of the mean axial load unlike previous studies. Also, the type of construction influences the recovery length of the cable. Later work of Raoof & Huang (1992) reported the friction transition in a parallel wire strand. They concluded that it is possible to estimate the magnitude of the recovery length in this type of cable under simplified assumptions. Raoof (1992) did another research in the free bending fatigue of axially loaded spiral strands and concluded that the primary cause of wire fractures is due to interlayer fretting. Raoof & Kraincanic (1995) did research in the recovery length

phenomenon in axially multilayers spiral strands. They made a model for the calculation of the recovery length in these types of cables. They concluded that the recovery length is a weak function of the mean axial load. They also conclude after carrying out multiple theoretical parametric studies that the lay angle is the primary factor regarding the magnitude of the recovery length. Raoof & Kraincanic (1998) did further research in the recovery length and in its practical use. They argued that a length of 2.5 times the lay length will be a reasonable control length for all types of cable for counting the broken wires for discard purposes.

According to Verreet (2005) a cable is still in good condition if every individual wire is broken 200 times. They concluded that a few millimetres from the broken wire the full capacity is back in the cable due to the friction of the broken wires to the surrounding wires. They also concluded that the breaking strength of a cable due to the failure of a single wire is reduced locally and with less than 1% in cables with multiple wires. In figure 8 this is shown. There are multiple wire breaks but each of these individual wire breaks lead to a local reduction of 1%.

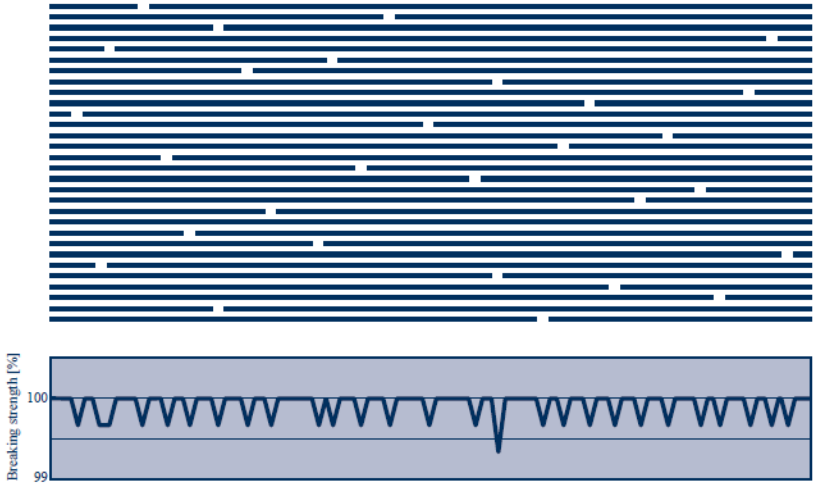

Figure 8 – Influence of an individual wire break to the capacity (Verreet, 2005)

2.4 Analytical Model to Predict Stress Distributions

2.4.1 Behaviour of the wires under axial loading

In case of a single wire the stress can be calculated in an easy way, namely dividing the force by the area of the wire. This principle works also for a bundle of straight wires. However, if that bundle of straight wires forms a helix around a core wire the stresses in the wires are different compared to the bundle of straight wires. According to Ivanov (2018) this is due to the effect that the shape of the cross-section is changing which results in a different stress level. This is illustrated in figure 9.

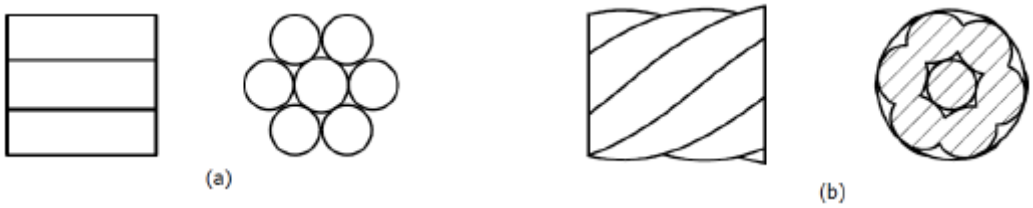

Figure 9 – Cross-section of single wires (a) and helical wires (b) (Ivanov, 2018)

In the application for bridges, all the cables are loaded in tension. To obtain more knowledge in understanding of the stresses on wire level due to the helical structure and the influence to the cable itself, a free body diagram of the outer wire is shown in figure 10. This behaviour under axial loading is investigated under the following assumptions:

- All the wires will start bearing stresses at the same time. The following things are assumed: wires do not have self-contained stresses and there are no loose wires or strands present.
- All the stresses in the wires are assumed to be in the elastic region.

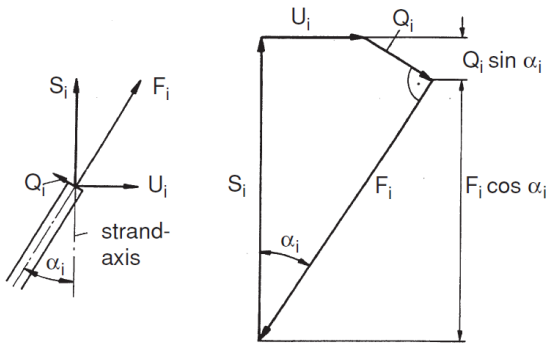

Figure 10 – Free body diagram (Feyrer, 2007)

A cable which is loaded in tension experiences a torque due to the helical structure of the cable. The torque in the cable causes loosening of the strands. To prevent this loosening, the cable can be secured at the cable ends. According to Feyrer (2007), non-rotating ropes can be used. In this type of ropes the left or right wound wires are compensating each other. In the following free body diagram it is assumed that the turning of the ropes is prevented. This results in the fact that the helical structure of the cable results in additional forces in the wires. The helical structure in the cable is introduced by the lay angle of the wires and strands. All the forces in the free body diagram are related to this lay angle. In the free body diagram the tension force in the strand (S_i) results in a tension force in the wire (F_i), a torque force (U_i) and a shear force (Q_i). Both the strand force (S_i) and the torque force (U_i) act as outer forces on the wires. Torsion and bending of the wires cause shear forces (Q_i) in the wires, these forces are limited due to the rope extension.

For this research, only the tension force in the wires will be worked out in more detail. Feyrer (2007) further elaborated the research of Benndorf (1904) to translate the effect of the helical structure to stresses in the wires. The forces in a certain wire k in strand l can be calculated by equation 2 and the stress in the wire can be calculated according to equation 3.

$$F_{kl} = \frac{\frac{\cos^2\beta_l}{1+\nu_l*\sin^2\beta_l} * \frac{\cos^2\alpha_{kl}}{1+\nu_{kl}*\sin^2\alpha_{kl}} * E_{kl} * A_{kl}}{\sum_{j=0}^{n_s}\left(z_j * \frac{\cos^3\beta_j}{1+\nu_j*\sin^2\beta_j} * \sum_{i=0}^{n_w} z_{ij} * \frac{\cos^2\alpha_{ij}}{1+\nu_{ij}*\sin^2\alpha_{ij}} * E_{ij} * A_{ij}\right)} * S \qquad (2)$$

$$\sigma_{tkl} = \frac{F_{kl}}{A_{kl}} \qquad (3)$$

In the above equations α_{kl} represents the lay angle of a wire in relation with a strand, β_l the lay angle of the strand in relation with the complete cable, A the cross-sectional area of the wire, E the modulus of elasticity, z the number of wires or stands, S the total force acting on the rope and ν the Poisson's ratio of the material.

The Poisson ratio for steel wires can be assumed to be equal to the Poisson ratio of normal steel. According to Feyrer (2007) this assumption can be made because there is a very small length related radial force between the wires. Feyrer (2007) did research into the influence of Poisson ratio for a 19-wire parallel wire strand and came to the conclusion that the influence of Poisson's ratio is relatively small. The influence of Poisson's ratio to the cable that is used in this research is investigated in paragraph 4.2. Equation 2 can be simplified to equation 4 when the Poisson ratio is neglected.

$$F_{kl} = \frac{\cos^2 \beta_l * \cos^2 \alpha_{kl} * E_{kl} * A_{kl}}{\sum_{j=0}^{n_s}\left(z_j * \cos^3 \beta_j * \sum_{i=0}^{n_w} z_{ij} * \cos^3 \alpha_{ij} * E_{ij} * A_{ij}\right)} \qquad (4)$$

2.4.2 Analytical model

The analytical model presented in this chapter is based on the behaviour of the wires under axial loading (described in paragraph 2.4.1). With the help of this analytical model the following things will be investigated:

- The stress distribution in the wires of the cable tested in the coming experiments.
- The influence of different cable configuration to the stress distribution in the wires.
- The influence of Poisson's ratio to the stress distribution.

The stress-strain relation used in this model for the individual wires is a bilinear relation. This bilinear relation is shown in figure 11. In this relation the yield stress is 1960 N/mm^2 at 0.01 strain and an ultimate stress of 2064 N/mm^2 at 0.03 strain. The wire failure criterium is set that wires will fail if the elongation is above 0.03.

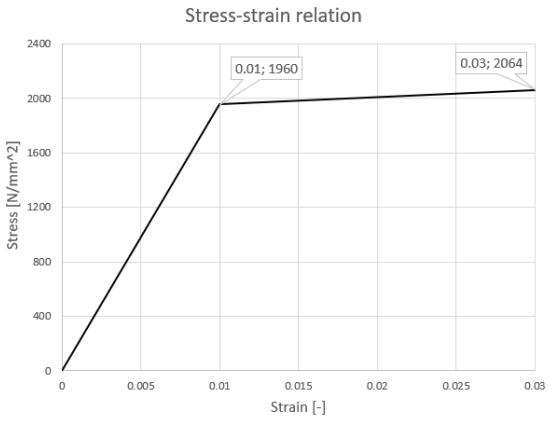

Figure 11 – Bilinear stress-strain relation

In figure 12, a flowchart that explains the logic behind the analytical model. In this model, only the stress due to axial loading is considered. Ivanov (2018) did research into the influence of secondary stress (friction stress) and torsion, moment and shear stresses. Ivanov (2018) concluded that secondary stress is negligible if the cable experiences no change in curvature. Another conclusion of his research is that the torsion, moment and shear stresses can also be considered neglectable. These stresses can be considered neglectable due to the fact that these stresses are the result of a change in lay angle that is caused by cable elongation. The cable elongation is considered as relatively small and so these stresses can be considered as neglectable.

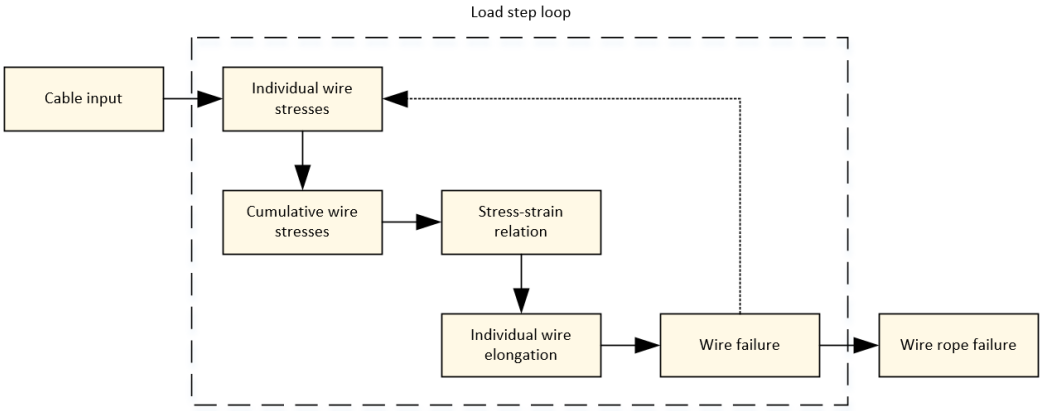

Figure 12 – Flowchart for the analytical model

This model starts with the cable input parameters. In Appendix 1 the (geometrical) properties of the cable and the applied load step is given. First the model starts with calculating more geometrical properties which are necessary for further calculations. At this moment in the model all the constant parameters and an incremental load step are defined. Now an iterative loop starts with (1) calculating the individual wire stresses based on equation 2. The next step (2) is adding the additional wire stresses to the wire stresses in the previous load step. Based on stress-strain relation the individual wire elongation is calculated (3). In the following step (4) each individual wire elongation is checked with the wire failure criterium based on the stress-strain relation. If the complete cable is not failed the next step is adding a new load and step 1 to 4 is repeated. If a wire reaches failure the additional stress due to an incremental load step is redistributed over the remaining wires. This loop is repeated until the remaining wires cannot withstand the additional stress without failure of these wires. This results in a capacity of the cable under pure axial loading.

3 PERFORMANCE OF AE SYSTEMS

The performance of AE systems is described in this chapter. This chapter is divided into four paragraphs. The first paragraph (3.1) contains the background of AE, in this paragraph topics like, the data acquisition system (3.1.1), the sensors (3.1.2) the couplant and mounting of the sensors (3.1.3) and the signal parameters (3.1.4) are described. In paragraph 3.2 the full scale (3.2.1) and the verification (3.2.2) experiments are stated. The results of those experiments are given in paragraph 3.3. Finally, the conclusions are stated in paragraph 3.4.

3.1 BACKGROUND

The damage process in steel structures can result in a release of energy and the generation of elastic waves (Nair & Cai, 2010). For instance, crack initiation or ultimate failure. AE as a SHM method is based on the generation of elastic waves in the structure. As described in paragraph 2.1 and 2.2 the elastic waves propagate in different modes. The elastic waves hit the transducer in the sensors and the sensors are converting these into electrical signals (Drummond et al., 2006). For the AE technique three essential components are needed: a source in form a damage process (1), a receiver in the form of a sensors with a transducer which catch up these waves and convert them to electrical signals (2) and a data acquisition signal which collect all the data and which is needed for further post-processing of the signals (3). Software packages are needed to analyse the data which is received by use of the sensors. In figure 13 the main principle of AE is represented (Nair & Cai, 2010).

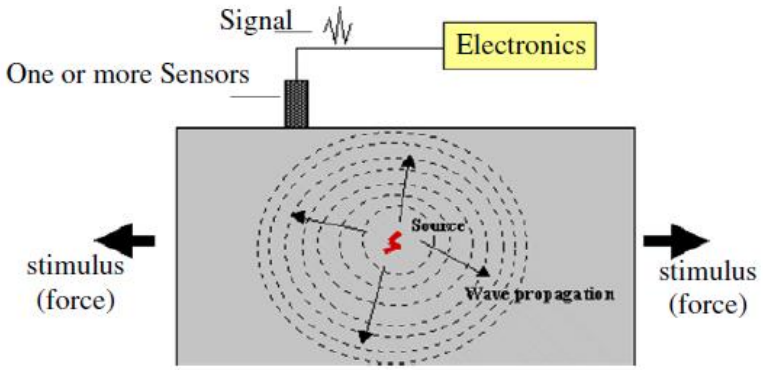

Figure 13 – Principle of AE (Nair & Cai, 2010)

There are more definitions made on AE. According to Weavers (1996) "Acoustic emission is a naturally occurring phenomenon within materials and term acoustic emission is used to define the resulting transient elastic waves when the strain energy is released suddenly within a material due to the occurrence of micro-structural changes in a material". Another definition of AE is given by the American Society for the Testing of Materials: "the class of phenomena whereby transient elastic stress waves are generated by the rapid release of energy of localised sources within a material" (Nair & Cai, 2010). According to Holford & Lark (2005) the main objectives for SHM with AE is the detection of the emission sources that are present in a material and to gain as much as possible information about the sources which are generated by different damage mechanisms.

The techniques of AE have both advantages and disadvantages. The following advantages and disadvantages of AE are given in table 1, with respect to the use of AE for bridge monitoring (Nair & Cai, 2010).

Table 1 – Advantages and disadvantages of AE

Advantages	Disadvantages
Damage growth generates AE	Background noise needed experienced people and more trial sessions
For the use of global, local, remote and continuously monitoring purpose AE technique is suited	Quantitative analyses with AE are a challenge
The detection and location of source is possible	There are no standardized procedures available

The parameters of AE signals, as described in paragraph 3.1.4, can be used to discriminate AE signals due to wire breaks from other sources. Next to these parameters, the frequency of the AE signals can also be used to discriminate AE signals due to wire breaks from other sources. The frequency of AE signals can be determined with wavelet transformations. Wavelet transformations cut the signals into different frequency bands. Each frequency will be studied and matched with its scale (Xin, Diender & Veljkovic, 2018). The wavelets transform the signals into the time-frequency domain. With the help of scalograms the characteristics of the time-frequency can be visualized. These scalograms can be used to identify the frequencies of the AE signals.

In figure 14, an overview of a typical AE instrumentation is given. This instrumentation exists of sensors, preamplifiers, measurement circuitry and a data acquisition system. The sensors will detect AE signals, they will convert it to electrical signals. These electrical signals are raised to an usable level by help of the preamplifiers. To eliminate background noises a threshold is set above the background emission level. The threshold is always a minimum amplitude level. This threshold determined which signals will be recorded and/or analysed. All the signals which are passing this threshold are stored in the data acquisition system. Next to the data storage function the data acquisition system have a data analysis and presentation function. The data acquisition system and the sensors will be explained further in paragraph 3.1.1 and 3.1.2.

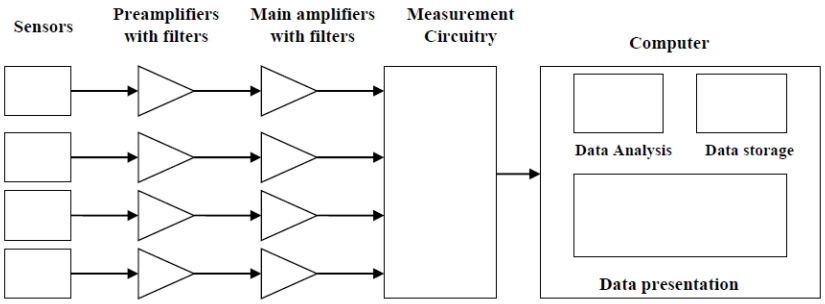

Figure 14 – Typical AE instrumentation (Xin, 2018)

3.1.1 Data acquisition system

The data acquisition system used in the experiments is the Sensor Highway III (SH-III) system. This system is available at the Delft University of Technology and contains 16 channels. In figure 15 this system is shown. According to the manufacturer (MISTRAS) this system is developed for AE, SHM and sensor fusion application. This system is designed in such a way that it can be used for applications in outdoor environments. The product sheet for this system according to the manufacturer is shown in Appendix 2.

Figure 15 – Sensor Highway III data acquisition system

3.1.2 Sensors

In figure 16 a typical example of a sensor is shown. Sensors for AE are always using piezoelectric elements as a transducer. This transducer transduces the received mechanical energy, which is received from the generated elastic wave in the material, into an electric signal (Holford & Lark, 2005). A piezoelectric element deforms by a stress wave and generates an electric signal (Niroula, 2014). In most modern sensors there is a pre-amplifier system built in, if this is not the case an extern preamplifier must be placed close to the sensor. Preamplifiers raise the electric signals to an usable level, because the piezoelectric crystal generates a very small voltage. The preamplifiers provide the necessary gain (40 dB), cable drive capability and filtering (Holford & Lark, 2005). This is mostly a low-noise amplifier. The choice of a specific sensor depends mainly on three parameters (Holford & Lark, 2005):

- Sensitivity of the sensor;
- Frequency range of the sensor;
- Physical and environmental characteristics of the sensor.

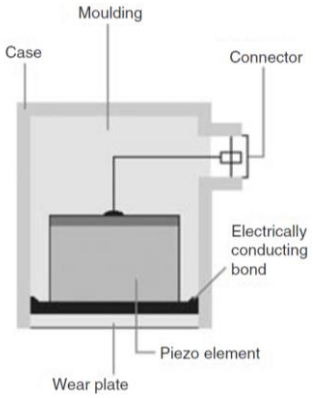

Figure 16 – Cross section of an AE sensor (Holford & Lark, 2005)

According to Holford and Lark (2005) there is a lot of confusion about the terms wideband, broadband, high fidelity, flat width frequency and resonant for the description of the characteristics of the transducer performance. The terms wideband and broadband implicate for sensors with large frequency ranges with a high sensitivity. High fidelity and flat width frequency are implicating that there are no resonances over the range of frequency which is of interest. The resonant implicates over a narrow frequency range a high sensitivity. Holford and Lark (2005) concluded that generally when high sensitivity is needed a resonant type of transducer is used. They also conclude that for practical usage the lower frequency range is governed by background noise and the high frequency range is governed by attenuation. They concluded that the frequency range which is most

common to use for general AE testing is the range of 100 – 300 kHz. Casey, White & Taylor (1985) performed a frequency analysis of the signals which are generated by failure of wires. They concluded the main frequency components of the transduces signal which is generated due a wire breakage lies in the range of 0 – 100 kHz. Sun and Qian (2011) performed experiment on wires and concluded that the main frequency peak for wire breaks was at 150 kHz. They also concluded that for AE signals due to a given impact are in a frequency range of 10 – 50 kHz. With a main peak frequency less than 20 kHz.

Sensors are applied on the surface of materials which have to be tested. The mounting and coupling of the sensors are important for a good transmission of the AE. According Niroula (2014) the following couplants are mainly used: hot glue, vaseline, vacuum grease and ultrasonic gel. The effectiveness of a specific type of couplants depends on a few parameters. Parameters like absorption, impedance, application thickness and the viscosity of the couplants determine the final effectiveness of the couplants. The use of couplants have to be carried out with a lot of care (Niroula, 2014).

In table 2 the characteristics of the available sensors for the experiments are shown. In total three different experiments will be carried out. The aim of the first experiment is to capture AE signals due to wire breaks and to localize them. The second and third experiments are verification experiments where the aim is to investigate the accuracy of linear source location techniques and the influence of different types of sensors. In last experiments impacts will be given to the cable. For a more detailed description of the experiments see paragraph 3.1.2. Based on the research that is carried out by Holford and Lark (2005), Casey et al. (1985) and Sun and Qian (2011) the decision is made which sensors will be used for which experiments. For the full scale experiment the R3I-AST and the R6I-AST sensors will be used. These sensors are covering an operating frequency range of 10 – 100 kHz. For the first verification experiment only the R6I-AST sensor is used because according to Sun and Qian (2011) the frequency range of AE signals due to impact is partly covered by this type of sensor. For the second verification experiment all the three types of sensors which are available are used. The R3I-AST sensors are used because this sensor type covers almost the complete frequency range of AE signals due to impact. The other two types of sensors are used to investigate the suitability of different types of sensors compared to the R3I-AST sensor. It is expected that the R3I-AST sensors are the most suitable type of sensors for AE signals due to impacts. The different types of sensors are shown in figure 17. The product sheets according to the manufacturer are shown in Appendix 3.

Table 2 – Characteristics of used sensors

	R3I-AST	R6I-AST	VS600-Z2
Operating frequency	10 – 40 kHz	40 – 100 kHz	400 – 800 kHz
Resonant frequency	31 kHz	98 kHz	600 kHz
Manufacturer	MISTRAS	MISTRAS	VALLEN

Figure 17 – AE sensors: R3I-AST sensor (l). R6I-AST sensor (m). VS600-Z2 sensor (r)

3.1.3 Couplant and mounting

The couplant that is used for this experiment is viscoelastic putty (Pritt®). Zhang, Pahlavan, Yang, & Hordijk (2017) did research on the behaviour of viscoelastic putty. They concluded that the amplitude variation could be ± 5 dB. This results in the fact that the material as couplant absorbs a part of the signal. A wire break will cause a signal with a high amount of energy which could damage the sensors if a couplant like vaseline is used. To prevent the sensors from being damaged during high amount of energies, this couplant will suit perfect. For all the sensors an equal amount of couplant is used and placed on the cable.

To ensure a good transmission of the elastic waves from the cable to the sensors the grease of the cable was removed. After removing the grease, the couplant and the sensors where placed on the cable. To ensure a constant pressure and attachment of the sensors to the cable insulation tape was used. Prestressing of the tape tackles the problem that the sensors could fall of when the diameter of the cable decreases during loading. Also, two sensors are attached to the socket of the cable. This is done with the same (amount of) couplant to obtain fair results, but with a clamp instead of tape. The process of mounting the sensors to the cable/socket is visualized in figure 18.

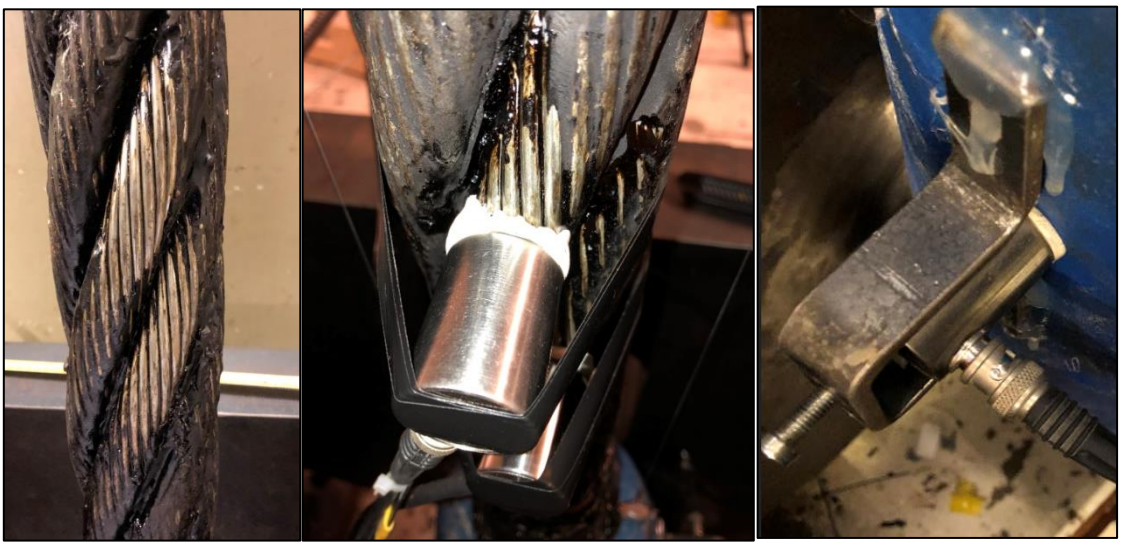

Figure 18 – Removing of grease (l). Sensor on cable (m). Sensor on socket (r)

3.1.4 Signal parameters of AE

Parameters like amplitude, hits, counts, events, rise time, duration, signal strength, (MARSE) energy and absolute energy are recorded for every signal. To obtain more knowledge about the source of the signal the parameters can be observed. The above-mentioned parameters are further explained.

Amplitude

A key parameter of an acoustic transducer signal is the voltage. The voltage level is rather small. With the use of amplifiers these small voltage levels are increased to a workable level. This conversion of voltage to decibel is done by equation 5. The peak amplitude is equal to the highest voltage in the voltage time waveform (figure 19). When AE tests are carried out a lot of amplitudes are recorded. In this equation, the peak voltage is given by V_p and V_{ref} is the reference voltage (Drummond et al., 2006).

$$A(dB) = 20 * \log\left(\frac{V_p}{V_{ref}}\right) \qquad (5)$$

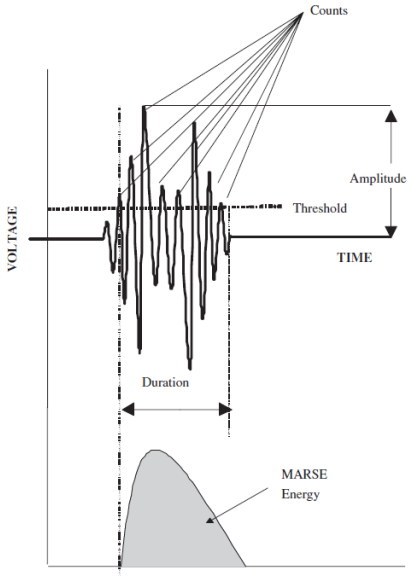

Figure 19 – A typical output waveform (Drummond et al., 2006)

Hits, counts and events

In figure 19 a typical result of AE is presented, this is a voltage time waveform. When an acoustic signal hits the transducer the result of this is a hit. The top part of figure 19 is a waveform, this is called a hit. During the test with AE a threshold is been set. Counts are the number of times when the threshold is passed. In figure 20 all the peaks which cross the threshold are counts. All the hits that make it possible to locate the source of the acoustic signal are called an event (Drummond et al, 2006). It is common to count both the negative as the positive threshold crossings and multiply this number by a half (Niroula, 2014).

Rise time and duration

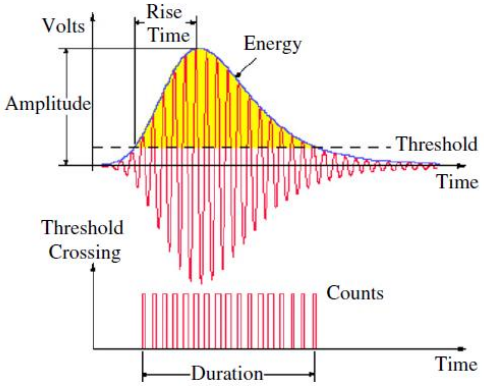

Figure 20 – A typical AE signal (Nair & Cai, 2010)

In figure 20 another result of an AE test is shown. In this figure the rise time and duration are presented. The rise time is equal to the time when the first threshold is crossed to the maximal peak. The duration of a waveform is the time between the first and last threshold crossing. Both parameters are measured in microseconds (Niroula, 2014).

Signal strength, marse energy and absolute energy

AE signals are generated due to the rapid release of energy, the energy amount of the transducer can be related to this energy release. In figure 20 the total energy of the transducer is equal to the area enclosed by the waveform. This measure of energy is called the signal strength or the (MARSE = measured area under the rectified signal envelope) energy, they are proportional to each other (Niroula, 2014). The (MARSE) energy/signal strength is shown in figure 20, the units of these parameters are pVs. The absolute energy is calculated by taking the time integral of the squared transducer output signal (Drummond et al., 2006). The absolute energy is measured in attojoules (aJ).

3.2 EXPERIMENTS

The full scale and verification experiments were all carried out on a 77-6x36WS-IWRC-1770/1960-zn-sz cable. In Appendix 4 the explanation and some geometrical properties of this type of cable are given. In total three experiments were performed: one full scale experiment where the cable was loaded until failure and two verification experiments where the cable was placed in the test setup without loading. The experiments were performed in a 10 MN test bench at the Stevin II Laboratory at the Delft University of Technology. More detailed information about the test bench can be found in the work of Ivanov (2018).

3.2.1 Full scale experiment

The aims of the full-scale experiment were to find the capacity of this type of cable and to investigate the AE behaviour related to wire breaks inside a cable. Figure 21 represent an (schematic) overview of the test bench. In this paragraph the following subjects will be further described: the test setup, test procedure, failure expectations, results related to the capacity, failure modes and the time identification of wire breaks.

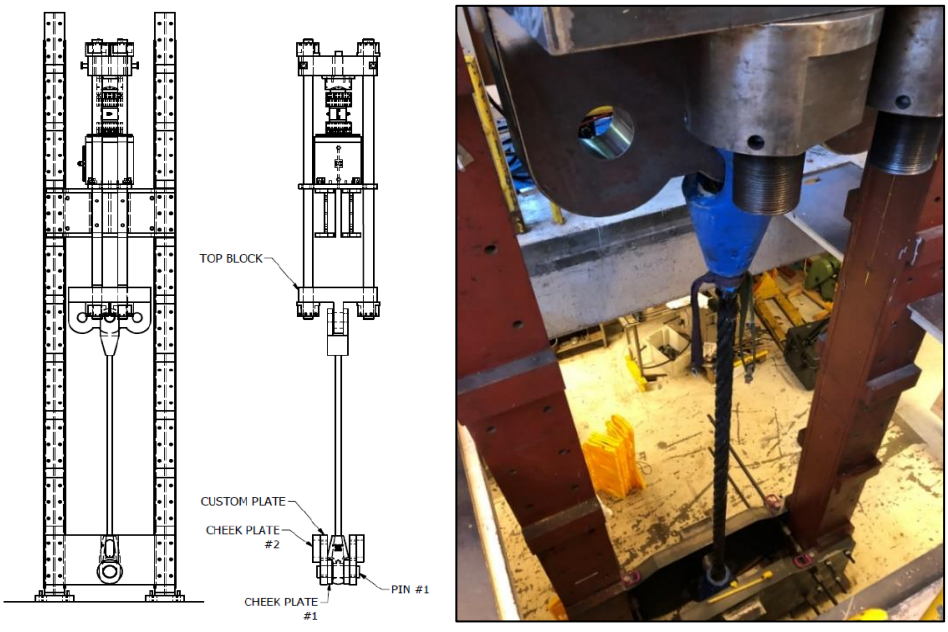

Figure 21 – An (schematic) overview of the test bench (Ivanov, 2018)

Test setup

In total six R6I-AST and four R3I-AST sensors were placed on the 3000 mm long cable. The reason why these types of sensors were chosen is explained in paragraph 3.1.2. The sensor layout and spacings are given in figure 22. In this figure the black sensors represent the R3I-AST sensors and the white sensors represent the R6I-AST sensors. The spacings in figure are given in mm. The testing machine is able to measure the elongation of the cable. However, this elongation can include possible displacement from the components of the test bench. These possible displacements can introduce an error in the actual elongation of the cable. To measure the actual elongation of the cable two LVDT (linear variable differential transformer) devices were attached to the cable to investigate the significance of the error in the elongation obtained by the testing machine. The LVDTs are attached to the sockets of the specimen. The red crosses in figure 22 represents the LVDTs. According to the manufacturer of the cable the minimum breaking load (MBL) is 4850 kN. The cable was prestressed to a level of 10% of the MBL.

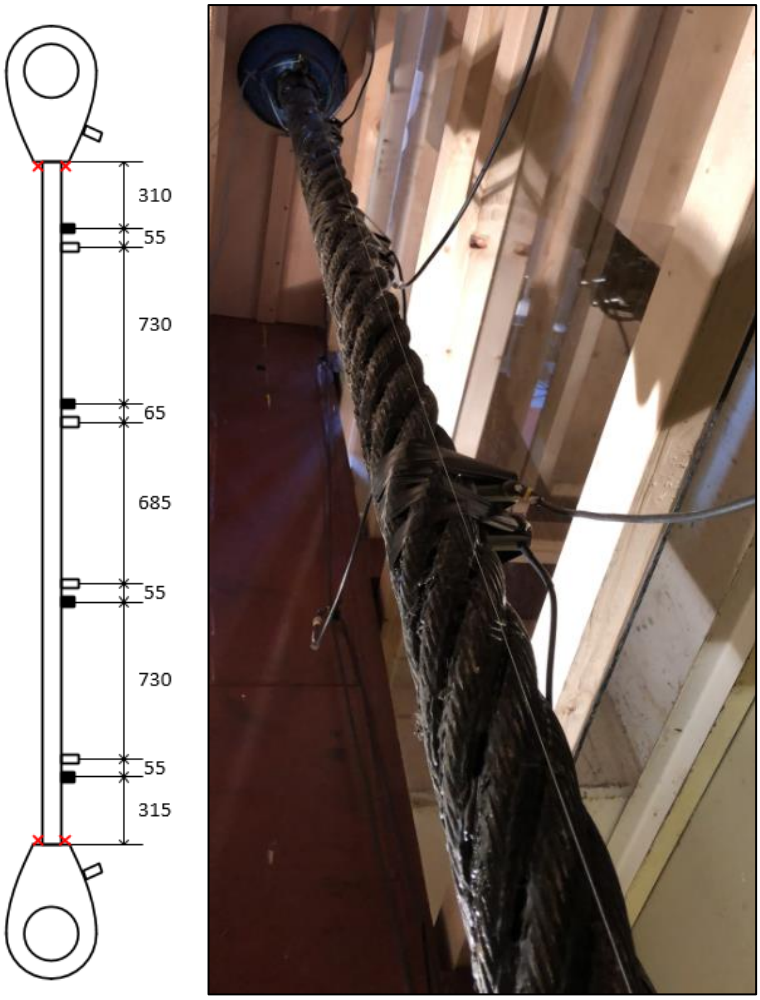

Figure 22 – Sensor layout and spacings

Test procedure

The cable was loaded until failure without any stops or unloading's. The loading speed that was used is 0.175 mm/s. Based on the MBL and the analytical model of stay cables the expected break force was around 4500 – 5200 kN.

Failure expectations

Based on Ivanov (2018), steel wires will change their mechanical properties due to the manufacturing process. According to Feyrer (2007), the total elongation for wires inside a cable is about 1.5 – 4 % and the yield strength is about 75 – 95 % of the ultimate strength. For single wires which are straightened the extension is even smaller, namely between 1.4 – 2.9 % and the yield strength is about 85 – 95 % of the ultimate strength. Comparing both situations, it can be concluded that the manufacturing process results in a decrease in ductility but in an increase in yield strength.

Based on previous experiences the failure modes of single wires can be categorized into cup and cone and shear failure. In the cup and cone failure mode the wires will neck due to high axial stresses. Necking is the effect of the reduction in cross-section. The cup and cone are visible due to the appearance of micro voids. Shear failure is failure of the wires under an opposing load, for instance friction. Shear failure can occur due to the helical structure of the cable. This helical structure results in shear force in the wires which can result in shear failure of the wires. It is expected that the cable will not be completely separated and that the single wires will fail due to cup and cone or shear failure.

Results

The most important results are shown in figure 23. The measured breaking force of the cable was 5138 kN. The measured breaking force is 5.9% higher compared to the MBL prescribed by the manufacturer. The measured breaking force of the cable is within the expected range. The elongation at failure according to the LVDT and the testing machine are respectively 0.0370 and 0.0458. The difference in elongation is expected due to the elastic deformation of the different components of the test bench. The difference in elongation is almost 1%. In the plastic region wire breaks start to occur, these wire breaks result in small load drops. These small load drops can be seen in the figure below.

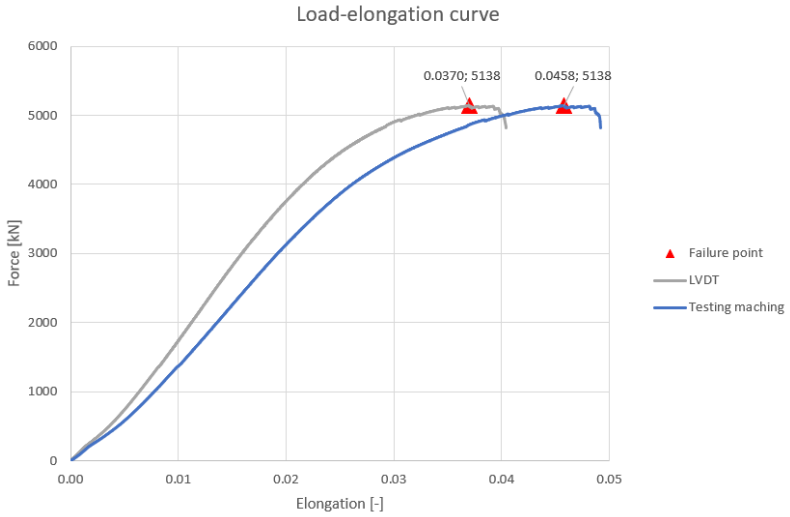

Figure 23 – Load-elongation curves

In figure 24 the failure of the cable is represented. The cable is, as expected, not completely separated. In total two outer strands are still intact, the other strands are completely separated from each other. The approximate position of the failure is around 1100 – 1200 mm from the top socket of the cable.

Figure 24 – Failure of the cable

As expected, the wires that failed can be split into two different failure modes, namely cup and cone and shear failure. In figure 25 the two different failure modes are clearly visible. The cup and cone failure mode is clearly visible in the left figure and shear failure of the wires is clearly visible in the right figure. The most occurring failure mode was cup and cone failure, due to the effect that the axial stress was governing in the wires.

Figure 25 – Cup and cone failure (l) and shear failure (r)

Time identification of wire breaks

For further post processing purposes, the approximate time of wire breaks are important. The small load drops (approximately 15 kN) in the load-time curve (figure 26) are the result of wire breaks in the cable. If a wire break occur the load will drop and the cable is searching for a new equilibrium. The cable will redistribute the force over the remaining wires. This phenomenon is repeated until too many wires are broken and the load cannot be redistributed anymore over the remaining wires. At the end the load drops are hard to see. The approximate time for every load drop is summarized in table 3.

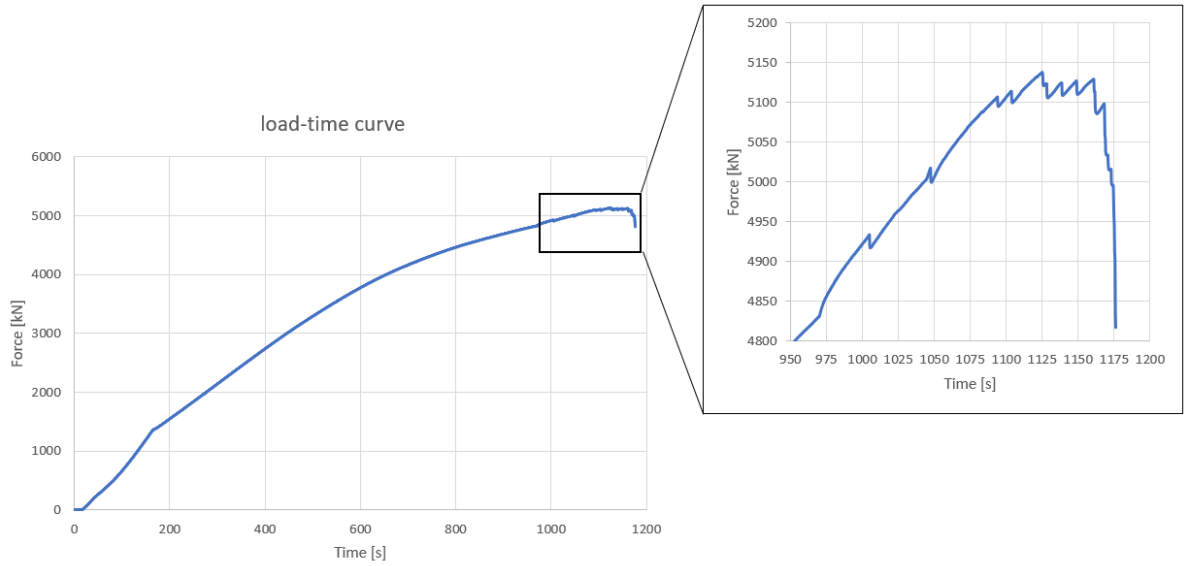

Figure 26 – Load-time curve and zoomed load-time curve of the black box

Table 3 – Approximate time values of load drops according to load-time curve

Time [s]	1005	1048	1094	1104	1126	1129	1139	1149	1161	1162	1169	1171	1173	1175
Load drops	1	1	1	1	1	1	1	1	1	1	3	1	1	3

To verify the above method of time identification of wire breaks, a device which recorded the sound was placed next to the test bench during the experiment. This device recorded continuously during the experiment. This record device recorded in total 20 wire breaks. In figure 27 the soundwaves for 20 different wire breaks are shown. For every sound wave the blue line is the start of a wire break. The time needs to be scaled with the time in figure 26. After scaling the time, the approximate time of wire breaks are summarized in table 4.

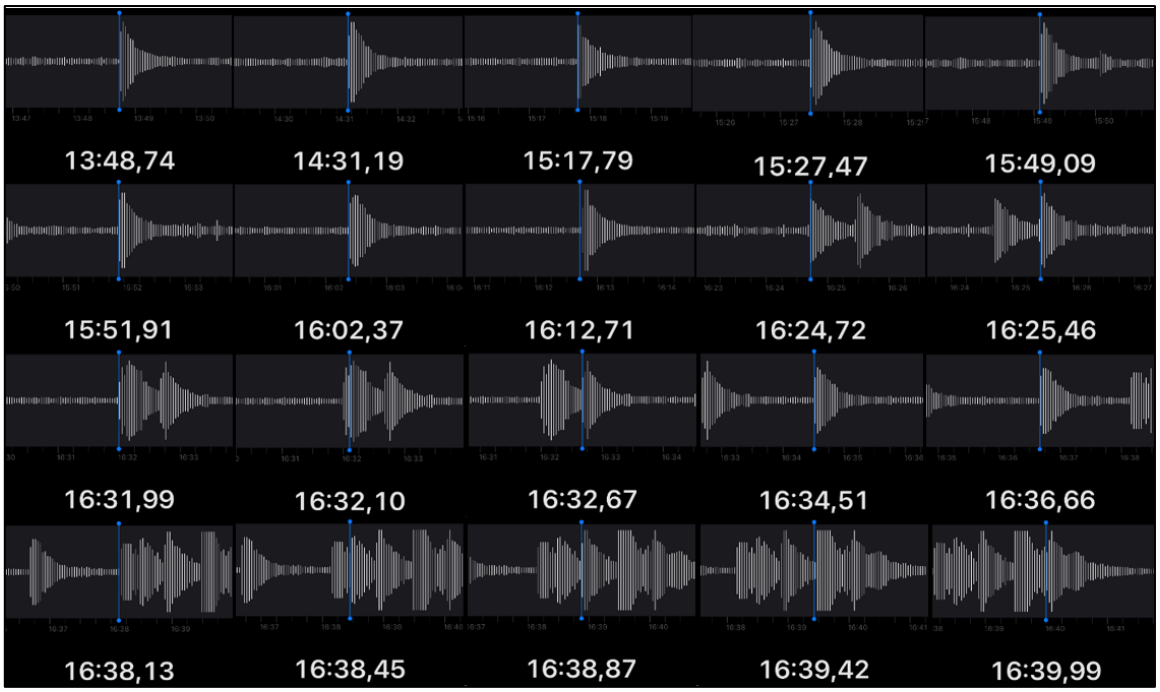

Figure 27 – 20 Soundwaves of the record device

Table 4 – Approximate time values of load drops according to record device

Time[s]	1005	1047	1094	1103	1125	1128	1138	1149	1161	1168	1169	1171	1173	1174	1175	1176
Wire breaks	1	1	1	1	1	1	1	1	2	2	1	1	1	2	2	1

The approximate time in table 3 and 4 are almost equal to each other. Some values have a difference of only 1 second, but this difference is not of importance. The aim is to identify the wire breaks at a certain time during the loading of the cable. As expected, the load drops at the end of the test in figure 26) are hard to see and compared to the record device two values are missing. For further post processing purposes (paragraph 3.2.3), the time of wire breaks in table 4 are used.

3.2.2 Verification experiments

The aim for the first experiment was to investigate the accuracy of a linear source location technique based on three different TDOA (see paragraph 2.2.2). The aims of the second experiment were to investigate also the accuracy of a linear source location techniques based on three different TDOA. But also, the wave speed of the AE signals and the suitability of different types of sensors. In figure 28 an (schematic) overview of the test bench is given. As can be seen in this figure the cable was bend around a sleeve. To be consistent in all the experiments in this research, both experiments were performed on the straight part of the bended cable. In the following paragraphs the test setup and the test procedures for both experiments are described further. The choice for using different types of sensors is explained in paragraph 3.1.2.

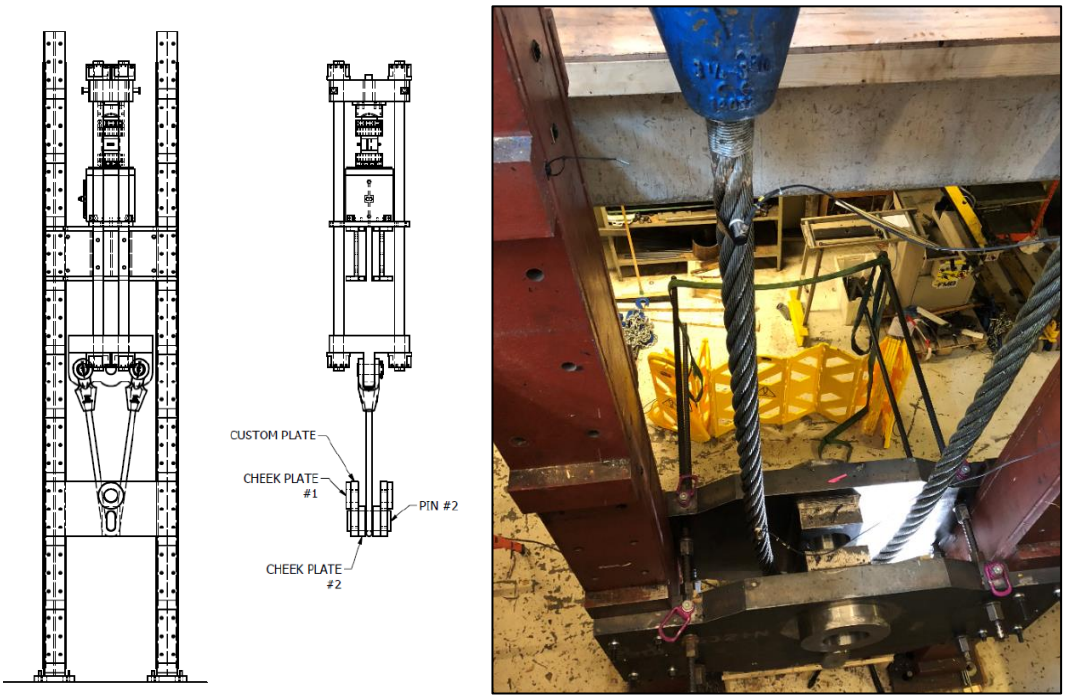

Figure 28 – Schematic overview of the verification experiments (Ivanov, 2018)

Test setup experiment 1

For this experiment only two R6I-AST sensors were placed on the cable. Next to this, three different positions were marked on the cable where the impact was given by a hammer. The spacing between the sensors and the location of the position (1,2 and 3) are given in figure 29. The values in this figure are given in mm.

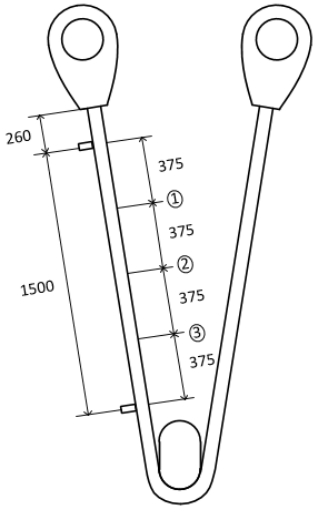

Figure 29 – Sensor and position layout for the first verification experiment

Test procedure experiment 1

To investigate the accuracy of a linear source location technique, a pencil break test was used five times at every position shown in figure 29. But, the AE signals due to the pencil break test were not strong enough to reach both sensors. This makes the pencil break test not suitable for investigation to the accuracy of a linear source location technique. Instead of using the pencil break test, the hammer in figure 30 was used. The AE signals due to the given impact by the hammer reaches both sensors. To obtain more data, the cable was given an impact 10 times at every location. To be as consistent as possible, the amount of power of each impact was tried to keep constant. In figure 29 the sensors and the position of the impacts are not on the same side of the cable, but during the experiment the cable was given an impact at the same side of the cable where the sensors were attached.

Figure 30 – Hammer used for impact

Test setup experiment 2

For the second verification experiment six sensors were placed on the cable. All the three available sensors (R3I-AST, R6I-AST and VS600-Z2) are used in this experiment. An overview of the spacing between the different sensors and the location of three different positions (A, B and C) are given in figure 31. Respectively, the black, white and grey sensors in figure 31 are representing the R3I-AST, R6I-AST and VS600-Z2 sensors. The locations and the sensors are not on the same side, but the impacts were given at the same side of the sensors.

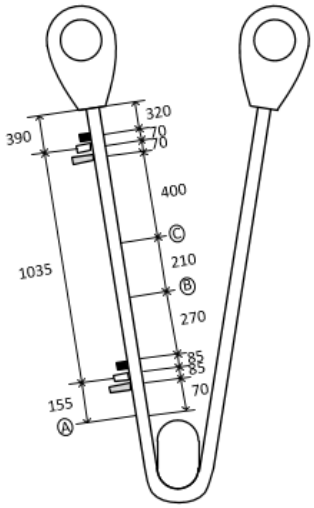

Figure 31 – Sensor and position layout for the second verification experiment

Test procedure experiment 2

To increase the level of consistency, a pendulum with and without an additional mass were used to give the cable an impact. The different pendulum configurations are showed in figure 32. The consistency level was increased because for every impact the divergence of the pendulum was kept the same which resulted in a constant amount of power for the impacts.

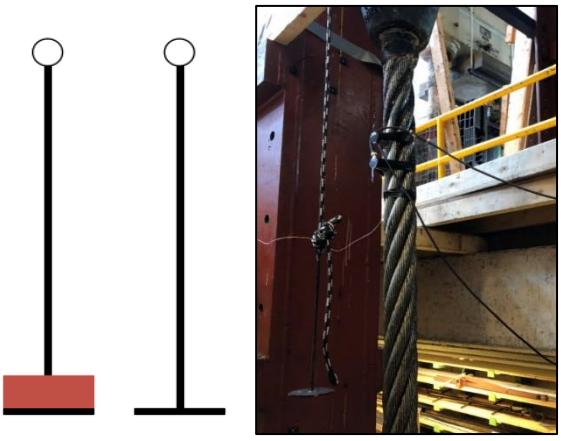

Figure 32 – Pendulum with (l) and without (m) mass and overview of the pendulum

To investigate the wave speed of the AE signals, the cable was given an impact 15 times at location A by the pendulum without an additional mass. The wave speed of the AE signals can be calculated according to equation 6. Only the TDOA obtained from first threshold passing (method 1) is used.

$$V = \frac{D}{\Delta t} = \frac{spacing\ sensors}{TDOA} \qquad (6)$$

To investigate the accuracy of a linear source location technique, the cable was given an impact 10 times at location B, half of the impacts were given with an additional mass and half of the impacts were given without an additional mass. Location C was given 20 times an impact by the pendulum. Also, for these impacts half of the impacts were given with an additional mass and half of the impacts are given without an additional mass.

3.3 RESULTS

3.3.1 Full scale experiment

Figure 33 presents the energy-time results for one R3I-AST sensor (sensor number 10) and for one R6I-AST sensor (sensor number 8). The graphs in this figure are scaled to the time scale ranging from 950 s to 1200 s, this is the region where the wire breaks occurred according to paragraph 3.2.1 Time identification of wire breaks. In table 5 the results are summarized for each time value.

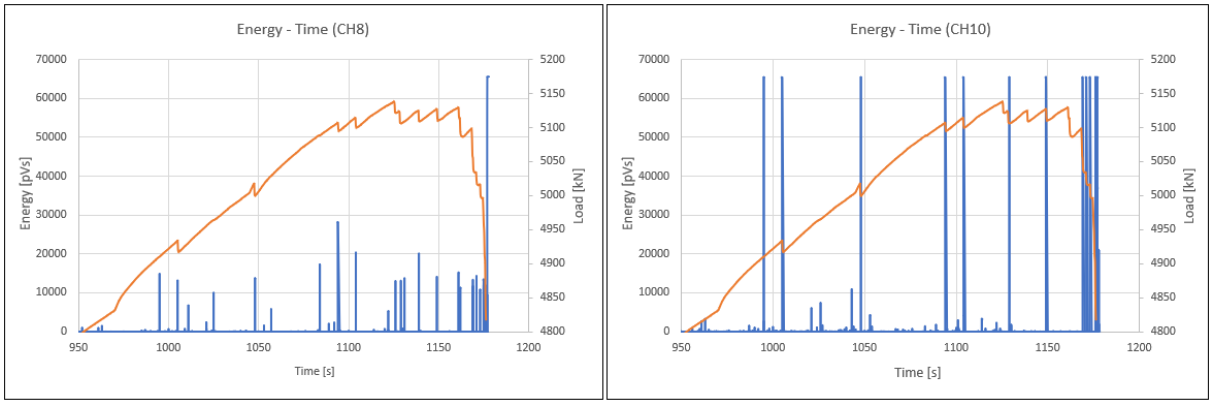

Figure 33 – Energy-time curve for sensors 8 and 10

Table 5 – Energy values for sensor 10 and 8

Time value [s]	1005	1047	1094	1103	1125	1128	1138	1149	1161	1161
Energy sensor 10 [pVs]	65535	65535	65535	65535		65535		65535		
Energy sensor 8 [pVs]	13197	13816	28206	20382	13062	13168	20124	14183	15301	11364
Time value [s]	1168	1168	1169	1171	1173	1174	1175	1175	1175	1176
Energy sensor 10 [pVs]			65535	65535	65535				65535	
Energy sensor 8 [pVs]	11761	13414	11487	14403	10857	11947	11158	13468	9519	65535

In figure 33 and table 5 the results of two different types of sensors are shown. In this figure the energy values related to wire breaks are much higher for the R3I-AST sensor compared to the R6I-AST sensor. Also, the R3I-AST did not catch all the wire breaks inside the cable. The R3I-AST sensor missed 11 out of 20 wire breaks. From these results it can concluded that the frequency of the AE signals caused by a wire break are more in the operating frequency range of 40 – 100 kHz. As expected, the R6I-AST sensors are more suitable for wire break identification compared to R3I-AST sensors.

According to Drummond et al. (2006) the amplitude and energy parameters are the most effective parameters to discriminate wire breaks from all the other AE sources. Figure 34 and 35 present the amplitude- and energy-time results obtained from the R6I-AST sensors (sensor numbers 3,4,5 & 8). The results for the R3I-AST sensors (sensor number 2,6,7 & 10) are given in Appendix 5. The threshold level during this experiment was 35 dB, but for the figures a threshold of 60 dB is used.

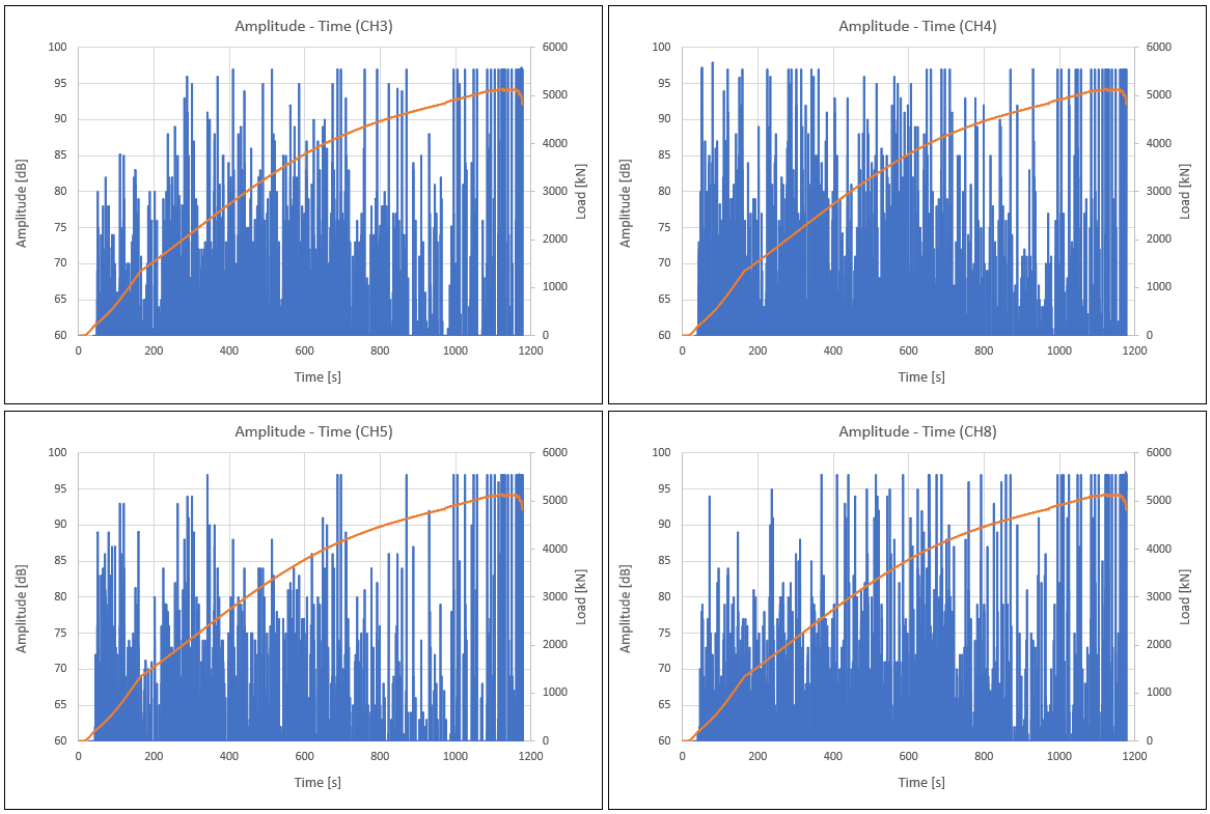

Figure 34 – Amplitude-time and load-time curve for sensors 3,4,5 & 8

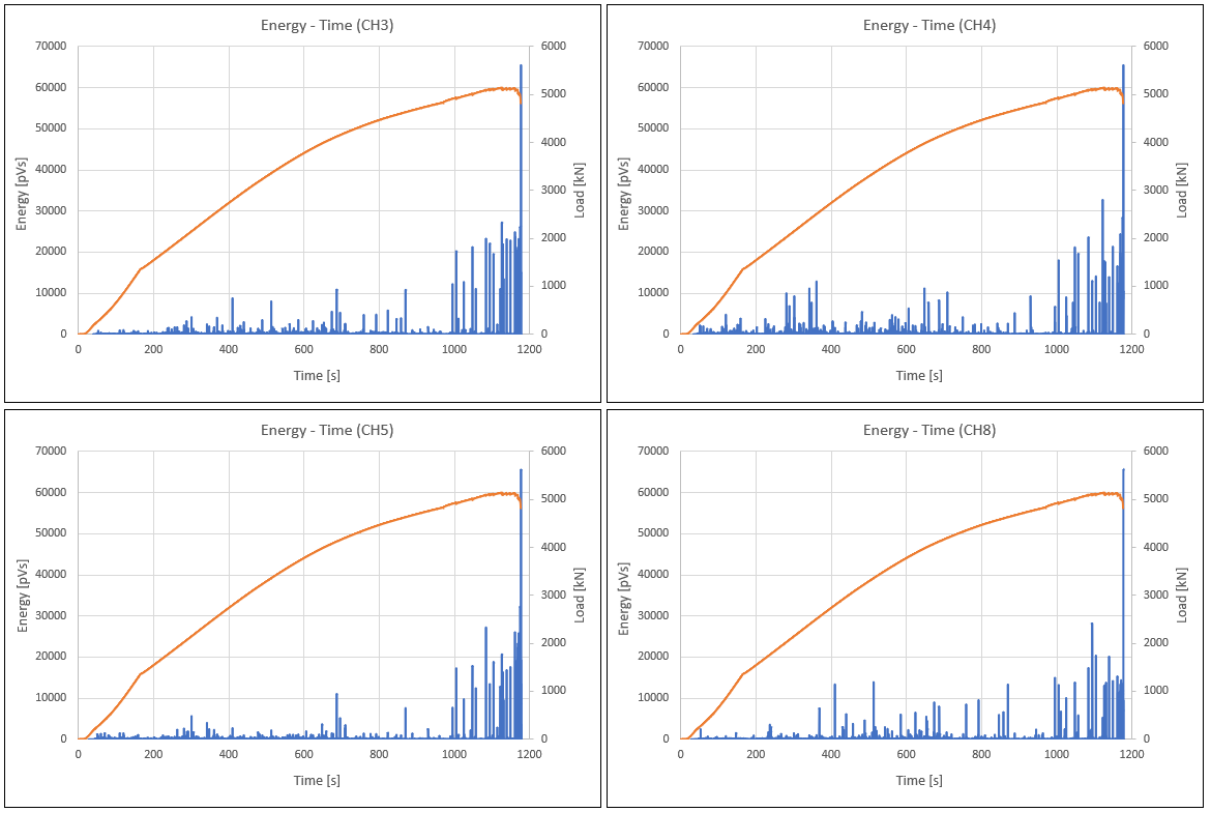

Figure 35 – Energy-time and load-time curve for sensors 3,4,5 & 8

According to paragraph 3.2.1 Time identification of wire breaks the first wire break occur at 1005 s. The amplitude values after the first wire break are approximately the same as before the first wire break occur. However, the energy values increased when wire breaks occur inside the cable. In figure 34 it can be seen that the sensors could not handle a higher amplitude than 97 dB. Even if the amplitude values are higher the sensors cut this off to a maximum value of 97 dB. The transducer output signal is converted into an amplitude according to equation 5 (page 22) and the energy is the time integral of the squared transducer output signal. This make the amplitude and the energy related to each other. Based on the relation between the amplitude and the energy it can be concluded that the energy values are lower compared to the real values due to the cut off of the amplitude. In table 6 a summary of the minimal values for different parameters is given.

Table 6 – Summary of minimal values for different parameters

Parameter	R6I-AST				
	CH3	CH4	CH5	CH8	Minimal values
Amplitude [dB]	97	97	97	97	97
Energy [pVs]	15107	10510	13432	9519	15107
Signal Strength [pVs]	9.4E+07	6.6E+07	8.4E+07	5.9E+07	9.4E+07
Absolute Energy [aJ]	3.5E+08	2.0E+08	2.9E+08	1.9E+08	3.5E+08
Duration [µs]	41428	48761	27940	42341	41428
Rise time [µs]	1315	212	969	418	1315
Counts [-]	778	1050	547	918	778

Next to the amplitude and energy, also the signal strength and absolute energy are related to the transducer signal output. These values are also cut off by the sensors due to the cut off limit. The real values are expected to be higher compared to the values given in table 6. This make the minimal values in table conservative minimal values for the discrimination of wire breaks from AE sources. By further analysing of the results caused by wire breaks the minimal values for the different parameters can be used.

Sensors on socket

Figure 36 present the amplitude- and energy-time results of the R6I-AST (sensor number 1 and 9) attached on the socket. Sensor 1 is attached to the top socket and sensor 9 is attached on the bottom socket. The amplitude and energy values for sensor 1 show over the first 800 seconds only high values, while sensor 9 show only high values in the first 200 seconds. As described in paragraph 3.2.1 the top socket is attached to a top block which is connected by four steel rods to the hydraulic jack of the test bench. The bottom socket is only attached to the cheek plates. During testing the different components of the test bench are experience stresses, which result in AE signals. Near the top socket more components are present which experience stresses compared to the bottom socket. This result in a longer period of high amplitudes and energy levels. Also, the energy values for sensor 1 are higher compared to sensor 9, this is clearly visible in table 7. Finally, these energy values are much higher compared with the energy values for sensor 8 in table 5. According to above observations the results of the sensors on the socket (sensor 1 and 9) are stated as non-usable for further post processing purposes.

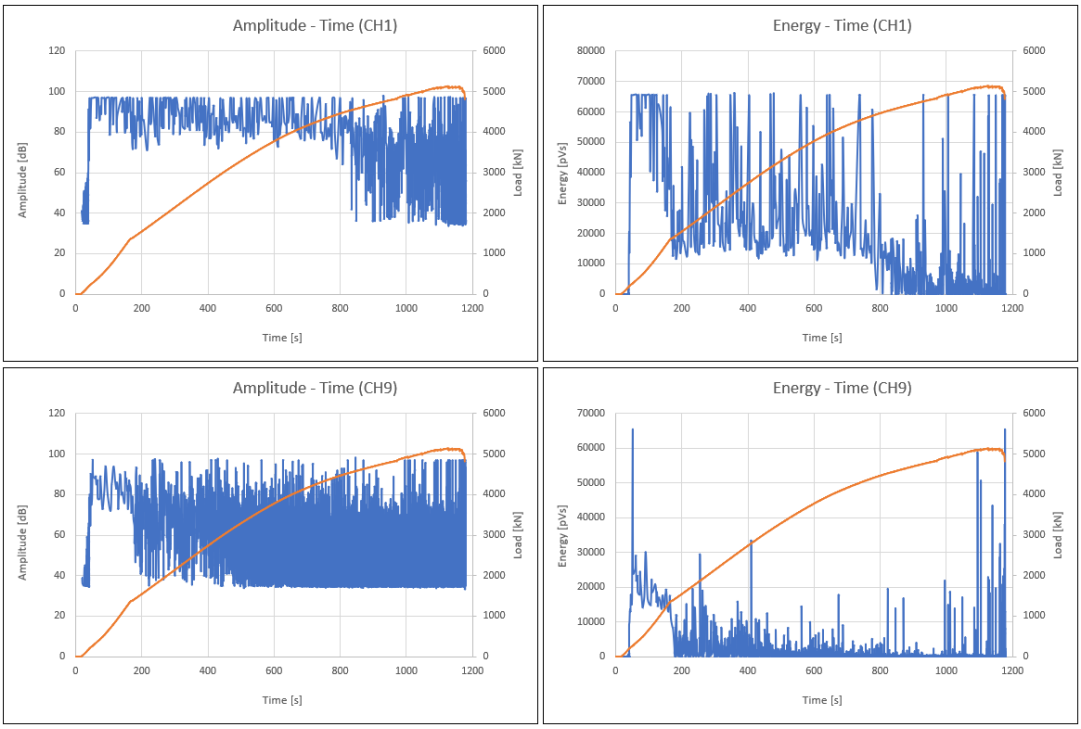

Figure 36 – Amplitude- and energy-time for sensors 1 & 9

Table 7 – Energy values for sensor 1 and 9

Time value	1005	1047	1094	1103	1125	1128	1138	1149	1161	1161
Sensor 1 [pVs]	65535	6634	31863	46998	58681	65535	29548	65535	36532	37879
Sensor 9 [pVs]	14991	17138	58909	50759	22942	22085	43556	19808	28706	32546
Time value	1168	1168	1169	1171	1173	1174	1175	1175	1175	1176
Sensor 1 [pVs]	65535	65535	65535	53148	65535	61662	49796	65535	65535	65535
Sensor 9 [pVs]	11537	20827	15668	23179	18624	20429	20187	25338	13071	65535

Source location

The cable failed globally between 1250 mm and 2250 mm from the bottom socket. In figure 37 this region is shown by the red lines.

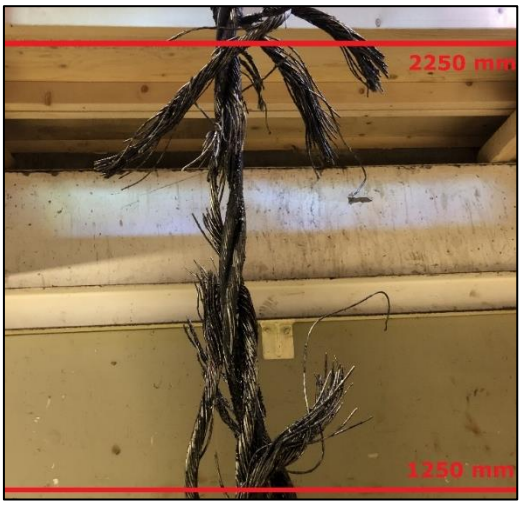

Figure 37 – Global region of failure

Next to the global failure of the cable three local wire breaks were clearly visible. In figure 38 the three local wire breaks and the distance from the bottom socket are given. The local wire breaks were located 440, 550 and 655 mm from the bottom socket.

Figure 38 – Locations of clearly visible wire breaks

The location of the source of an AE signal can be determined according to paragraph 2.2. The method that is used to determine the location of the sources is a linear source location technique. For this technique the wave speed and the TDOA are unknown parameters. The wave speed of the signals is calculated based on the determination of the sequence of sensor hits. In this case sensors 3,4,5 and 8 are attached to cable. For example, the wire break occur between sensor 3 and 4. The signal will travel through the whole cable and all the sensors record the signal. The wave speed of the signal can be calculated by the time difference between sensor 4 and 5 or 5 and 8, because the spacing between the sensors is known. With this wave speed and the TDOA the location of the source can be calculated. In figure 39 the location of the wire breaks for both types of sensors and the three local wire breaks level are shown. This location is based on the TDOA obtained from the sensors.

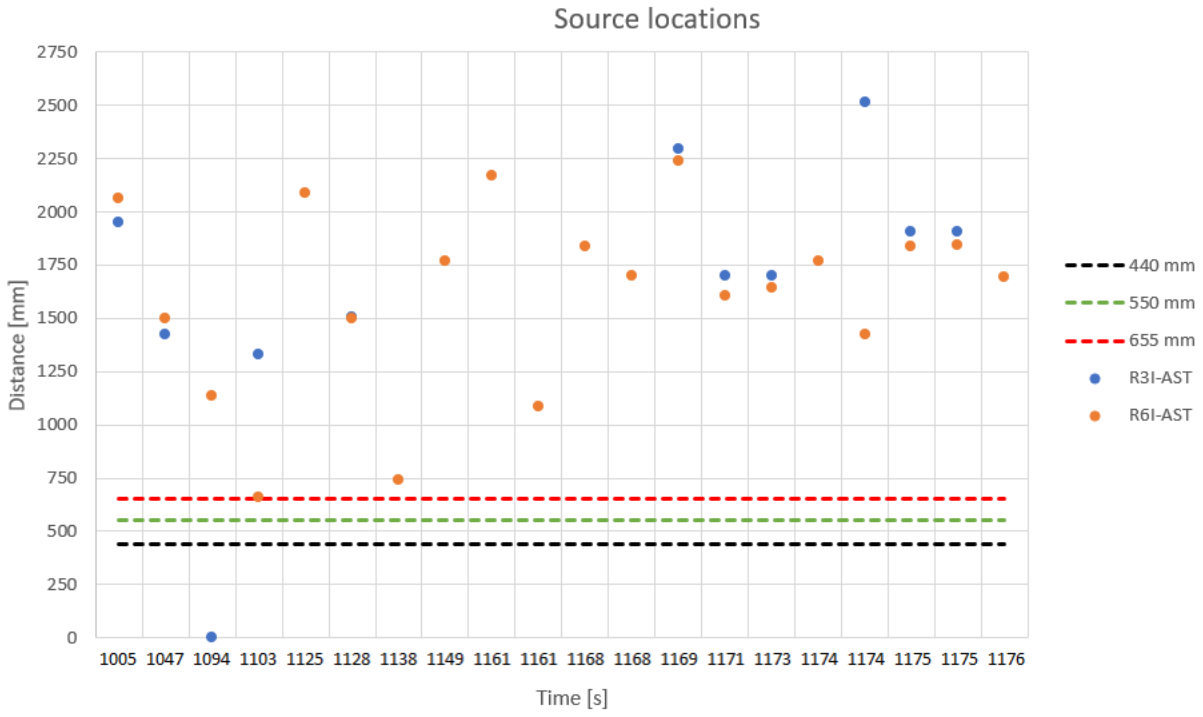

Figure 39 – Location of wire breaks and local wire break levels

Most of the wire breaks according to the sensors are within the range of 1250 – 2250 mm. The exact position of the wire breaks in this range is impossible to determine because the wires will deform heavily, as can be seen in figure 37. The accuracy is determined for the R6I-AST sensors based under the assumption that the smallest distances are corresponding to each other (the location for 1103, 1138 and 1161 s correspond respectively to 440, 550 and 655 mm). The accuracy for the three local wire breaks (440, 550, 655 mm) are respectively 7.2, 6.4 and 14.4%.

A comparison between the different types of sensors is given in table 8. As expected, the R3I-AST sensors were not able to capture all the wire breaks, in total 11 out of 20 locations are determined and compared with the R6I-AST sensors. The highest differences in locations are 37.8%, 36.4% and 22.4%. The difference between the other locations is much smaller, namely in the range of 0.2% - 3.6%.

Table 8 – Location of wire breaks

Time value [s]	R3I-AST distance [mm]	R6I-AST distance [mm]	difference [mm]	difference [%]
1005	1952	2061	109	3.6
1047	1424	1498	73	2.4
1094	0	1133	1133	37.8
1103	1328	656	672	22.4
1125		2087		
1128	1503	1498	5	0.2
1138		743		
1149		1767		
1161		2169		
1161		1087		
1168		1840		
1168		1702		
1169	2298	2238	60	2.0
1171	1699	1607	92	3.1
1173	1699	1642	56	1.9
1174		1767		
1174	2514	1422	1092	36.4
1175	1905	1840	65	2.2
1175	1905	1843	62	2.1
1176		1695		

3.3.2 Verification experiments

According to Sun & Qian (2011) the frequency range of impacts lie in the range of 10 – 50 kHz. It is expected regarding to the sensor choice that the R3I-AST sensors will perform better compared to the R6I-AST sensors. Because the operating frequency range for the R3I-AST sensor is 10 – 40 kHz.

First verification experiment

Table 9 present the comparison between the impact location and the location determined by the linear source location technique based on the three different TDOA.

Table 9 – Results of first verification experiment

	(1) First threshold passing		(2) P-wave analysis		(3) Wavelet analysis		
Impact	Δ [mm]	Δ [%]	Δ [mm]	Δ [%]	Δ [mm]	Δ [%]	
1	13.5	0.9%	1.5	0.1%	190.0	12.7%	location 1
2	32.6	2.2%	20.6	1.4%	212.0	14.1%	
3	32.6	2.2%	22.6	1.5%	52.0	3.5%	
4	13.5	0.9%	4.5	0.3%	662.0	44.1%	
5	13.5	0.9%	0.5	0.0%	438.0	29.2%	
6	13.5	0.9%	2.5	0.2%	756.0	50.4%	
7	13.5	0.9%	3.5	0.2%	758.0	50.5%	
8	13.5	0.9%	4.5	0.3%	154.0	10.3%	
9	13.5	0.9%	1.5	0.1%	16.0	1.1%	
10	13.5	0.9%	3.5	0.2%	200.0	13.3%	
11	0.0	0.0%	5.0	0.3%	157.0	10.5%	location 2
12	0.0	0.0%	2.0	0.1%	1.0	0.1%	
13	0.0	0.0%	2.0	0.1%	1024.0	68.3%	
14	0.0	0.0%	2.0	0.1%	993.0	66.2%	
15	0.0	0.0%	2.0	0.1%	353.0	23.5%	
16	0.0	0.0%	2.0	0.1%	703.0	46.9%	
17	76.3	5.1%	77.3	5.2%	929.0	61.9%	
18	0.0	0.0%	4.0	0.3%	1056.0	70.4%	
19	0.0	0.0%	6.0	0.4%	988.0	65.9%	
20	0.0	0.0%	4.0	0.3%	951.0	63.4%	
21	69.8	4.7%	67.8	4.5%	200.0	13.3%	location 3
22	82.8	5.5%	86.8	5.8%	343.0	22.9%	
23	82.8	5.5%	82.8	5.5%	503.0	33.5%	
24	82.8	5.5%	84.8	5.7%	405.0	27.0%	
25	69.8	4.7%	67.8	4.5%	214.0	14.3%	
26	69.8	4.7%	84.8	5.7%	340.0	22.7%	
27	82.8	5.5%	92.8	6.2%	715.0	47.7%	
28	69.8	4.7%	86.8	5.8%	597.0	39.8%	
29	82.8	5.5%	63.8	4.3%	443.0	29.5%	
30	69.8	4.7%	61.8	4.1%	216.0	14.4%	

The linear source location technique based on TDOA (1) and (2) are approximately equal to each other. TDOA (1) gives a maximum difference of 82.8 mm (5.5%) and TDOA (2) gives a maximum difference of 92.8 mm (6.2%). The biggest difference in source location occurs in location 3, while location 2 is almost exactly the same. The TDOA in method (1) is obtained by the first threshold passing, while the second method (2) obtained the TDOA when the first longitudinal wave (also called the P-wave, see paragraph 2.1.1) hit the sensor. In most of the cases the P-wave is the first wave which hit the sensor, because this wave travel with the highest wave speed. The first P-wave is not automatically the first threshold passing, this results in the differences between the two methods.

TDOA (3), which is based on a wavelet analysis, shows in contradiction with TDOA (1) and (2) some really big difference. The maximum difference based on the wavelet analysis is 1056 mm (70.4%). Which is over one meter while the spacing between the two sensors is only 1.5 meter. Both sensors receiving signals, these signals can be converted to waveforms. With a wavelet analysis these waveforms are decomposed and finally compared with each other. The shift in the two different decomposed waves is equal to the TDOA between the two sensors. The inaccuracy of this method compared to the other methods could be explained by the effect of this decomposition of the waveforms. Only 3 out of 30 source locations determined by the wavelet analysis show a higher accuracy then 6.2%. While the other two methods do not have lower accuracies then 6.2%.

Second verification experiment

According to Sun and Qian (2011) the frequency range of impact lie between 10 – 50 kHz and the wave speed of impact lie between 5078 – 5155 m/s. Table 10 present the wave speed which are calculated for each impact. The wave speeds for 15 different impacts and three different sensors are shown. Also, the average and range of the wave speed are given.

Table 10 – Wave speed for different types of sensors

	VS600-Z2	R6I-AST	R3I-AST
Impact	Wave speed [m/s]	Wave speed [m/s]	Wave speed [m/s]
1	1753	1406	4650
2	4665	5537	4691
3	1860	659	4610
4	2597	1317	3932
5	2597	2826	3820
6	4440	4845	4313
7	1298		4610
8	2220		4775
9	1251		4456
10	1251		4178
11	1251		4178
12	1638	2188	3932
13	1186		3714
14	3441	2339	3714
15	3622	1995	4456
Average	2338	2568	4269
Range	1186 - 4665	659 - 5537	3714 - 4775

As can be seen from this table the R6I-AST sensors did not capture every impact which results in no calculation for the wave speed. The values in wave speed for the different type of sensors are lower compared to the range according to Sun and Qian (2011). The difference could be explained by the fact of different specimens. In their research the specimen was a single wire, while in this research study the specimen is a complete cable which exists of multiple wires. In the complete cable more factors could influence the propagation of the waves, like oil and voids, and thus influence the wave speed of the AE signals. Sun and Qian (2011) concluded that the wave speed decreases when the frequency increases. This phenomenon is clearly visible in the results of this experiment, see table 10. The R3I-AST sensors show the closest wave speed compared to Sun and Quan (2011). This type of sensor shows the highest sensitivity in the frequency range of 10 – 50 kHz. The average wave speed is used for the calculation of the location of the source. In table 11 the results for the R3I-AST sensors are shown.

Table 11 – Source location results for R3I-AST sensors

	(1) First threshold passing		(2) P-wave analysis		(3) Wavelet analysis		
Impact	Δ [mm]	Δ [%]	Δ [mm]	Δ [%]	Δ [mm]	Δ [%]	
1	7.9	0.9%	10.5	1.0%	5032.2	493.4%	Location B
2	20.2	2.0%	25.3	2.5%	2738.1	268.4%	
3	20.6	2.0%	30.0	2.9%	865.8	84.9%	
4	20.6	2.0%	1.6	0.2%	49.6	4.9%	
5	12.0	1.2%	22.1	2.2%	538.0	52.7%	
6	12.0	1.2%	12.0	1.2%	265.6	26.0%	
7	44.6	4.4%	7.0	0.7%	293.8	28.8%	
8	44.6	4.4%	12.1	1.2%	455.2	44.6%	
9	20.6	2.0%	23.1	2.3%	625.9	61.4%	
10	20.6	2.0%	19.7	1.9%	378.3	37.1%	
11	13.4	1.3%	15.2	1.5%	1749.9	171.6%	Location C
12	85.9	8.4%	97.2	9.5%	221.8	21.7%	
13	5.2	0.5%	7.8	0.8%	31.7	3.1%	
14	19.7	1.9%	5.5	0.5%	17.0	1.7%	
15	3.1	0.3%	3.8	0.4%	26.5	2.6%	
16	13.4	1.3%	21.3	2.1%	134.1	13.2%	
17	13.4	1.3%	13.4	1.3%	20.4	2.0%	
18	30.0	2.9%	55.2	5.4%	28.3	2.8%	
19	3.1	0.3%	14.2	1.4%	61.2	6.0%	
20	30.0	2.9%	38.7	3.8%	23.8	2.3%	
21	30.0	2.9%	28.3	2.8%	356.3	34.9%	
22	30.0	2.9%	26.5	2.6%	52.5	5.2%	
23	30.0	2.9%	20.4	2.0%	114.2	11.2%	
24	30.0	2.9%	30.9	3.0%	30.0	2.9%	
25	3.1	0.3%	4.0	0.4%	31.7	3.1%	
26	3.1	0.3%	4.9	0.5%	115.1	11.3%	
27	30.0	2.9%	18.7	1.8%	29.9	2.9%	
28	30.0	2.9%	30.9	3.0%	30.0	2.9%	
29	30.0	2.9%	39.6	3.9%	80.4	7.9%	
30	30.0	2.9%	29.1	2.9%	28.3	2.8%	

The differences for TDOA (1) and (2) are respectively 85.9 mm (8.4%) and 97.2 mm (9.5%) and the average difference is respectively 22.90 mm (2.3%) and 22.30 mm (2.2%). TDOA (3) decreases the accuracy of the linear source location technique. The highest difference is 5032.2 mm (493.4%), which is over 5 meters. The explanation between the difference for the different TDOA is the same as explained in paragraph 3.3.2 First verification experiment.

In table 12 the results are shown for the R6I-AST sensors. In total four hits during experiment 2 are not recorded by the sensors. These points are deleted due missing information.

Table 12 – Source location results for R6I-AST sensors

	(1) First threshold passing		(2) P-wave analysis		(3) Wavelet analysis		
Impact	Δ [mm]	Δ [%]	Δ [mm]	Δ [%]	Δ [mm]	Δ [%]	
1	57.9	5.6%	55.9	5.4%	180.0	17.4%	Location B
2	57.9	5.6%	55.3	5.4%	281.3	27.2%	
3	103.7	10.0%	111.4	10.8%	429.7	41.5%	
4	43.2	4.2%	44.2	4.3%	541.0	52.3%	
5	84.1	8.1%	67.7	6.5%	113.2	10.9%	
6	201.7	19.5%	219.7	21.2%	64.4	6.2%	
7	33.4	3.2%	35.0	3.4%	541.0	52.3%	
8	103.7	10.0%	103.7	10.0%	377.2	36.4%	
9	84.1	8.1%	84.1	8.1%	559.0	54.0%	
10	162.5	15.7%	162.5	15.7%	162.5	15.7%	
11	22.9	2.2%	20.3	2.0%	642.7	62.1%	Location C
12	2.2	0.2%	2.2	0.2%	299.3	28.9%	
13	93.3	9.0%	27.3	2.6%	45.8	4.4%	
14	163.4	15.8%	167.8	16.2%	60.5	5.9%	
15	51.9	5.0%	49.3	4.8%	51.0	4.9%	
16	130.3	12.6%	147.7	14.3%	211.6	20.4%	
17	47.5	4.6%	47.5	4.6%	97.9	9.5%	
18	80.6	7.8%	75.4	7.3%	49.2	4.8%	
19	47.5	4.6%	46.6	4.5%	138.7	13.4%	
20	18.7	1.8%	20.5	2.0%	101.3	9.8%	
21	85.0	8.2%	52.0	5.0%	433.8	41.9%	
22	47.5	4.6%	53.6	5.2%	130.0	12.6%	
23	47.5	4.6%	47.5	4.6%	36.7	3.6%	
24	146.9	14.2%	146.9	14.2%	45.8	4.4%	
25	18.7	1.8%	18.7	1.8%	37.6	3.6%	
26	47.5	4.6%	70.9	6.9%	47.5	4.6%	

The accuracy of the linear source location with the R6I-AST sensors decrease compared to the R3I-AST sensors. The maximum differences for three different TDOA are: 201.7 mm (19.5%), and 219.7 mm (21.2%) and 642.7 mm (62.1%). The average difference for TDOA (1) and (2) are respectively 76.3 mm (7.37%) and 74.4 mm (7.2%). The differences for TDOA (1) and TDOA (2) are almost doubled compared to the results of the R3I-AST sensors. The explanation between the difference for the different TDOA is the same as explained in paragraph 3.3.2 First verification experiment. The only difference is that the

wavelet analysis method increases the accuracy of the linear source location technique for the R6I-AST sensors compared to the R3I-AST sensors. For the R3I-AST sensors the maximum difference was 5032.2 mm (493.4%), but for the R6I-AST sensors the maximum difference is 642.7 mm (62.1%). The origin of this increase in accuracy can be explained by the difference in shape of the waveforms. In figure 40 for both the R6I-AST and the R3I-AST the waveforms for both sensors are shown. The waveform for the R6I-AST sensors show a more similar form compared to the waveform of the R3I-AST sensors. During the decomposition of the waveform the waveform for the R6I-AST sensor keep the same shape which results in less time differences which finally results in a higher accuracy of the linear source location technique.

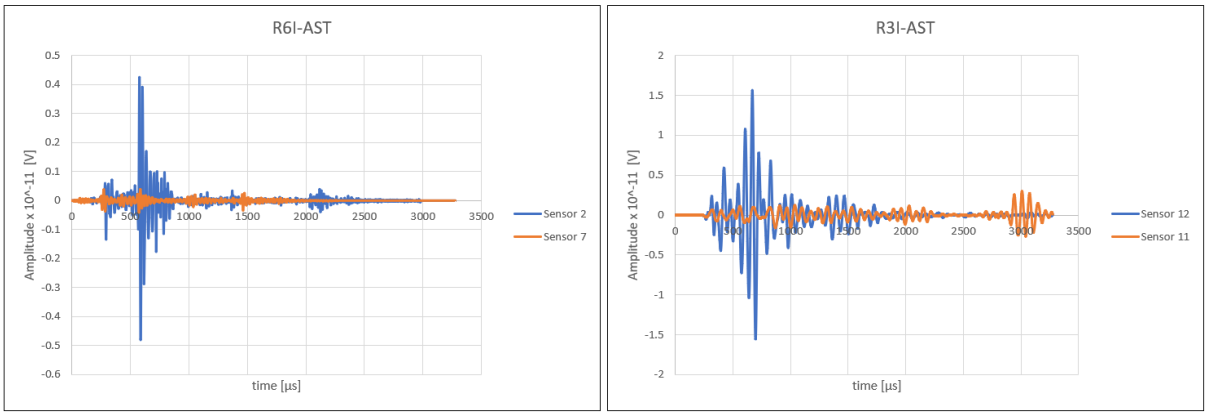

Figure 40 – Two waveform for both the R6I-AST and R3I-AST sensors

In table 13 the results are shown for the VS600-Z2 sensors. The accuracy of the VS600-Z2 sensors are even lower compared to the R6I-AST sensors. The difference for TDOA (1) is maximum 239.3 mm (22.8%), for TDOA (2) 332.9 mm (31.7%) and for TDOA (3) 2787.9 mm (265.5%). The explanation between the difference for the different TDOA is the same as explained in paragraph 3.3.2 First verification experiment.

Table 13 – Source location results for VS600-Z2 sensors

	(1) First threshold passing		(2) P-wave analysis		(3) Wavelet analysis		
Impact	Δ [mm]	Δ [%]	Δ [mm]	Δ [%]	Δ [mm]	Δ [%]	
1	35.4	3.4%	35.4	3.4%	148.1	14.1%	Location B
2	30.9	3.0%	30.9	3.0%	517.1	49.2%	
3	75.5	7.2%	140.1	13.3%	529.7	50.5%	
4	22.0	2.1%	22.0	2.1%	549.8	52.4%	
5	57.7	5.5%	126.4	12.0%	504.0	48.0%	
6	93.4	8.9%	57.8	5.5%	264.6	25.2%	
7	13.6	1.3%	13.6	1.3%	290.3	27.7%	
8	93.4	8.9%	118.6	11.3%	157.0	15.0%	
9	93.4	8.9%	55.5	5.3%	265.0	25.2%	
10	93.4	8.9%	121.9	11.6%	2787.9	265.5%	
11	21.5	2.1%	6.7	0.6%	1514.1	144.2%	Location C
12	116.7	11.1%	205.3	19.6%	623.4	59.4%	
13	65.4	6.2%	65.4	6.2%	492.2	46.9%	
14	25.6	2.4%	25.6	2.4%	1542.8	146.9%	
15	57.2	5.4%	30.5	2.9%	154.5	14.7%	

16	57.2	5.4%	104.0	9.9%	1705.1	162.4%	
17	24.0	2.3%	32.7	3.1%	437.6	41.7%	
18	25.6	2.4%	70.7	6.7%	468.0	44.6%	
19	25.6	2.4%	3.9	0.4%	441.9	42.1%	
20	25.6	2.4%	45.5	4.3%	1682.6	160.2%	
21	239.3	22.8%	195.9	18.7%	232.7	22.2%	
22	206.2	19.6%	295.6	28.2%	122.4	11.7%	
23	140.0	13.3%	145.2	13.8%	1107.8	105.5%	
24	173.1	16.5%	173.1	16.5%	14.7	1.4%	
25	206.2	19.6%	332.9	31.7%	426.3	40.6%	
26	106.8	10.2%	145.0	13.8%	349.9	33.3%	
27	7.5	0.7%	80.4	7.7%	76.4	7.3%	
28	73.7	7.0%	101.5	9.7%	1318.8	125.6%	
29	125.0	11.9%	231.8	22.1%	151.9	14.5%	
30	206.2	19.6%	231.4	22.0%	500.9	47.7%	

Table 14 present a summary of the accuracies obtained by the three different TDOA methods and for the three different types of sensors. From the tested sensors, the R3I-AST sensors show for method 1 and 2 the lowest average and standard deviation of the difference in location of the source. It was expected that the R3I-AST sensors show the highest accuracy, followed by the R6I-AST sensors and that the VS600-Z2 sensors show the lowest accuracy. Because, the R3I-AST show the highest sensitivity over the frequency range related to impacts followed by the R6I-AST sensors and the VS600-Z2 sensors.

The highest accuracy is obtained by TDOA method (1) and (2). These two methods are closely related to each other. These two methods are not dependent on the waveform shape or other parameters, but only on the first threshold passing and P-wave hit to the sensor.

Table 14 – Summary of accuracies

Sensor type	Variable	R3I-AST	R6I-AST	VS600-Z2
		Δ [%]	Δ [%]	Δ [%]
Method 1 – First threshold passing	Average	2.3%	7.4%	8.1%
	Standard deviation	1.6%	4.9%	6.3%
	Maximal difference	8.4%	19.5%	22.8%
Method 2 – P-wave analysis	Average	2.2%	7.2%	10.3%
	Standard deviation	1.9%	5.3%	8.3%
	Maximal difference	9.5%	21.2%	31.7%
Method 3 – Wavelet analysis	Average	47.1%	21.1%	61.5%
	Standard deviation	101.6%	18.8%	61.1%
	Maximal difference	493.4%	62.1%	265.5%

3.4 Conclusions

Based on this chapter the following conclusions can be drawn:

- Based on the source location accuracies the choice for different types of sensors is mainly depending on the frequency of the AE signals generated by different sources. Wire break leads to AE signals with higher frequencies compared to given impacts which leads to lower frequencies.
- Wire breaks inside a stay cable in the experiment performed in this research can be detected with the help of AE sensors.
- For the experiment performed in this research the R6I-AST type of sensors (100% wire break detection) are more suitable to detect wire breaks inside a cable compared to the R3I-AST type of sensors (45% wire break detection).
- The minimal values of different parameters in the table below can be used to discriminate signals due to wire breaks by other sources in the experiment performed in this research. Due to the cut off limit in the transducers output signal of the sensors the values for amplitude, energy, signal strength and absolute energy are conservative. All these parameters are related to the transducers output signal.

Table 15 – Minimal values for wire breaks

Parameter	R6I-AST
	Minimal values
Amplitude [dB]	97
Energy [pVs]	15107
Signal Strength [pVs]	9.4E+07
Absolute Energy [aJ]	3.5E+08
Duration [µs]	41428
Rise time [µs]	1315
Counts [-]	778

- The sensors attached on the cable perform much better compared to the sensors attached on the socket due to a lot of background noise by the components of the test bench.
- The location of three local wire breaks can be determined with accuracies of 6.4, 7.2 and 14.4%. This location is determined with a linear source location technique which used a TDOA obtained from the first threshold passing (method 1).
- For the verification experiments performed in this research the R3I-AST type of sensors are the most suitable type of sensors to locate the given impact to the cable.
- The best methods to obtain the TDOA for the linear source location technique are method 1 (first threshold passing) and method 2 (P-wave analysis). The first method shows lower averages but less spread and the second method show higher averages but more spread compared to each other.
- The wave speed of the AE signals decreases when the frequency of the AE signals increases.

4 ANALYTICAL MODEL OF STAY CABLES

The analytical model made in this research is further used for analysis in this chapter. In paragraph 4.1 an introduction in cables is given followed by the different type of (stay) cables (4.1.1). Paragraph 4.2 contains multiple analysis with the help of the analytical model. Analysis like, the validation of the model (4.2.1), the stress distributions during the experiment (4.2.2), the influence of Poisson's ratio to the stress distribution (4.2.3) and finally the influence of the double helical structure (4.2.4) are given. The chapter ends with the conclusions of this chapter (4.3).

4.1 INTRODUCTION

Nowadays steel cables are frequently used in the application of bridges, offshore industry, ships, power lines and even in elevators. Findings of a copper cable in the ruins of Nemeveh show that the cable was already used as a structural element about 700 B.C. (Costello, 1997). Iron chains and hemp ropes were the commonly used elements for lifting purposes before the steel cable was invented. A huge disadvantage of the iron chain was the linear arrangement of the chains. A linear arrangement has the consequence if one chain fail (the weakest link) the whole system will fail. The high strength of the iron chain was a big advantage. Hemp ropes had parallel arrangements which made the rope more reliable but these ropes could only be used in dry pits. By combining the advantages of both the iron chain and the hemp rope, the mining engineer Albert from Claustal invented around 1830 the steel cable (Verreet, 2001). The cable industry keeps improving and nowadays a widely amount of different cables are available for structural purposes in different fields of Civil Engineering.

4.1.1 Stay Cables

According to CEB FIB (2005) the last 10 to 20 years cable stayed structures have increased in popularity. A lot of long span stay cables bridge are built for both railway and highway traffic. The longest cable stayed bridge nowadays has a main span over 1000 meter. The stay cables of bridges are key load bearing elements. The cables carrying the load of the main girders of the bridge and transfer the load into the pylons and the anchorage of the back stays (Tang, 2000). The exact amount of load bearing function is different for every bridge. All the design parameters can influence the amount of load bearing function of the cables. According to Lin & Yoda (2017) corrosion and the anchorage system were the biggest problems that occurred in early cable stayed bridges. Nowadays, this are still problems that occur in cable stayed bridges. Next to these problems, fatigue problems in orthotropic steel decks are nowadays an important problem as well. To get more familiar with the state of the bridge and to ensure enough safety in bridge the need for good working SHM methods is growing. Nowadays, steel cables can be manufactured in different ways. In table 6 an overview is given of the different types of steel cables which can be used as stay cables.

Table 16 – Overview of different types of steel cables (Feyrer, 2007)

Round ropes	spiral rope	open spiral rope (strand with round wires) half-locked coil rope full-locked coil rope
	stranded rope (round strands)	single-layer rope (one layer of strands) multi-strand rope (several layers of strands)
	shaped strand rope	triangular strand rope oval strand rope
	cable-laid rope	round stranded ropes around a core
Braided rope		round strands interlaced or plaited together
Flat rope		four strand ropes stitched or riveted together

Spiral ropes can be divided into open spiral cable, half-locked coil cable and the full-locked coil cable. In old cable stayed bridge the half-locked or full-locked coil cable are frequently used as stay cables. The placing of the cables, the economic benefits because ducts and grouting are unnecessary and the corrosion resistance of these type of cable were huge advantages compared to other types of cables. According to Walther, Houriet, Isler, Moïa and Klein (1999) these types of cables can be used for bridges with saddle points and the use of a saddle point has a great advantage instead of using intermediate anchorage. Saddle points result in continuously stay cables, because the stay cable is not anchored at the pylon but is running over the pylon. The stranded ropes can be divided into the single-layer rope and the multi-layer rope. The difference between those two is the number of strand layers. This type of cable exists of parallel wires which are laid down in a protective grouting to prevent corrosion problems. To achieve a higher strength, the strands exist of a centre wire with wires wrapped around. These wires form a single helix around the centre wire of the strand. These strands are also wrapped around a core element and form a double helix. The mechanical properties of such a cable depend greatly on the number of wires and configuration but also on the steel grade that is used (Lin & Yoda, 2017). A typical cable build-up for a multilayer strand rope is shown in figure 23.

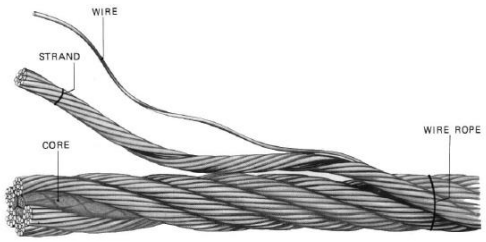

Figure 41 – Typical cable build-up (De Jong, 2015)

These types of cables can have different types of strand configurations. The strand configuration is on cross-sectional level. Nowadays, a lot of different stand configurations are available. These configurations are invented for different purposes. In figure 41 the most used strand configurations according to Ivanov (2018) are presented.

Figure 42 – Mostly used strand configurations (Ivanov, 2018)

The lay direction, lay length and the lay angle are specific parameters for stranded ropes. The lay direction of stranded ropes can be categorized in four different options. These options can be noted with the symbols Z,S,z and s. The direction of the strands can be noted by Z (right) or S (left) and the direction of the wires can be z (right) or s (left). In figure 25 an overview is given of the different lay directions. When the strands are in the opposite direction of the outer wires of a strand the lay direction is also called an ordinary lay rope. If the strands are in the same direction of the outer wires of a strand the lay direction is usually called a lang lay rope, formerly a Lang's lay or Albert's Lay. The Albert's lay is named after the inventor of the cable in the 1830 (Feyrer, 2007).

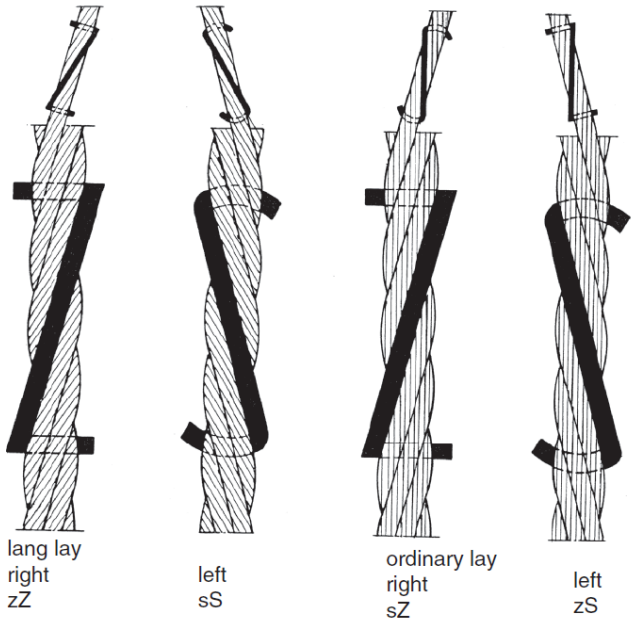

Figure 43 – Lay direction configurations (Feyrer, 2007)

The lay length and the lay angle are directly related to each other. The length of the strand along the axis of the strand in which a strand makes a 360 degrees turn is called the lay length (h_w). In figure 26 the relation between the lay angle and the lay length is shown (Feyrer, 2007).

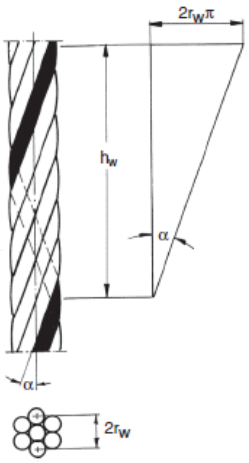

Figure 44 – Relation between lay angle and lay length (Feyrer, 2007)

4.2 Analytical Model

In the following paragraphs three different case studies are performed with the help of the analytical model which is described in paragraph 2.4. In paragraph 4.2.1 a validation of the model is made based on the experiment performed in the work of Ivanov (2018). In paragraph 4.2.2 the stress distribution in the wire for different moments during the experiment are visualized. In paragraph 4.2.3 the influence of Poisson's ratio to the stress distribution in the wires is investigated and in paragraph 4.2.4 the influence of the double helix structure (lay angle β) is investigated. Lay angle α is the lay angle of the wires related to the core wire of a specific strand and lay angle β is the lay angle of the strands related to the core of the cable.

4.2.1 Validation of the model

Validation is an important aspect for the reliability of the analytical model. De Jong (2015) and Ivanov (2018) did both research into the reduction in capacity of cables subjected to forced bending. They performed proof load experiments on straight cables to investigate the capacity of the cables to pure tension. After the capacity of the straight cables was obtained the bended cables were tested and the reduction in capacity could be determined. Ivanov (2018) made an analytical model to predict the capacity of the cables. The model that is made is based on the sample principle as described in paragraph 2.4 in this research study. In table 17 the results of the proof load experiments and the predictions according to the analytical model are presented.

Table 17 – Results of proof load experiments (Ivanov, 2018 & De Jong, 2015)

Rope Configurations	MBL	Analytical Model	Experiment	Accuracy
20-6x25F-IWRC	279 kN	336 kN	325 kN	+3.4 %
20-6x36WS-IWRC	279 kN	330 kN	322 kN	+2.5 %
77-6x36WS-IWRC	4850 kN	5210 kN	5138 kN	+1.4 %

From the table it can be noticed that the MBL according to the manufacturer of the cables is quite conservative. The MBL is not a good indicator of the actual capacity of the cable. Comparison between the capacity of the analytical model and the experiments show an overestimation of the capacity by the analytical model. The overestimation of the capacity is maximum 3.4%. The overall estimation of the capacity of the cables by the analytical model show a good correlation. The analytical model can predict the capacity of a cable in quite a good way. According to Ivanov (2018) the overestimation of the capacity can be explained due to the effect of additional coupling stresses due to torsion, bending and shear which are not included in the model.

4.2.2 Stress distributions during experiment

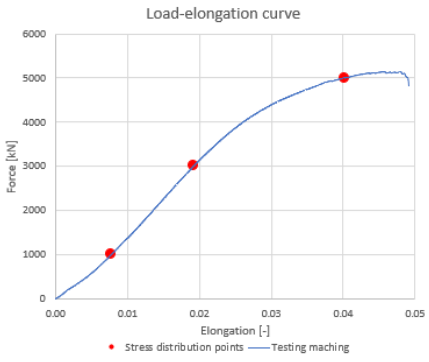

Figure 45 – Wire stress distributions points

In figure 45 the load-elongation curve of the full-scale experiment is given. The stress distribution in the wires of the cable are visualized by the help of the analytical model for the three red dots in the figure. The wire stress distributions are shown in figure 46.

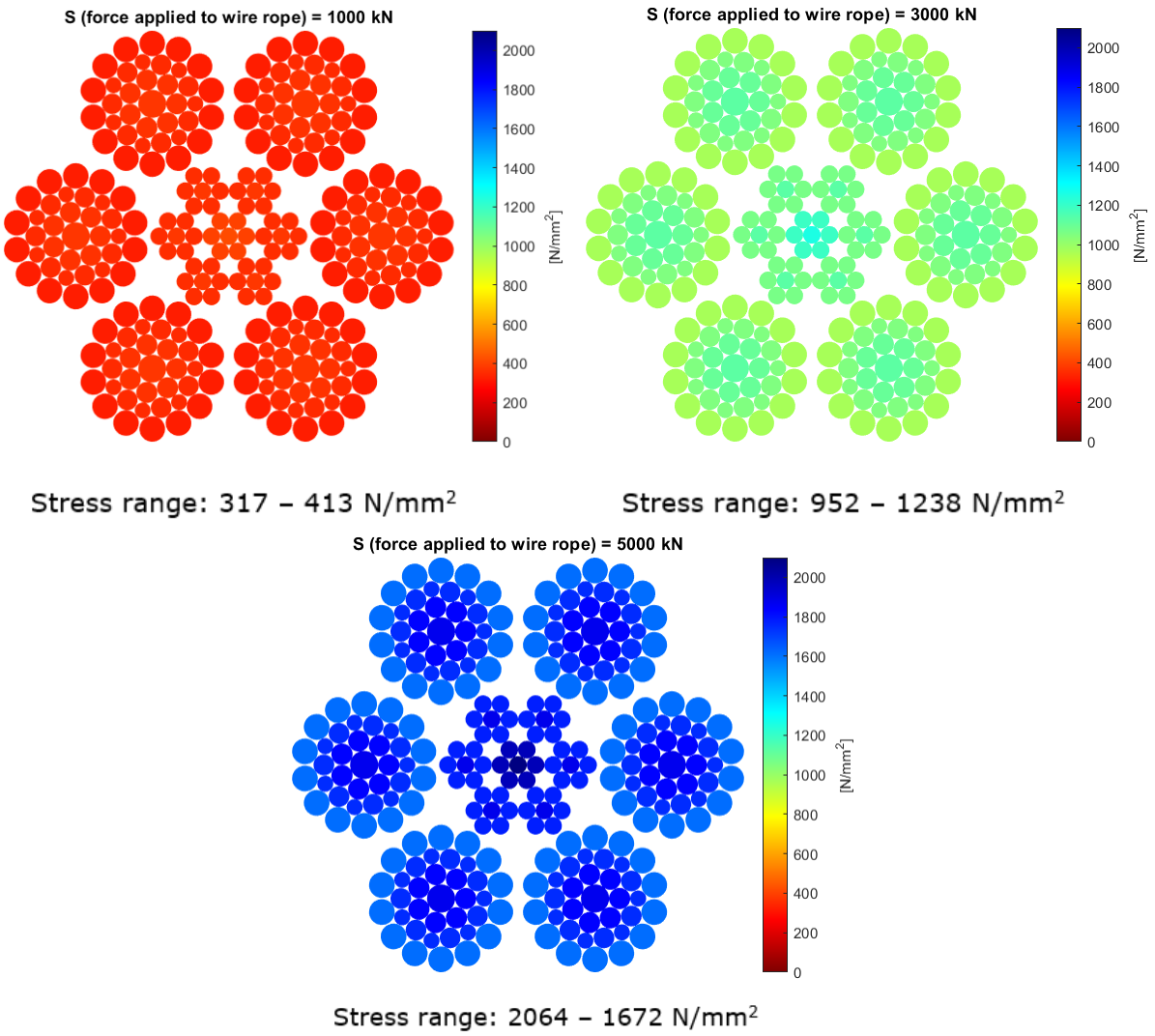

Figure 46 – Wire stress distributions for three different loads

As can be seen in the figure the range of wire stresses for an applied load of 1000 kN is from 317 – 413 N/mm^2. The core wire experiences a stress of 317 N/mm^2 while the outer strands experience a stress of 413 N/mm^2. The different between the stress levels is not really high. The stress differences in the wires for the applied load of 3000 kN is higher. The difference between the core wire in the outer strand compared to the outer wire in the outer strand is also clearly visible. It can be concluded that the core wires of a strand experiences higher stresses compared to the outer wires of the strands. The higher stresses in the core wire can be explained by the effective area of the wires. The core wire is a straight wire and all the other wires have a single or even a double helical structure. The effective area of the wires increases which result in a decrease of stress in these wires. The differences in stress levels become higher when a higher load is applied to the cable. The core wire of the cable experiences the highest stress, it is expected under ideal circumstances that the core of the cable fails at first.

4.2.3 Influence of Poisson's ratio

As described in paragraph 2.4 the influence of Poisson's ratio is almost neglectable. Feyrer (2007) concluded that the stresses in the inner wires are lower and the stresses in the outer wires are higher when Poisson's ratio is neglected. The influence of Poisson's ratio for the analytical model that is described in paragraph 2.4 is shown in figure 47. In this figure the normalized stresses with and without Poisson's ratio are shown for the different wire numbers. In figure 48 the influence of neglecting Poisson's ratio to the stress change is visualized.

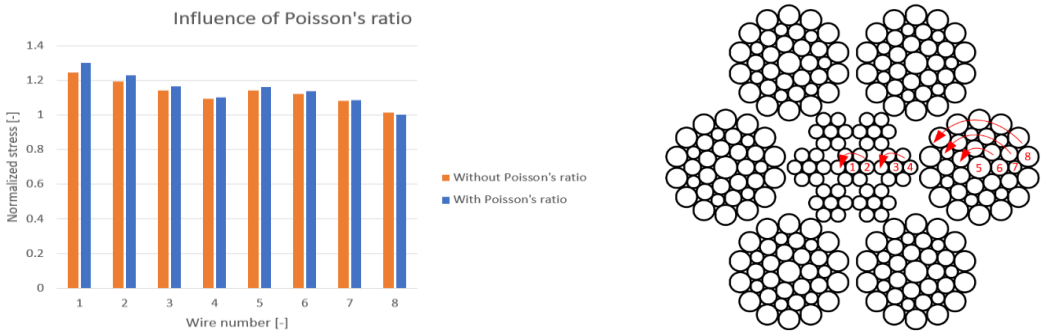

Figure 47 – Influence of Poisson's ratio and wire number explanation

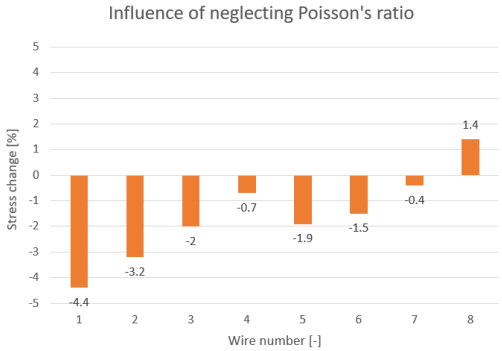

Figure 48 – Influence of neglecting Poisson's ratio

The influence of Poisson's ratio is different for the different wire numbers. For all the inner wires (wire number 1 – 7) the stresses in the wires decrease when Poisson's ratio is neglected. The stress in the outer wire increases when Poisson's ratio is neglected. This supported the conclusion Feyrer (2007) made. Equation 2 (in paragraph 2.4.1) is the basic of the model, as can be seen from this equation an important parameter for determining the stresses in the wires is the lay angle α. According to the figure above and the important role of the lay angle α it is expected that the lay angle α influences the effect of Poisson's ratio. In figure 49 the influence of the lay angle α to the stress distribution for the inner and outer wire are presented. Next to this the influence of Poisson's ratio is visualized. Between the stresses in the inner and outer wires a nonlinear relation is visible. An increase in lay angle α changes the effective area of the outer wires. Due to this change the effective area of the strand changes. The additional load will be resisted less by the outer wires and more by the inner wires. Which resulted in this nonlinear behaviour. The difference in stresses increases when the lay angle α increases. In case of the analytical model in this research the maximum stress change according to figure 48 for respectively the inner and outer wires is -4.4% and +1.4% and according to figure 49 -3.7% and 0.0% when neglecting Poisson's ratio. The influence of Poisson's ratio is depending on the lay angle α but also on lay angle β and also on the magnitude of both lay angles.

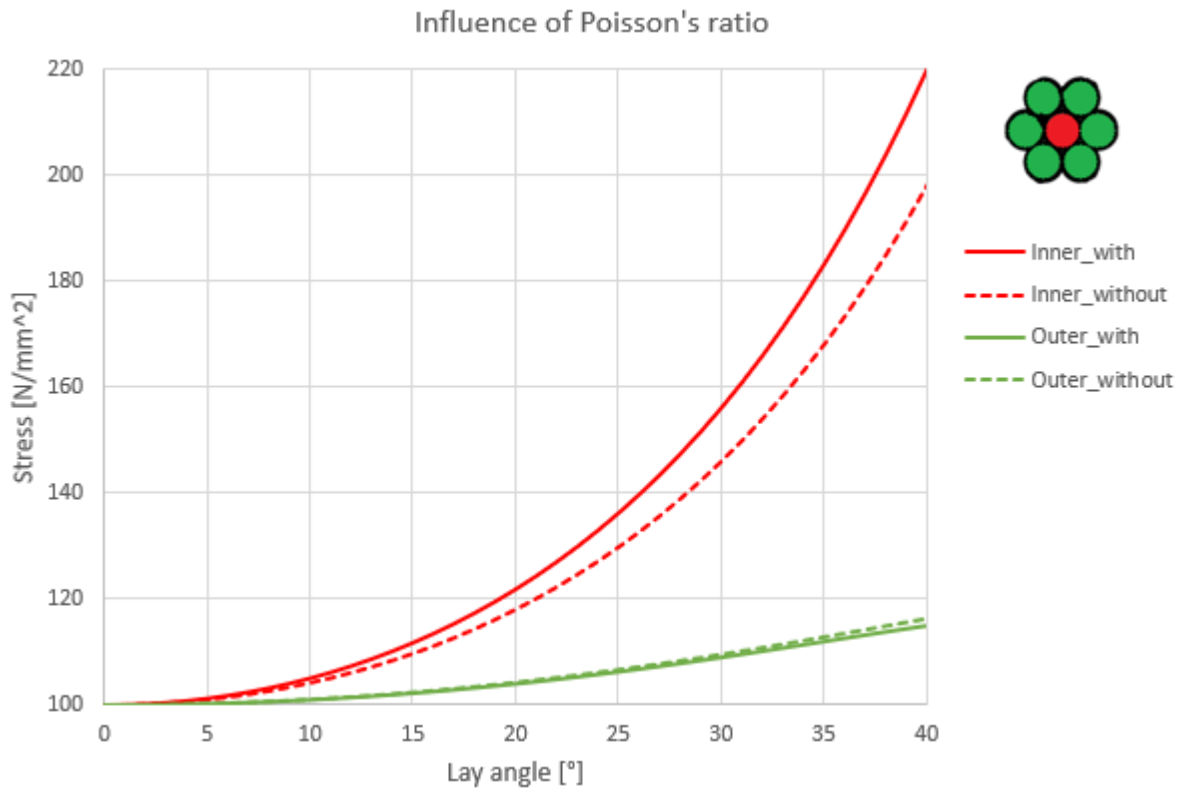

Figure 49 – Effect of lay angle (α) and Poisson's ratio to stresses

4.2.4 Influence of Double Helix (Lay Angle β)

The lay angle β in the cable configuration was equal to 16.7°. The wire stress distribution with three different lay angles β is analysed. With these wire stress distributions, the influence of lay angle β is investigated. In total three different cases are investigated with β values equal to: 8°, 16.7° and 25°. In figure 50 the wire stress distributions are shown for the different β values with an applied load of 4000 kN. In figure 51 the values for different wire number are compared.

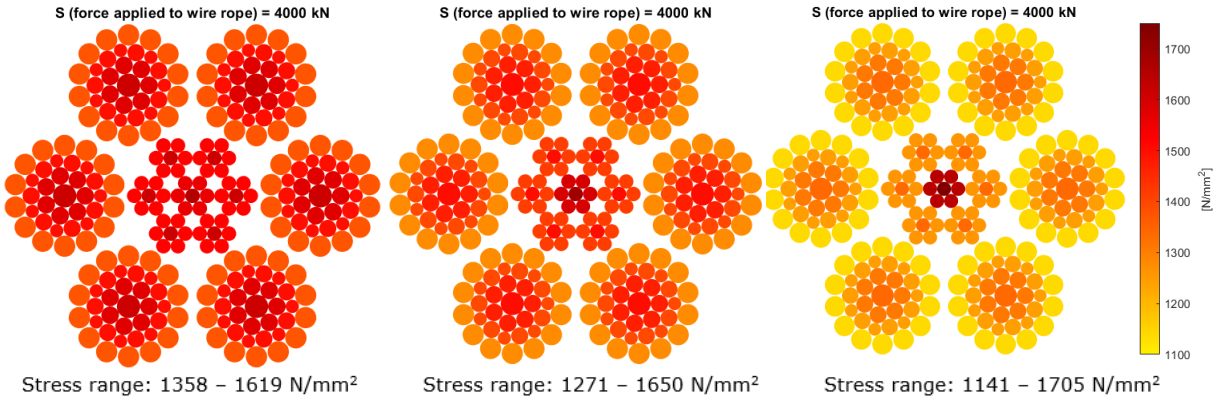

Figure 50 – Stress distribution for β values of 8° (l), 16.7° (m), 25° (r)

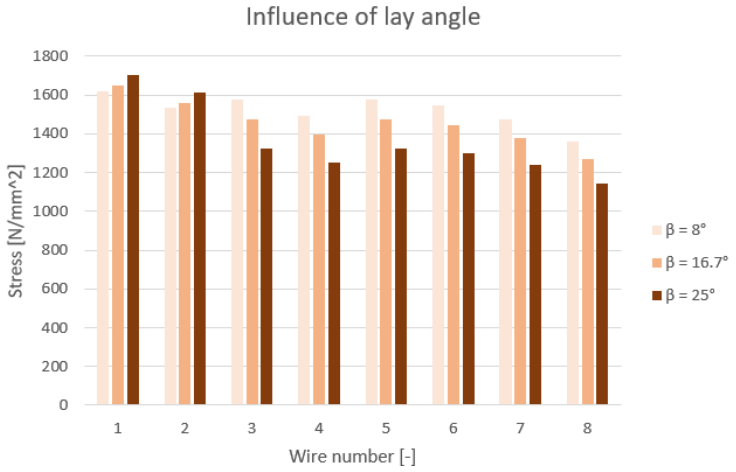

Figure 51 – Stress distribution at 4000 kN load

The stress distribution in the individual wires is quite depending on the lay angle β. For an increase in lay angle β, the stress in the core wire increase while the stresses in the outer wires decreases. Also, the difference in stress level (maximum and minimum value) become greater if the lay angle β increases, see figure 50. The increase of lay angle β results in less contribution of the outer wires to the axial stiffness of the cable. This can also be explained by the effect of the decrease of the effective area of the outer wires. Which resulted in less resistance of the outer wires and more resistance of the inner wires to the applied load to the cable.

4.3 Conclusions

Based on this chapter the following conclusions can be drawn:

- Under the assumptions that all wires will start bearing stresses at the same time and that all the stresses in the wires are in the elastic region the analytical model in this research study can predict the capacity in a quite accurate way. For three different cables the accuracy is +3.4, +2.5 and +1.4%. The analytical model overestimates the capacity a little bit. Which is the effect of not including additional coupling stresses due to torsion, bending and shear in this model.
- For this specific type of cable, the influence of neglecting Poisson's ratio leads to a maximum decrease in stress level in the core wire by 4.4% and an increase in stress level of 1.4% in the outer wires.
- The influence of Poisson's ratio is depending on the (magnitude of the) lay angles α and β. The influence of Poisson's ratio increases when the lay angle α increases.
- For this specific type of cable, the lay angle β influence the stress distribution in the wires of the cable. An increase in lay angle β results in a wider stress range over the different wire layers. The stress level in the first two wire layers increases while the stress level in the other layers decreases by an increase in lay angle β.

5 LOAD BEARING DISTRIBUTION

Chapter 5 is divided into five paragraphs. In paragraph 5.1 an introduction to the Galecopperbrug is given with the design guidance of RWS (5.1.1) and the current design of the Galecopperbrug (5.1.2). The SCIA model that is used in this research is described in paragraph 5.2. With the help of this SCIA model a case study is performed to investigate the load bearing distribution of the different structural elements (5.3). In paragraph 5.4 the application for the Galecopperbrug is given. This paragraph is divided into the costs of a SHM method with AE (5.4.1), the fire protection cover of the stay cables of the Galecopperbrug (5.4.2) and finally fracture based versus status driven AE (5.4.3). This chapter is finalized by the conclusion (5.5).

5.1 INTRODUCTION

As described earlier, the Galecopperbrug is a cable stayed bridge which carries the A12 highway and local roads over the ARK. The Galecopperbrug is located in the southern part of Utrecht in the Netherlands. The bridge is a part of the ring of Utrecht and it plays an important role in the highway infrastructure of the Netherlands. In fact, the Galecopperbrug exist of two cable stayed bridges, one bridge for every direction of traffic. The south bridge for the direction The Hague – Arnhem and the north bridge for the direction Arnhem – The Hague. Each bridge exists at this moment in time of three lanes and a hard shoulder for the main carriageway (A12 highway) and for the parallel carriageway (local roads) two lanes and an on and off slip road. The total length of the bridge is approximately 320 m. The bridge exists of three spans with the following length: 70 m – 180 m – 70 m. The total width of the bridge is two times 34.6 m, which is 69.2 m. The bridges cross the ARK at a skewed angle of 52 degrees. The south bridge is constructed in 1971 and the north bridge is constructed in 1976 under the design of engineers from Rijkswaterstaat (ARUP, 2009). In figure 52 an overview and in figure 53 a schematic overview of the Galecopperbrug is presented.

Figure 52 – Overview of the Galecopperbrug (Beeldbank RWS, 2004)

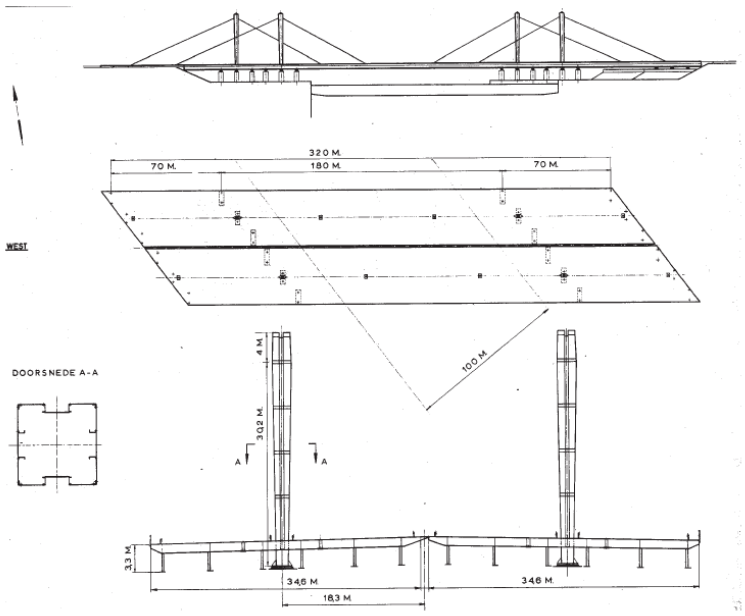

Figure 53 – Schematic overview of the Galecopperbrug (ARUP, 2009)

5.1.1 RBK Rijkswaterstaat

The bridges in and over the main roads and waterways are controlled by Rijkswaterstaat. To give guidelines and additional requirements for existing bridges, Rijkswaterstaat developed in 2013 the "Richtlijnen Beoordeling Kunstwerken (RKB)" document. This document is an addition to the set of standards NEN-EN 1990 till NEN-EN1999, NEN8700, NEN8701 and the ROK. A bridge must be safe during the remaining life span of the bridge. If there are any reasons for doubts related to this safety, the bridge has to be assessed by research and (re)calculations. The main aim of the RBK is to assess the structural safety and the usability of the bridges. A bridge needs to be assessed if the structural safety can be questioned. Some examples of these situations are given below (Rijkwaterstaat, 2013):

- Damage to the bridge with structural consequences. For example, corrosion of reinforcement steel, deformation due to damage or collision or by crack initiation.
- An increase of the characteristic traffic load or dead load with respect to the designed characteristic traffic load or dead load.
- Missing of relevant design information.
- New developments or insights in the behaviour of the structure of parts of the structure.
- A conservation inspection which led to an advice.

The purpose of this remaining paragraph is explaining the procedure for assessment of (current) bridges according to the RKB. The assessment levels, the usability and durability and the assessment and measures will be described further.

Assessment levels

The minimum reliability index used for existing bridges by Rijkswaterstaat is equal to $\beta = 4.3$. The bridge has to fulfil the requirements according the "new" safety level. In table 1 the different safety levels and the corresponding safety factors according to Rijkswaterstaat (2013) are given:

Table 18 – Safety levels (Rijkswaterstaat, 2013)

Structural safety level	β	Formula 6.10 a	Formula 6.10 b	Traffic	Wind	Other variable
		$\gamma G_{j,sup}$	$\varepsilon\gamma_{Gj,sup}$	$\gamma_{Q,1}$	$\gamma_{Q,1}$	$\gamma_{Q,1}$
New	4.3	1.40	1.25	1.50	1.65	1.65
Renovation	3.6	1.30	1.15	1.30	1.60	1.50
Usage	3.3	1.25	1.15	1.25	1.50	1.30
Reject	3.1	1.25	1.10	1.25	1.50	1.30

The above table applies to bridges whose environmental permit was granted before 2012 "Bouwbesluit". Bridges, whose environmental permit was granted after 2012 "Bouwbesluit", have to fulfil the new construction level. Safety levels "new" and "renovation" apply to new parts or parts which will be renovated in the near future. Parts of the bridge or complete bridges which are in use, have to fulfil the usage level requirements. The rejection levels are used for parts of the bridges or complete bridges which will not be renovated, are not in used but will be demolished.

According to Rijkswaterstaat (2013) the reference life span and the remaining life span for the new construction level are both 100 years, for the renovation and usage level both 30 years and for the reject level the reference life span is 15 years and the remining life span is only 1 year. The use level is quite different compared to the new construction level. The use level is only allowed under some additional requirements (Rijkswaterstaat, 2013):

- No reduction in resistance of the bridge compared to the design criteria.
- No structural damage or damage which influences the resistance of the bridge.
- No further increase in load during the remaining life span compared to the original design.
- If extra attention is paid to the management and maintenance of the bridge which results in an appropriate level of structural safety.

According to Rijkswaterstaat (2013) the safety level "renovation" has to be equal to the safety level "new". If this results in a disproportionate increase of work, an exception can be made and the minimum values of the renovation levels may be applied. This has to be approved by the contract manager and the management committee of the RBK. Only parts which are physically renovated can be included. Parts of the bridge or the complete bridge which are not renovated have to fulfil the level "use".

Usability and durability

In the Eurocode some material related requirements are given for the usability and durability of bridges. For existing bridges it is not always possible to fulfil these requirements. For instance, due to the influence of the current status of the structures which influences the usability and durability during the remaining life span. For the structural safety and usability assessment the bridges do not have to fulfil the material related requirements for the usability and durability requirements. However, the condition and the expected decrease of this during the remaining life span has to be taken into account. If the decrease of the condition is critical for the structural safety, further measures have to be taken. The usability related to the deformation of bridges must be considered (Rijkswaterstaat, 2013). For example, the vertical clearance of bridges.

Assessment and measures

In the structural safety assessment, the limit states are verified by unity checks. The requirement for structural safety is fulfilled, if the value is smaller or equal to 1,0. Only the ultimate limit state and fatigue are assed in the recalculations. Instead of judging the serviceability limit state and durability the expected decrease of the condition of the bridge has to be taken into account for the remaining life span. The assessment of the bridge will be performed by the following scheme:

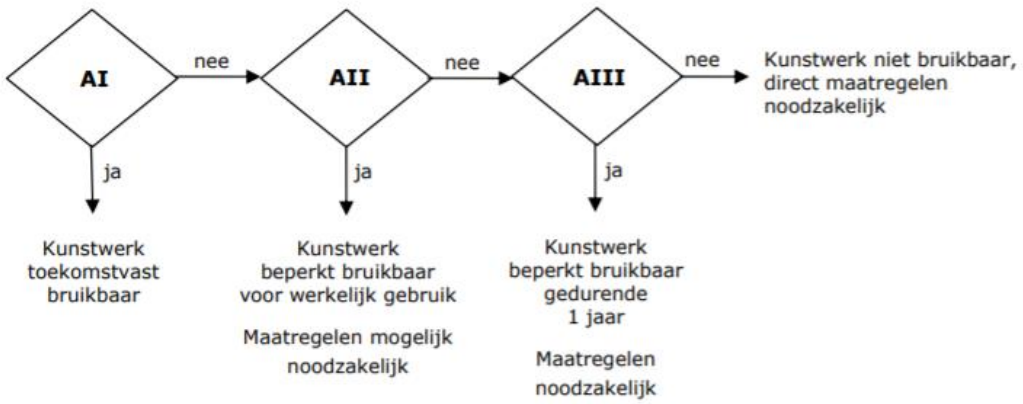

Figure 54 – Assessment scheme for the structural safety (Rijkswaterstaat, 2013)

Situation AI assesses the bridge for the future-proof use. If the bridge fulfils this, the bridge can be used by traffic without limitations. Situation AII assess the bridge for actual use. If the bridge fulfils the requirement for situation AII, further research has to be carried out to see if more management measures are necessary to deal with situation AII during the remaining life span. Situation AIII asses the direct disapproval of the bridge. If the bridge fulfils the situation AIII requirements, but not the requirements for the AII situation, necessary implementing measures must be taken within one year. If the engineering structure not fulfil the requirement for the AIII situation, direct necessary measures have to be taken to guarantee the structural safety (Rijkswaterstaat, 2013), for instance demolishing. According to Rijkswaterstaat (2013) the following measures to guarantee the structural safety for the remaining life span can be taken: Lower the traffic load, lower the dead load, reinforce, replace or prevent the decrease of the condition.

5.1.2 Design of the Galecopperbrug

The aim of this paragraph is gaining more knowledge about the design of the Galecopperbrug and some specific parameters are given. This knowledge is necessary to understand the structural behaviour of the Galecopperbrug and to model this. A central suspension plane is used to suspend the bridge. The suspension plane exists of two stays for the main span and two back stays which are anchored to the abutments (see figure 53). A central suspension plane is formed if the cables are from a top view in a straight line which each other. The cables of the Galecopperbrug exist of two times six full-locked coil cables with each 76 mm in diameter. The total cross-sectional area of one cable is 3955 mm^2. The cables are arranged in a modified mono design, which is a design where only one cable is used, but instead of using only one cable there are two cables used. The suspended span of 180 m is divided into three segments with the following lengths: 54.75 m – 70.50 m – 54.75 m measures between the pylons. The stay cables are continuously running from the bridge deck through the pylon to the bridge deck on the other side of the pylon. A saddle is used at the top of the pylon which results in equal forces on both sides

in the cables. Or in other words the cable behaves like a back stay on one side and like a main stay at the other side of the pylon. The forces in the back and main stay are equal to each other, if friction force is neglected. The cables are connected to main girders 3 and 4 of the bridge (ARUP, 2009). The pylons rise in total 34.2 m above the supported bearing. The pylons have a squared shaped steel box cross section with changing dimension over the height. At the bottom the dimension of the steel box is approximately 1500 mm and at the top the dimension of the steel box is approximately 2500 mm (ARUP, 2009).

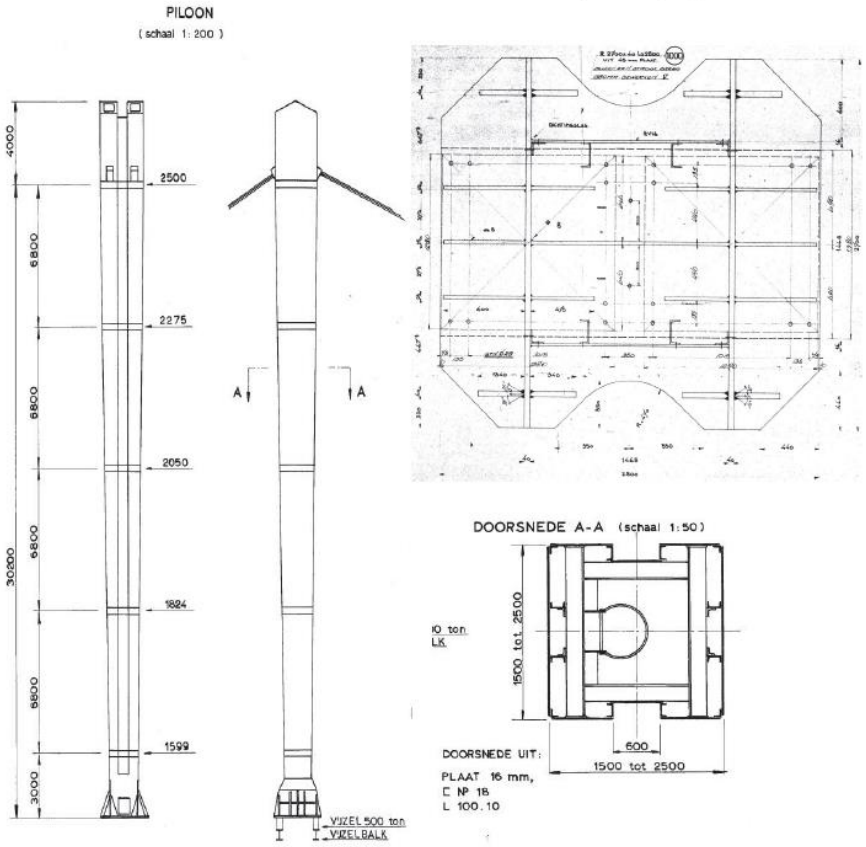

Figure 55 – Bridge pylons of the Galecopperbrug (ARUP, 2009)

The bridge deck of both bridges exists of an orthotropic steel deck. The orthotropic steel deck structure of the Galecopperbrug consists of a grid of cross girders and longitudinal stiffeners. At every 3.33-meter cross girders with a height of 800 mm are placed. The orthotropic steel deck is supported by main girders and they are supported by an abutment and a pier on both sides. The north and south bridges are both supported on six steel I profile beams with a total height of 3300 mm. This height is inclusive the partition and the deck plate. The width and thickness of the bottom flange of the main girders are depending on the location. The width can vary between 600, 800 or 1000 mm and the thickness varying between 20 and 66 mm. The web of the main girders varies between 10 – 12 mm and where the connection is made with the cables the web thickness is 40 mm. In figure 8 it can be seen that the distances between the main girders is 6.1 m, 6.8 m, 4.9 m, 6.8 m and 6.1 m. At both sides of the end main girders (girder 1 and 6) there are two cantilevers. Next to girder 1 the cantilever is 2.425 m and next to girder 6 the cantilever is 1.5 m. On the web of the main girder vertical stiffeners and up to three horizontal stiffeners are used at the connection with the cross girders to prevent the main girders form plate buckling (ARUP, 2009).

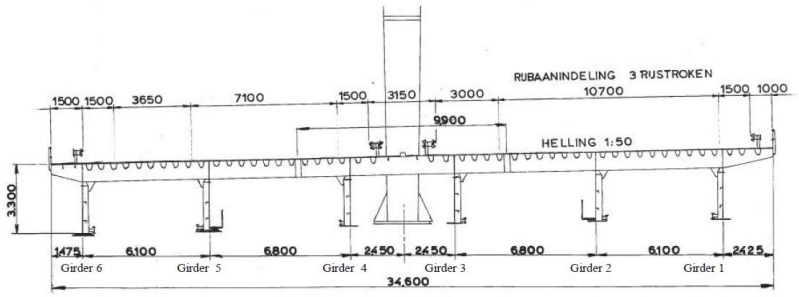

Figure 56 – Cross section orthotropic steel deck of the Galecopperbrug (ARUP, 2009).

At the places where the connection is made between the cables and the main girders the total height of the cross beams is 2600 mm. These crossbeams connect all the main girders and transfer the load to the central suspension plane. The deck plate acts for both the cross and the main girder as a top flange (ARUP, 2009). The deck plate has a thickness 10 mm and 12 mm on top of the main girders. Originally the bridge deck was covered with a 50 mm thick layer of asphalt pavement. Due to fatigue problems, cracks were discovered in the deck plate of the bridge. To reinforce this bridge deck the asphalt layer was removed, the cracks were repaired and a new High Strength Concrete (HSC) layer is placed (ARUP, 2012). The deck plate is stiffened by troughs and these troughs have different dimensions. The depth of these troughs are 250, 275 or 325 mm and with a maximum width of 300 mm. The thickness of the throughs is either 6 mm or 8 mm, this is depending on the location of the troughs. For both the south and north bridge the same geometry is used, the only difference is the type of troughs that is used. For the north bridge angular shaped troughs are used. Troughs next to the main girders are 325 mm deep and 8 mm thick and the other ones are 275 mm deep. The troughs of the south bridge are rounded troughs which are 250 mm deep. At the south bridges the troughs are not closed at the position of the suspension plane, but strips of 160 mm are used (ARUP, 2009).

During the recent renovation of the Galecopperbridge in 2014, for every bridge two prestress girders are placed on the sides of the bridge. This renovation was part of the strengthening and widening project of the Galecopperbrug (ARUP, 2012). These prestress girders are placed to carry the additional load in the near future. In the near future the Galecopperbrug will be widened and this results in more self-weight and traffic load.

5.2 SCIA Model

The design of the Galecopperbrug, which is described in paragraph 5.1.2, can be used to model the bridge in SCIA. The SCIA model used in this research is made by RWS. The aim of this SCIA model is to investigate the structural behaviour of the different components of the Galecopperbrug. By use of this model more structural insight of the Galecopperbrug is obtained.

Three main load bearing elements of the Galecopperbrug can be distinguished. The main girders, the prestress girders and the stay cables are the main load bearing elements of the Galecopperbrug. These elements ensure the load distribution from the bridge to the supports of the bridge. In this model the following elements are modelled:

- Orthotropic steel deck (existing of the deck plate, throughs and cross beams);
- Main girders;
- Prestress girders;
- Stay cables.

The pylons of the bridge are not modelled. Because the stay cables are continuously running through the saddle point in the pylon only this saddle point is modelled. All the elements except the stay cables are modelled in 2D plate elements. The stay cables are modelled in 1D beam elements. In figure 57 an overview of the model is given and in figure 58 a side view of the model is shown.

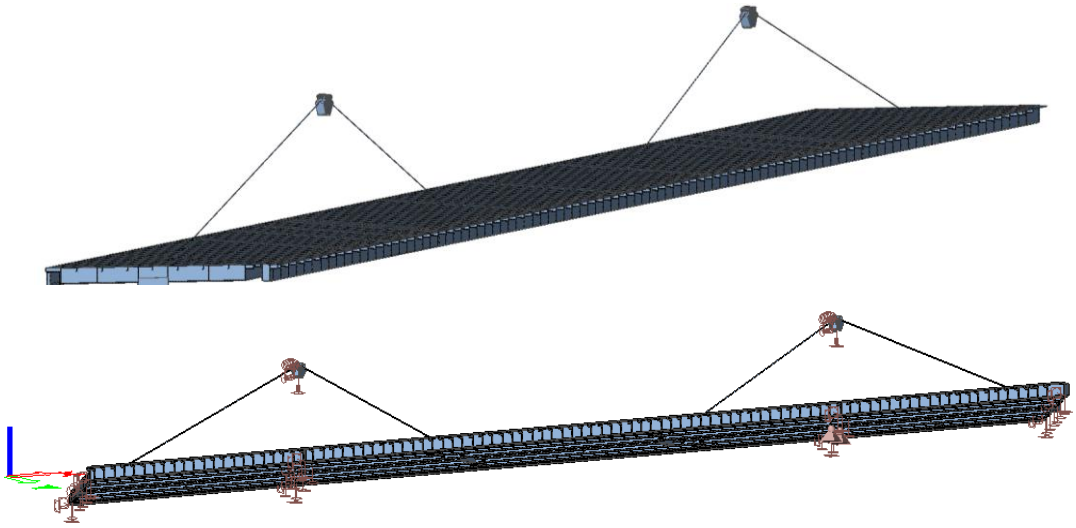

Figure 57 – Overview of the SCIA model (RWS)

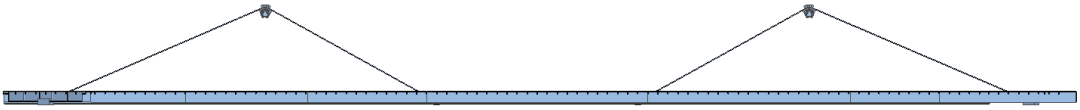

Figure 58 – Side view of the SCIA model (RWS)

In figure 57 the supports in the model of the Galecopperbrug are shown. Both prestressed girders are supported at four different locations. These four locations are at the abutments of the bridge and at the location where the pylons are located. Four main girders of the Galecopperbrug are supported on the same four locations as the prestressed girders. The stay cables are supported at the location of the pylon. For further investigations a linear calculation is performed.

5.3 Case Study

In this case study the load bearing distribution of the Galecopperbrug is investigated by three different load scenarios. The following load scenarios are analysed:

1) Self-weight of the bridge elements;
2) Distributed load of 5 kN/m^2 (simplification for the permanent load from the HSC layer);
3) The self-weight and the distributed load combined.

In figure 59 the distributions of the loads over the three main load bearing elements is visualized. These three different load scenarios are used to investigate the load bearing role of the stay cables of the bridge based on the static loading of the Galecopperbrug. The static loading of the Galecopperbrug is based on the self-weight of the bridge elements and the distributed load, which is equal to the HSC layer on top of the bridge deck.

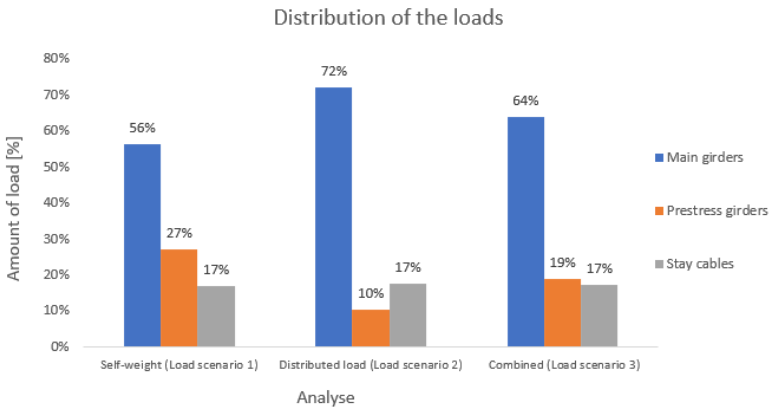

Figure 59 – Distributions of the three main load bearing elements

As can be seen from figure 59, the main girder of the Galecopperbrug carry most of the load in all the different load scenarios. In case of the self-weight of the bridge the main girders carry 56% of the applied load, while the prestress girders carry 27% and the stay cables carry the remaining 17% of the applied load. The distributed load of 5 kN/m^2 is mostly carried by the main girders. The stay cables carry the same amount compared to load scenario 1. The prestress girders carry 17% less loads compared to load scenario 1. The prestress girders are connected to the sides of the bridge but these prestress girders are attached recently. This is the reason why prestressed girder are carrying less distributed load compared to load scenario 1. Load scenario 3 is a mix of load scenario 1 and 2. The stay cables of the Galecopperbrug are carrying in all the load scenarios the same amount of load, which makes the stay cables an important load bearing element. In table 3 a summary of the utilisation factors of the main girders and the prestress girders is given. All the utilisation factors are satisfying the criterium (≤1,0). Without the stay cables the main girders and the prestress girders has to carry the load of the stay cables (17%). The utilisation factors for main girder 3 and the outer prestress girder are respectively 0.92 and 0.93. The extra load of 17%, cannot be taken by the main girders and the prestress girders. Which will result in a collapse of the bridge if the stay cables of the bridge cannot carry the load. This increases the need for a SHM method which can monitor the stay cables of the Galecopperbrug.

Table 19 – Summary of utilisation factors (ARUP, 2013)

Scenario under Consideration	New Inner Prestressed Girder	Main Girder 1	Main Girder 2	Main Girder 3	Main Girder 4	Main Girder 5	Main Girder 6	New Outer Prestressed Girder
Prior to the Renovation Works	Not Applicable	**1.60**	**1.72**	**1.45**	**1.39**	**1.31**	**1.28**	Not Applicable
After Prestressing New Girders	0.81	0.87	0.82	0.89	0.85	0.77	0.71	0.68
After Jacking the Bridge	0.84	0.78	0.72	0.83	0.76	0.68	0.65	0.65
After Completion of Renovation	0.90	0.92	0.87	0.88	0.79	0.76	0.72	0.69
After Widening the Bridge	0.87	0.88	0.87	0.92	0.83	0.74	0.86	0.93

The replacement of the stay cables of the Galecopperbrug needs to be done with the minimal amount of traffic hindrance. The Galecopperbrug plays an important role in the Dutch infrastructure network, complete closure of the bridge will cause high amount of traffic hindrance and problems. It is not possible to close the complete bridge during the replacement of the stay cables. Instead of a complete closure of the bridge another option will be the closure of multiple lanes. This ensures that the bridge can still be used but with less capacity. According to ARUP (2013) the bridge can resist 95% of the full Eurocode live load if two stay cables of the Galecopperbrug are destressed. With traffic restrictions the live load can be decreased which makes it possible to replace the stay cables of the Galecopperbrug. An additional supporting structure to restrain the pylon when the cables are destressed is necessary. In figure 60 and 61 the global displacements of the Galecopperbrug are shown for two different cases. The two following situations are investigated: situation of the complete bridge (figure 60) and the other situation where one bundle of stay cable is destressed (figure 61). These two global displacements are based on the SCIA model which is described in paragraph 5.2.

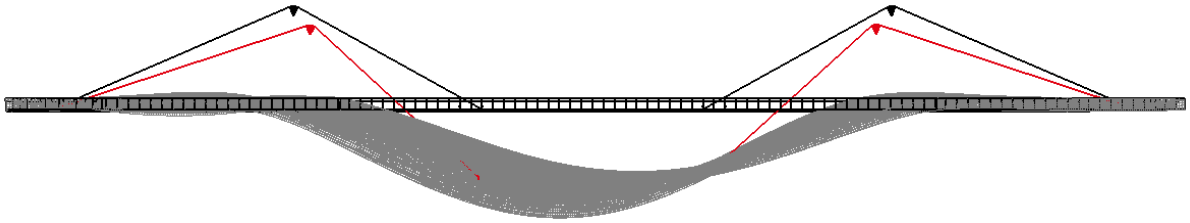

Figure 60 – Bridge displacement situation 1

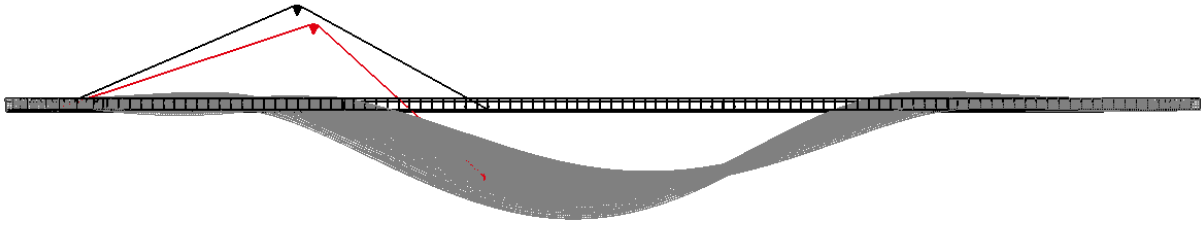

Figure 61 – Bridge displacement situation 2

In both situations the self-weight of the bridge elements is investigated. In the first situation the maximum displacement of the bridge is 769 mm. In the second situation, where one bundle of stay cable is destressed, the maximum displacement of the bridge is 847 mm. Based on this SCIA model the additional displacement due to the self-weight of the bridge will be 78 mm. Next to the self-weight of the bridge, the additional distributed load due to the HSC layer and the live loads are also acting on the bridge during replacement of the stay cables. To increase the reliability of this investigation more analysis need to be completed. More analysis with respect to the stresses and displacements for both the static and live loads need to be carried out. Next to destressing of one bundle of stay cables, other options are possible for the replacement of the stay cable. For example, the progressive installation of new stay cables parallel to the current stay cables of the Galecopperbrug, or installing a temporary support for the bridge underneath the main span of the Galecopperbrug. These two options need further investigation to ensure enough safety for both the users and construction people. According to ARUP (2013) there are options to replace the stay cables of the Galecopperbrug without a complete closure of the Galecopperbrug.

5.4 Application for the Galecopperbrug

5.4.1 Costs

The costs for SHM systems are of great importance for the responsible party. In case of a SHM system with AE for the stay cables of a cable stayed bridge (Galecopperbrug) in the Netherlands, Rijkswaterstaat is the responsible party. The approximate costs are obtained by speaking with the manufacturer of AE equipment MISTRAS. The total costs for a SHM method for the Galecopperbrug can be divided into four important categories:

- Equipment costs;
- Installation costs;
- Maintenance costs;
- Analyse costs.

Equipment costs

Equipment costs are highly related to the total amount of sensors needed. For example, if the sensors will be placed on the anchorage zones of the cable and with a spacing of 50 meters (Rule of thumb according to MISTRAS) the total amount of sensors will be (in case of the Galecopperbrug): two anchorage points and a total length of stay cables of approximately 150 meters. In total for one bundle of stay cables there are 4 sensors needed. The north bridge of the Galecopperbrug contains 2 bundles of stay cables for each pylon. This gives a total amount of sensors equal to 16. The costs are in the range of €2500 – €3000 per sensor, this is including the waterproof sensors, cables, data acquisition system and lightning protection. The total amount of sensors is highly depending on the purposes of the SHM system. The total amount of sensors can be reduced if the AE behaviour is well known.

Installation costs

Installation costs are highly depending on the type of bridge. On average the installation costs are 70% of the equipment costs. This could be more if the accessibility of the stay cables is hard or due to the traffic hindrance on the bridge. The installation costs are also depending on the number of sensors that are used, but if more sensors are needed the costs are relatively decreasing.

Maintenance costs

The sensors and the system need maintenance. Maintenance costs exist of calibration of the sensors and the system and the basis maintenance of the sensors and the system given by the manufacturer.

Analysing costs

Analysing of the costs are highly depending on the purpose of the SHM method. The intensity of the monitoring requires labour costs. For example, the data can be analysed every day with a report every week or the data can be analysed every week with a weekly or monthly report. A daily analysis and reporting, costs approximately more than €4000 a month. A weekly analysis and a monthly report is approximate €1000 a month. These costs are depending on the bridge, the first months takes more analysing time. Due to the fact that the methods of discrimination of the noise signals need to be investigated. If the bridge is monitored over a long period of time, these costs will reduce due to the fact of automation.

The total costs for a SHM method are highly depending on multiple reasons, but the biggest reason is knowledge. If more knowledge is available on the behaviour of the cable (attenuation and individual wire breaks) the plan for sensors could be optimized. This will lead automatically to a reduction in costs.

5.4.2 Fire protection cover

For implementing AE as a SHM method for the Galecopperbrug the practical issues related to the accessibility of the cable need to be investigated. The fire protection covers for the stay cables of the Galecopperbrug are shown in figure 62. The fire protection cover for the stay cable is placed to a height of 18 meters above the bridge deck. These covers are placed to fulfil the requirements according to fire. The decision to protect only the first 33 meters of the stay cables at the canal side and 42 meters of the stay cables at the abutments side are made based on a fire which can occur with a truck which is transporting flammable gasses/liquids (DeBoer, 2015).

Figure 62 – Fire protection cover for the stay cables

The fire protection covers are placed around the bundle of stays cables. Which makes it almost impossible to placed AE sensors on the stay cables at the position where the fire protection cover is placed. Drummond et al. (2006) concluded that the signals are not significantly attenuating over distances of 30 meters. The longest fire protecting cover is 42 meters, this is more than the 30 meters Drummond et al. (2006) recommended. According to MISTRAS a rule of thumb for the spacing of sensors on the stay cables is once every 50 meters, according to the attenuation behaviour. Based on this research individual wire breaks show AE signals with amplitudes equal to the maximum allowable amplitude of the sensors. AE signals due to individual wire breaks show high (absolute) energy, signal strength and relative long durations of the AE signals. In the performed experiments the maximum distance between the sensors was relatively small, namely maximum 2.4 meters. Due to the relatively small distance between the sensors the behaviour of the AE signals over distances of 42 meters is hard to predict. More research is necessary to understand the behaviour of the AE signals over longer distances.

5.4.3 Fracture based versus status driven AE

Fracture based AE is the main aim of the experiments performed in this research. The focus of fracture-based AE is wire break detection in a stay cable. Wire break detection is an important issue in monitoring of stay cables, but next to this (due to the environmental conditions) the cable is corroding. Corrosion of cables results in a gradually increase of brittleness of the material and a decrease of cross-sectional area. Damage due to corrosion is hard to diagnose by visual inspection due to the (fire resistant) covering of the stay cables. But, also due to corrosion in unreachable places. This results in a huge requirement

for the developing of status driven AE instead of fracture-based AE. Status driven AE is focussing on the current status of the stay cables, which included the level of corrosion and the remaining fatigue life. Xin et al. (2018) propose a status driven AE monitoring method for stay cables to identify the status and the remaining fatigue life by combining wavelet scalograms and transfer learning (TL) convolutional neural networks (CNNs). In figure 63 the proposed scheme for status driven AE is shown.

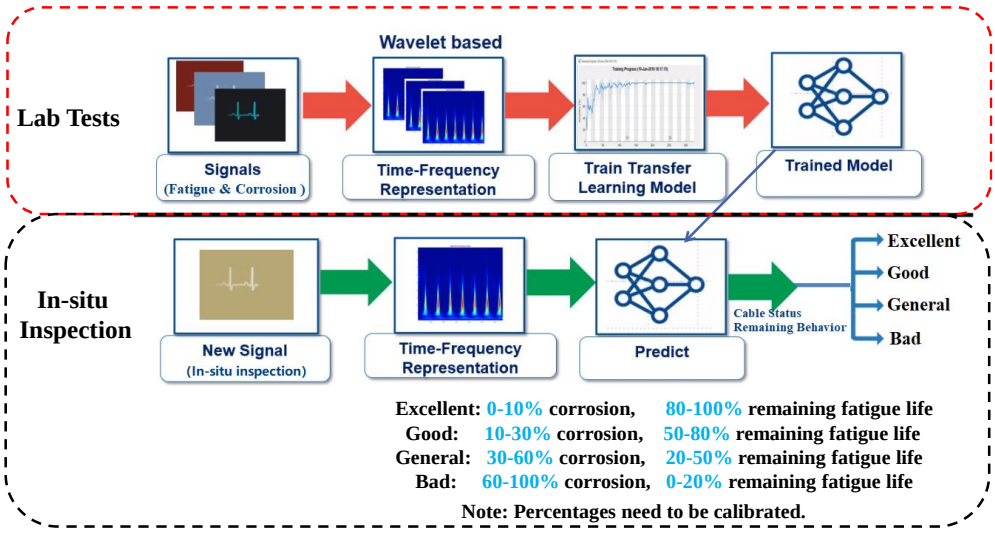

Figure 63 – Status driven AE monitoring (Xin et al., 2018)

Machining learning (ML), artificial intelligence (AI) and especially deep learning (DL) in computer vision are developing at a high speed (Mayrbaurl & Camo, 2004 and Krizhevsky, Sutskever, & Hinton, 2012). The aim is to let computers perform identification, which are labour intensive and time consuming, by learning from past experience. This is done by implementation of artificial neural networks (ANNs) with ML or DL methods. According to Tong, Gao, Sha, & Hu (2018), Gao & Mosalam (2018), Wang, Zhao, Li, Zhao, & Zhao (2018) and Kerh, Su, & Mosallam (2017) DL techniques could improve the classification accuracy in civil engineering applications. CNNs are developed around the 1990s, this was developed to solve problems related to handwritten-digits recognition. These types of models are increasing in depth to improve accuracy, robustness, performance and for adaptability in image classification. According to Xin, Diender, & Veljkovic (2018) the building of new CNNs requires a lot of effort and time, especially a CNN in hyper-parameters optimization. The search time for this optimization can cover weeks or even months. According to Xin et al. (2018) there is required a huge amount of data to configure and optimize this during the training process. A new ML technique is called TL. TL uses knowledge from source domains to target domains which could be related but still are different. The reuse of a model is the starting point for another model, in this case the big amount of data which is required for training deep CNN is combined. According to Xin et al. (2018) AE signals classification is promising due to the high performance in image classification of TL CNNs.

As shown in figure 61 fatigue tests are carried out on cables with different corrosion levels to obtain the remaining fatigue life and the AE signal characteristics. By the help of wavelet transformations, the AE signals are transformed from the time domain to the time-frequency domain to obtain data sets full of scalograms. To obtain the relationship between the cable status and the signal due to AE the CNN is implemented. A trained CNN model is constructed. For in situ inspection of bridges this trained CNN model can be used to

translate the signals obtained from in situ monitoring to useable information regarding to the status and the remaining fatigue life of the cable. Rijkswaterstaat can make decisions based on the reported status of this status driven AE monitoring.

A pilot study which consists of a binary AE signal classification based on the experiment performed during this research is achieved in the study of Xin et al. (2018), see figure 64. All the data of fracture and noise signals are collected during the test. Because a small amount of data is obtained from this experiment, TL CNNs based on GoogleNet are used for the noise and fracture classification of the signals. With the help of other AE signals this trained CNN was validated. This model was validated by other AE signals.

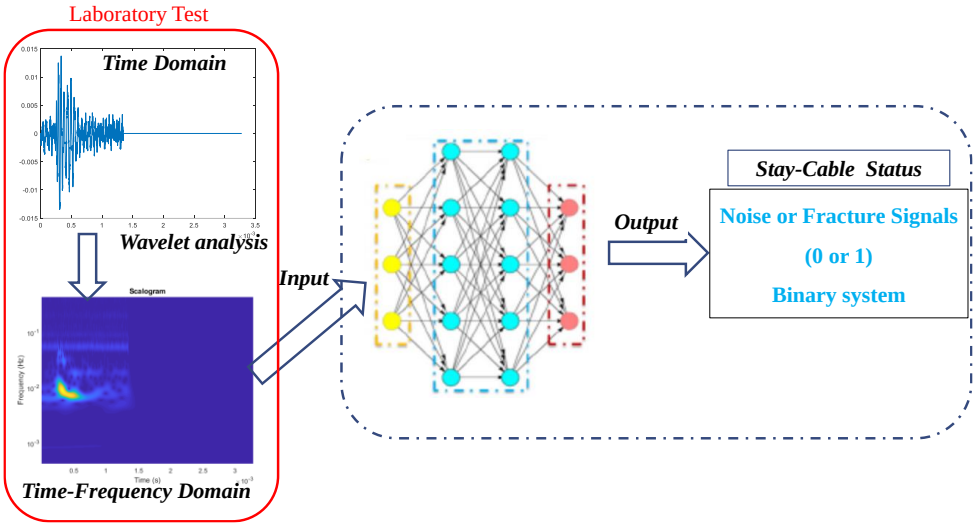

Figure 64 – Pilot binary AE signal classification

5.5 Conclusion

Based on this chapter the following conclusions can be drawn:

- Under the assumptions made in the SCIA model, the stay cables of the Galecopperbrug carry for two different load scenarios 17% of the total load.
- There is not enough capacity left in the main and prestress girders to carry the total load if the stay cables of the Galecopperbrug fail.
- The costs of AE as a SHM method for the Galecopperbrug is mainly depending on the amount of knowledge that is available. With more knowledge the best suitable sensors can be used, the best sensor layout can be made and less analysing time is required.
- According to the manufacturer of AE equipment, the fire protecting covers of stay cables of the Galecopperbrug give not a problem for the AE sensor. A rule of thumb for stay cables is a sensor spacing of 50 meters.
- Status driven AE as a monitoring technique by combining wavelet analysis and deep transfer learning could have a promising future.

6 SUMMARY OF CONCLUSIONS

This chapter contains the final conclusions and the summary of conclusions of this research. These conclusions are made based on the research that is carried out.

The main objective of this research study was to do research into the possibilities of AE as a SHM method for the stay cables of the Galecopperbrug. To give answer to the research questions the state of the art was investigated. Next to this, experiments were carried out, an analytical model was made and a SCIA model of the Galecopperbrug was used to investigate the structural behaviour of the Galecopperbrug. The main research question of this research study was: "Is the AE-system used in a fracture-based assessment suitable for structural health monitoring of the stay cables of the Galecopperbrug?". Using all the findings in this research, the conclusion regarding the main research question can be drawn: Wire breaks inside (stay) cables will generate elastic stress waves which can be captured and recorded by AE sensors. Based on an experiment where multiple wire breaks occur, it is shown that wire breaks can be identified with the help of the technique of AE. However, the identification of wire breaks is mainly depending on the correct choice of sensor type. In the experiments performed in this research the R6I-AST sensors identified 100% of the wire breaks, while the R3I-AST sensors identified only 45% of the wire breaks. Conservative minimal values are found for different parameters to identify the wire breaks. Wire breaks can be localized by the help of a linear source location technique. In the experiments, is it found that three wire breaks can be localized with an accuracy of 6.4, 7.2 and 14.4%. Using the TDOA method 1 (first threshold passing) in the other experiments performed, the average accuracy for the given impacts is found to be 2.3% and 7.4% for respectively the R3I-AST and R6I-AST sensors. The sensor type is depending on the source of AE signals. In the experiment performed in this research the R6I-AST sensors were more suitable for AE signal due to wire breaks while the R3I-AST sensors are more suitable for AE signal due to impacts. Based on the assumptions and the experiments performed in this research it can be concluded that AE can be used in a fracture-based assessment for SHM of the stay cables of the Galecopperbrug.

Next to this, more conclusions can be drawn regarding the remaining research questions:

- Wire breaks will affect the local load bearing resistance only by 1%. If multiple wire breaks occur within a distance of 2.5 times the lay length the load bearing resistance will decrease more. The load bearing resistance will decrease further until to many wires are broken within this range and the cable cannot redistribute the stresses anymore. This will result in a failure of the cable.
- The expected stress distribution in the wires of a stay cable can be predicted with the analytical model described in this research. These expected stresses can be justified if multiple strain gauges are attached to the cable to verify the stresses obtained from the analytical model.
- Sensors attached on the cable perform much better compared to sensors attached on the socket, due to a lot of background noise by the components of the test bench.
- The minimal values of different parameters can be used to discriminate signals due to wire breaks by other sources in the experiment performed in this research. Due to the cut off limit in the transducers output signal of the sensors the values for amplitude, energy, signal strength and absolute energy are conservative. All these

parameters are related to the transducers output signal. In the table below the different parameters with their minimal values related to AE signals due to wire breaks are given. These values are obtained by the R6I-AST sensors.

Table 20 – Minimal values for wire breaks

Parameter	R6I-AST
	Minimal values
Amplitude [dB]	97
Energy [pVs]	15107
Signal Strength [pVs]	9.4E+07
Absolute Energy [aJ]	3.5E+08
Duration [µs]	41428
Rise time [µs]	1315
Counts [-]	778

- Under the assumptions that all wires will start bearing stresses at the same time and that all the stresses in the wires are in the elastic region the analytical model in this research can predict the capacity in a quite accurate way. For three different cables the accuracy is +3.4, +2.5 and +1.4%. The analytical model overestimates the capacity a little bit. Which is the effect of not including additional coupling stresses due to torsion, bending and shear in this model.
- For this specific type of cable, the influence of neglecting Poisson's ratio leads to a maximum decrease in stress level in the core wire by 4.4% and an increase in stress level of 1.4% in the outer wires.
- The influence of Poisson's ratio is depending on the (magnitude of the) lay angles α and β. The influence of Poisson's ratio increases when the lay angle α increases.
- For this specific type of cable, the lay angle β influence the stress distribution in the wires of the cable. An increase in lay angle β results in a wider stress range over the different wire layers. The stress level in the first two wire layers increases while the stress level in the other layers decrease by an increasing lay angle β.
- Under the assumptions made in the SCIA model, the stay cables of the Galecopperbrug carry for two different load scenarios 17% of the total load.
- There is not enough capacity left in the main and prestress girders to carry the total load if the stay cables of the Galecopperbrug fail.
- The costs of AE as a SHM method for the Galecopperbrug is mainly depending on the amount of knowledge that is available. With more knowledge the best suitable sensors can be used, the best sensor layout can be made and the less amount of analysing is required.
- According to the manufacturer of AE equipment, the fire protecting covers of stay cables of the Galecopperbrug is not a problem for the AE technique. A rule of thumb for stay cables is a sensor spacing of 50 meters.
- Status driven AE as a monitoring technique by combining wavelet analysis and deep transfer learning could have a promising future.

7 RECOMMENDATIONS

The recommendations of this research are given in this chapter. These recommendations are made based on the research that is carried out.

Resulting from the research that is carried out, some recommendations are stated below:

- Wire breaks are identified with sensors which operate in a frequency range of 10 – 100 kHz. It is recommended to carry out more experiments with a slightly higher operating frequency range to improve the wire break identification.
- In this research, only a stranded cable with an IWRC is tested. In reality different type of cables are used for the stay cables of bridges. To improve the insight in AE behaviour for different types of cables more experiments with different cable types need to be carried out.
- The costs for AE as a SHM method for the stay cables of the Galecopperbrug can be reduced. If the knowledge regarding to the AE behaviour for a full-locked coil cable is improved, the costs for a SHM method for the Galecopperbrug can be reduced.
- The analytical model developed in this research assumes stresses in the elastic region and do not take into account the stresses in the plastic region. Also, the coupling stresses are neglected in this model, which results in a small overestimation of the capacity of cables. Incorporating of these two assumptions in the model, can improve the accuracy for the prediction of the capacity of the cables.

REFERENCES

ARUP. (2009). Galecopperbrug: Bridge Specific Design Basis. 9V3175-42-A2-DB-GALEDESB-001004.

ARUP. (2012). Galecopperbrug: Phase 3c Design Report. 9V3175-42-D3c-RP-GALE_DREP-097802.

ARUP. (2013). Galecopperbrug: Cable replacement studies. 9V3175-42-TR-RP-CABLE_RPL-100748.

Bakht, B., & Mufti, A. (2008). *Bridges: Analysis, Design, Structural Health Monitoring, and Rehabilitation.* New York: Springer.

Balageas, D., Fritzen, C. P., & Güemes, A. (2006). *Structural Health Monitoring.* London: ISTE Ltd.

Carrión, F. J., Quintana, J. A., & Crespo, S. E. (2017). SHM of a stayed bridge during a structural failure, case study: the Rio Papaloapan Bridge. *Journal of Civil Structural Health Monitoring, 7,* 139-151.

Casey, N. F., & Laura, P. A. A. (1996). A review of the acoustic-emission monitoring of wire rope. *Ocean Engineering, 24(10),* 935-947.

Casey, N. F., White, H., & Taylor, J. L. (1985). Frequency analysis of the signals generated by the failure of constituent wires of wire rope. *NDT International, 18(6),* 339-344.

CBS. (2018). *Trends in Nederland.* Downloaded on 26 September 2018, from https://www.cbs.nl/nl-nl/publicatie/2018/26/trends-in-nederland-2018

CEB FIB. (2005). *Acceptance of stay cable systems using prestressing steels.* Stuttgart: Federation for Structural Concrete (FIB).

Chien, C. H., & Costello, G. A. (1985). Effective Length of Fractured Wire in Wire Rope. *Journal of Engineering Mechanics, 111(7),* 952-961.

Costello, G. A. (1997). *Theory of Wire Rope.* New York: Springer.

DeBoer. (2015). Tekeningen brandwerende voorzieningen tuien. Netherlands: Gelderland.

De Jong, B. C. (2015). *Analytical and experimental analysis of the capacity of steel wire ropes subjected to forced bending.* University of Delft, Delft.

Drouillard, T. F. (1996). A history of Acoustic Emission. *Journal of Acoustic Emission, 14(1),* 1-34.

Drummond, G., Watson, J. F., & Acarnley, P. P. (2006). Acoustic emission from wire ropes during proof load and fatigue testing. *NDT&E International, 40,* 94-101.

Feyrer, K. (2007). *Wire Ropes: Tension, Endurance, Reliability*. Stuttgart: Springer.

Gaillet, L., Zejli, H., Laksimi, A., & Tessier, C. (2009). Detection by acoustic emission of damage in cable anchorage. *Non-Destructive Testing in Civil Engineering.*

Gao, Y., & Mosalam, K. M. (2018). Deep Transfer Learning for Image-Based Structural Damage Recognition. *Computer-Aided Civil and Infrastructure Engineering, 33,* 748-768.

Garvan, F. (2001). The maple book. New York: CRC Press.

Gokhale, M. Y., & Khanduja, D. K. (2010). Time Domain Signal Analysis Using Wavelet Packet Decomposition Approach. *International Journal of Communications, Networks and System Sciences, 3,* 321-329.

Grosse, G. U., & Ohtsu, M. (2008). *Acoustic Emission Testing.* Berlin: Springer.

Holford, K. M., & Lark, R. J. (2005). Acoustic emission testing of bridges. In G. Fu, *Inspection and monitoring techniques for bridges and civil structures* (pp. 183-215). Cambridge: Woodhead Publishing Limited.

Ito, M. (2005). Cable-Supported Bridges. In Chen, W. F., & Lui, E. M., *Handbook of Structural Engineering (pp. 26-1–26-31).* New York: CRC Press.

Ivanov, H. I. (2018). *Reduction in capacity of steel wire rope slings subjected to forced bending.* University of Delft, Delft.

Kerh, T., Su, Y. H., & Mosallam, A. (2017). Incorporating global search capability of a genetic algorithm into neural computing to model seismic records and soul test data. *Neural Computing Application, 28,* 437-448.

Krizhevsky, A., Sutskever, I., & Hinton, G. E. (2012). ImageNet classification with deep convolutional neural networks. *Advances in Neural Information Processing systems, 25(2),* 1097-1105.

Li, H., & Ou, J. (2016). The state of the art in structural health monitoring of cable-stayed bridges. *Journal of Civil Structural Health Monitoring, 6,* 43-67.

Lin, W., & Yoda, T. (2017). *Bridge Engineering: Classification, Design Loading, and Analysis Methods.* Oxford: Butterworh-Heinemann.

Mayrbaurl, R. M., & Camo, S. (2004). Guidelines for inspection and strength evaluation of suspension bridge parallel-wire cables. *Transportation Research Board.*

Nair, A., & Cai, C. S. (2010). Acoustic emission monitoring of bridges: Review and case studies. *Engineering Structures, 32,* 1704-1711.

NEN. (2011). *Eurocode: Grondslagen van het constructief ontwerp.* Delft: NEN.

Niroula, K. (2014). *Acoustic monitoring of the main suspension cables of the Anthony Wayne Bridge.* University of Toledo, Toledo-Ohio.

Raoof, M. (1991). Wire recovery length in a helical strand under axial-fatigue loading. *International Journal of Fatigue, 13(2),* 127-132.

Raoof, M. (1992). Free bending fatigue of axially pre-loaded spiral strands. *Journal of strain analysis, 27(3),* 127-136.

Raoof, M., & Kraincanic, I. (1995). Recovery Length in Multilayered Spiral Strands. *Journal of engineering mechanics, 121(7),* 795-800.

Raoof, M., & Kraincanic, I. (1998). Determination of wire recovery length in steel cables and its practical applications. *Computers and structures, 68,* 445-459.

Raoof, M., & Huang, Y. P. (1992). Wire Recovery Length in Suspension Bridge Cable. *Journal of Structural Engineering, 118(12),* 3255-3267.

Rijkswaterstaat. (2013). Richtlijnen Beoordeling Kunstwerken: Beoordeling van de constructieve veiligheid van een bestaand kunstwerk bij verbouw, gebruik en afkeur (RBK 1.1). Netherlands: Rijkswaterstaat.

Rizzo, P., & di Scalea, F. L. (2001). Acoustic Emission Monitoring of Carbon-fiber-reinforced-polymer Bridge Stay Cables in Large-scale Testing. *Experimental Mechanics, 41,* 282-290.

Sun, L., & Qian, J. (2011) Experimental study on wire breakage detection by acoustic emission. *Frontiers of Architecture and Civil Engineering in China, 5(4),* 503-509.

Svensson, H. (2012). *Cable-stayed bridges: 40 Years of Experience Worldwide.* Berlin: Wilhelm Ernst & Sohn.

Tong, Z., Gao, J., Sha, A., & Hu, L. (2018). Convolutional Neural Networks for Asphalt Pavement Surface Texture Analysis. *Computer-Aided Civil and Infrastructure Engineering,* 1-17.

Van Dooren, F., Gration, D., Den Blanken, S., Nagtegaal, G., Ashurst, D., & Kunst, P. (2010). Orthotropic deck fatigue: renovation of 8 bridges in the Netherlands. *13th International Conference.*

Verreet, R. (2001). *A Short History of Wire Rope.* Aachen: PR GmbH.

Verreet, R. (2005). *Steel Wire Ropes for Cranes.* Aachen: PR GmbH.

Wang, N., Zhao, Q., Li, S., Zhao, X., & Zhao, P. (2018). Damage Classification for Masonry Historic Structures Using Convolutional Neural Networks Based on Still Images. *Computer-Aided Civil and Infrastructure Engineering.*

Weavers, M. (1996). Fundamentals in acoustic emission. *22nd European conference on acoustic emission testing.*

Webb, G. T., Vardanega, P. J., Fidler, P. R. A., & Middleton, C. R. (2014). Analysis of Structural Health Monitoring Data from Hammersmith Flyover. *Journal of bridge engineering, 19(6),* 05014030-1 – 05014030-11.

Xin, H. (2018, 24 August). RWS, TNO and TUD meeting on use of AE for cable monitoring [Powerpoint].

Xin, H., Diender, R. J., & Veljkovic, M. (2018). Status-driven Acoustic Emission Monitoring for Stay Cables in Bridge Engineering Application Using Deep Transfer Learning and Wavelet Analysis.

Zejli, H., Gaillet, L., Laksimi, A., & Benmedakhene, S. (2012). Detection of the Presence of Broken Wires in Cables by Acoustic Emission Inspection. *Journal of bridge engineering, 17(6),* 921-927.

Zhang, F. (2017). *Evaluation of acoustic emission monitoring of existing concrete structures*. University of Delft, Delft.

Zhang, F., Pahlavan, L., Yang, Y., & Hordijk, D. (2017). Influence of cracks on the reliability of Acoustic Emission monitoring of concrete structures. *2nd International RILEM/COST Conference on Early Age Cracking and Serviceability in Cement-based Materials and Structures (EAC2).*

Zhang, G., Zhang, Z., & Fischer, C. (2007). Structural Health Monitoring of a Long-span Cable-stayed Bridge. *Journal of Intelligent Material Systems and Structures, 18,* 835-843.

Zhou, Z., Zhou, J., Dong, L., Cai, X., Rui, Y., & Ke, C. (2017). Experimental study on the location of an acoustic emission source considering refraction in different media. *Scientific reports, 7,* 7472.

APPENDICES

APPENDIX 1 – GEOMETRICAL PROPERTIES

In figure 65 the red number are representing the different wires and the green circles and number are showing the strand layers. The geometrical properties of the cables are listed in the table below (table 21). The Poisson's ratio is equal to 0.3 and the incremental load step is equal to 50 kN.

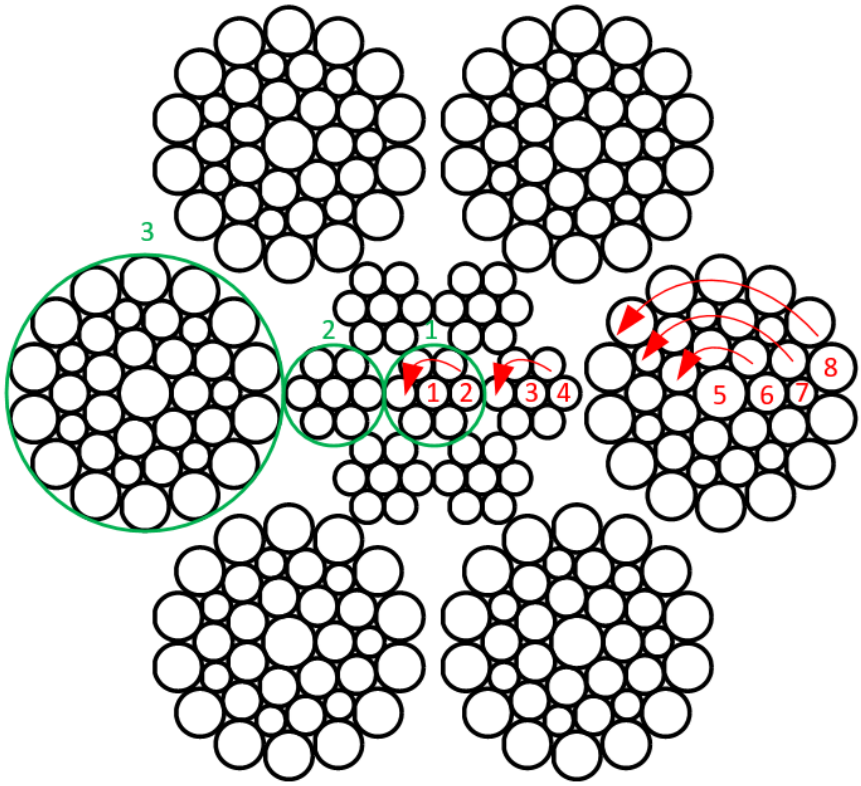

Figure 65 – Wire indication

Table 21 – Geometrical properties

Wire	ϕ [mm]	α [°]	β [°]	number of wires in strand	wire layer in strand	strand layer
1	3	0	0	1	1	1
2	3	11.8	0	6	2	1
3	3	0	16.7	1	1	2
4	3	11.8	16.7	6	2	2
5	4.81	0	16.7	1	1	3
6	3.62	7.2	16.7	7	2	3
7	3.53/2.73	13.1	16.7	7/7	3	3
8	4.39	19.3	16.7	14	4	3

APPENDIX 2 – PRODUCT SHEET DATA ACQUISITION SYSTEM

The product sheet obtained from the manufacturer for the Sensor Highway III system is shown below.

MISTRAS

PHYSICAL ACOUSTICS

PRODUCT DATA SHEET

Sensor Highway III

DESCRIPTION

The Sensor Highway III (SH-III) system has been developed for continuous outdoor, Acoustic Emission (AE), Structural Health Monitoring (SHM) and Sensor Fusion applications.

The SH-III has been designed for monitoring applications in outdoor environments, without the use of costly heaters, air conditioners or fans. 32 channels of AE are built within its small, weatherproof outdoor enclosure, with sealed inputs, protected from the environment including heat, cold, rain, hail, snow, and lightning. 8 AE channels per module, with a maximum of 4-modules provide 32 channels of full AE signal processing including waveform processing and the full data set of AE time based, hit based, and frequency based feature extraction and digital signal processing.

FEATURES

- Direct On-Board Terminal Block connections and DIN rail mounts for other external sensor inputs
- Parametric Input Connections for other analog sensors
- Solid State Weather Station option with over 20 weather parameters to AEwin
- Multiple units can be connected and synched to system clocks for large, location groups.
- Various communication interfaces available for digital parametrics
- Various options for data/network communications including Ethernet, Wireless, & Cellular Modem
- Uses AEwin software for remote data collection, alarm detection and email alarm notification
- Optional Battery backup. Keeps system running during short power loss
- Remote Boot, built-in. Provides remote access to reset or reboot

OPERATING SPECIFICATIONS

Dynamic

Enclosure Size: 20" x 16" x 7"
Weight: < 30 lbs. with enclosure for 17-32 ch
Operating Temp: -22˚-149˚F (-30˚ to + 70˚C)
Storage Temp: -40˚-167˚F (-40˚ to + 85˚C)

Power Requirements

Power Requirements: 85-260 VAC or 9-28 VDC, surge protected
Power Consumption: 12W system + 0.25W/channel

Analog Channels

# of AE Channels: 8 per module, up to 4 modules or 32 channels
Bandwidth: 1 kHz – 400 kHz
ADC: 18 bit, 2 MSPS
Sensor Power: 5V phantom power

Digital

Waveform Buffer: 2k FIFO & 8k Circular Buffer
DSP: 4 million gate FPGA
Digital I/O: 8 inputs & 8 outputs

Communication

Network: 1 Gigabit Ethernet
USB: 3 USB 2.0, 1 USB 3.0
Serial: One RS-232, One RS-485

Parametrics

Single ended inputs: 100kSPS, 0-10V input, qty: 8/module, max. 16
Tachometer input: 2 Digital Tach inputs with time marks

Com Express CPU

Processor: 1.6 GHz Atom N2600, Hyperthreading
Memory: 4 Gbyte DDR3
Storage: Internal 60 GB SSD, Internal 256 GB SSD

CE

WORLDWIDE HEADQUARTERS:
195 Clarksville Rd •
Princeton Jct, NJ 08550 • USA
T: +1.609.716.4000 • F: +1.609.716.0706
E-MAIL: sales.systems@mistrasgroup.com

CANADA	T: +1.403.556.1350	**GREECE**	T: +30.210.2846.801	**SCANDINAVIA**	T: +46(0)31.252040
CHINA	T: +86.10.5877.3672	**HOLLAND**	T: +31.010.245.0325	**S. AMERICA**	T: +55.11.3082.5111
FRANCE	T: +331.498.26040	**INDIA**	T: +91.22.2586.2444	**UK**	T: +44(0)1954.231.612
GERMANY	T: +49.211.730940	**MIDDLE EAST**	T: +44(0)1954.231.612		

www.mistrasgroup.com

Figure 66 – Product sheet of the Sensor Highway III system

APPENDIX 3 – PRODUCT SHEETS SENSORS

The products sheets obtained from the manufacturer for respectively the R3I-AST, R6I-AST and the VS600-Z2 sensors are given.

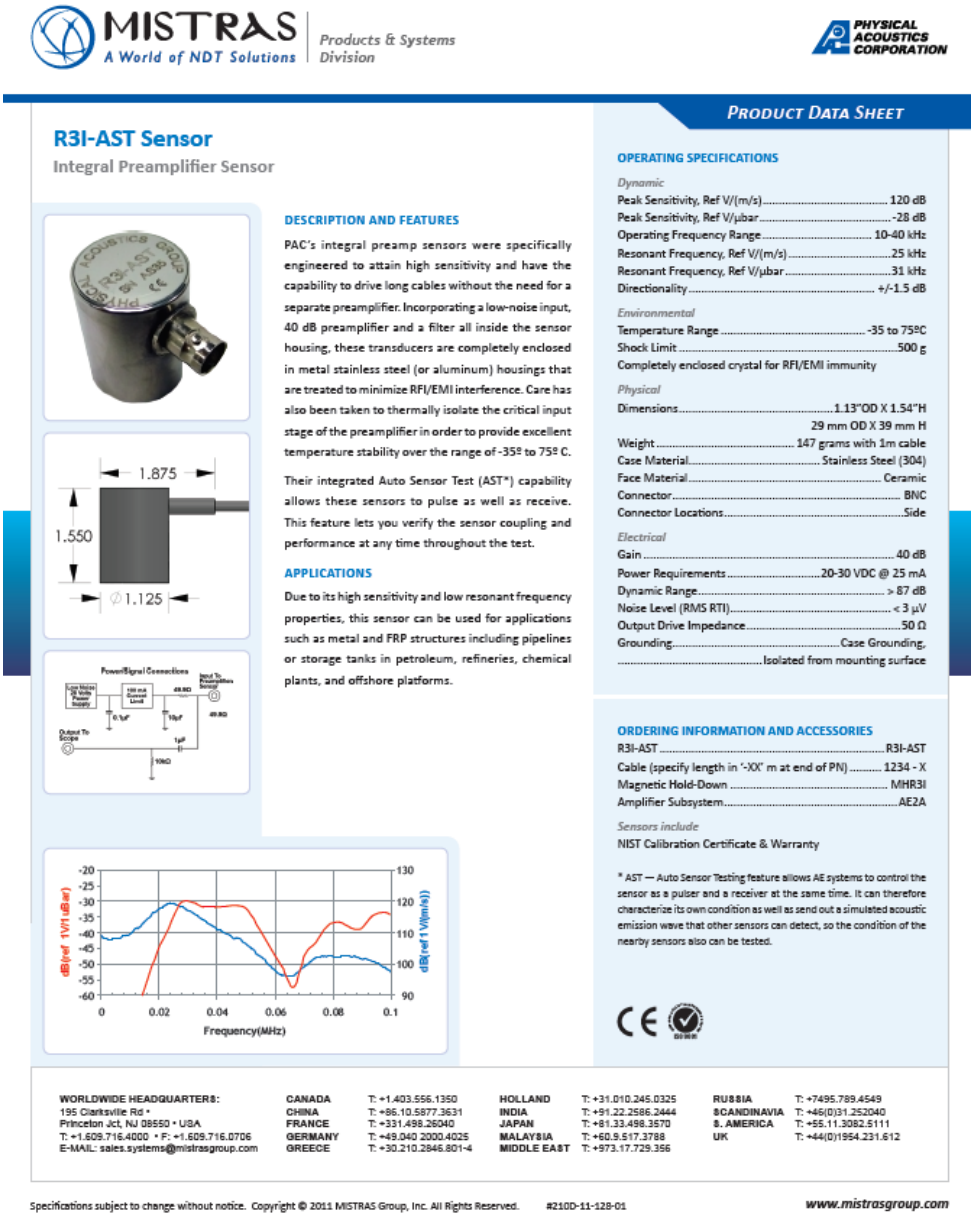

MISTRAS A World of NDT Solutions | Products & Systems Division

PHYSICAL ACOUSTICS CORPORATION

PRODUCT DATA SHEET

R3I-AST Sensor

Integral Preamplifier Sensor

DESCRIPTION AND FEATURES

PAC's integral preamp sensors were specifically engineered to attain high sensitivity and have the capability to drive long cables without the need for a separate preamplifier. Incorporating a low-noise input, 40 dB preamplifier and a filter all inside the sensor housing, these transducers are completely enclosed in metal stainless steel (or aluminum) housings that are treated to minimize RFI/EMI interference. Care has also been taken to thermally isolate the critical input stage of the preamplifier in order to provide excellent temperature stability over the range of -35º to 75º C.

Their integrated Auto Sensor Test (AST*) capability allows these sensors to pulse as well as receive. This feature lets you verify the sensor coupling and performance at any time throughout the test.

APPLICATIONS

Due to its high sensitivity and low resonant frequency properties, this sensor can be used for applications such as metal and FRP structures including pipelines or storage tanks in petroleum, refineries, chemical plants, and offshore platforms.

OPERATING SPECIFICATIONS

Dynamic

Peak Sensitivity, Ref V/(m/s)	120 dB
Peak Sensitivity, Ref V/µbar	-28 dB
Operating Frequency Range	10-40 kHz
Resonant Frequency, Ref V/(m/s)	25 kHz
Resonant Frequency, Ref V/µbar	31 kHz
Directionality	+/-1.5 dB

Environmental

Temperature Range	-35 to 75ºC
Shock Limit	500 g

Completely enclosed crystal for RFI/EMI immunity

Physical

Dimensions	1.13"OD X 1.54"H 29 mm OD X 39 mm H
Weight	147 grams with 1m cable
Case Material	Stainless Steel (304)
Face Material	Ceramic
Connector	BNC
Connector Locations	Side

Electrical

Gain	40 dB
Power Requirements	20-30 VDC @ 25 mA
Dynamic Range	> 87 dB
Noise Level (RMS RTI)	< 3 µV
Output Drive Impedance	50 Ω
Grounding	Case Grounding, Isolated from mounting surface

ORDERING INFORMATION AND ACCESSORIES

R3I-AST	R3I-AST
Cable (specify length in '-XX' m at end of PN)	1234 - X
Magnetic Hold-Down	MHR3I
Amplifier Subsystem	AE2A

Sensors include

NIST Calibration Certificate & Warranty

* AST — Auto Sensor Testing feature allows AE systems to control the sensor as a pulser and a receiver at the same time. It can therefore characterize its own condition as well as send out a simulated acoustic emission wave that other sensors can detect, so the condition of the nearby sensors also can be tested.

WORLDWIDE HEADQUARTERS:
195 Clarksville Rd •
Princeton Jct, NJ 08550 • USA
T: +1.609.716.4000 • F: +1.609.716.0706
E-MAIL: sales.systems@mistrasgroup.com

CANADA	T: +1.403.556.1350	HOLLAND	T: +31.010.245.0325	RUSSIA	T: +7495.789.4549
CHINA	T: +86.10.5877.3631	INDIA	T: +91.22.2586.2444	SCANDINAVIA	T: +45(0)31.252040
FRANCE	T: +331.498.26040	JAPAN	T: +81.33.498.3570	S. AMERICA	T: +55.11.3082.5111
GERMANY	T: +49.040 2000.4025	MALAYSIA	T: +60.9.517.3788	UK	T: +44(0)1954.231.612
GREECE	T: +30.210.2846.801-4	MIDDLE EAST	T: +973.17.729.356		

 #210D-11-128-01 www.mistrasgroup.com

Figure 67 – Product sheet R3I-AST sensor

MISTRAS
A World of NDT Solutions | Products & Systems Division

PHYSICAL ACOUSTICS CORPORATION

PRODUCT DATA SHEET

R6I-AST Sensor

Integral Preamplifier Sensor

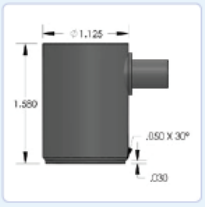

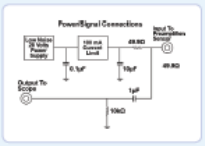

DESCRIPTION AND FEATURES

PAC's integral preamp sensors were specifically engineered to attain high sensitivity and have the capability to drive long cables without the need for a separate preamplifier. Incorporating a low-noise input, 40 dB preamplifier and a filter all inside the sensor housing, these transducers are completely enclosed in metal stainless steel (or aluminum) housings that are treated to minimize RFI/EMI interference. Care has also been taken to thermally isolate the critical input stage of the preamplifier in order to provide excellent temperature stability over the range of -35º to 75º C.

Their integrated Auto Sensor Test (AST*) capability allows these sensors to pulse as well as receive. This feature lets you verify the sensor coupling and performance at any time throughout the test.

APPLICATIONS

Due to its high sensitivity and low resonant frequency properties, this sensor can be used for applications such as metal and FRP structures including pipelines or storage tanks in petroleum, refineries, chemical plants, and offshore platforms.

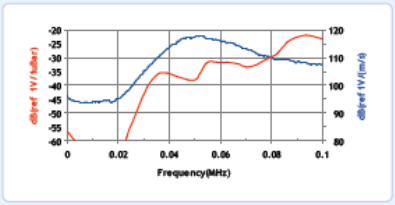

OPERATING SPECIFICATIONS

Dynamic

Peak Sensitivity, Ref V/(m/s)	117 dB
Peak Sensitivity, Ref V/µbar	-23 dB
Operating Frequency Range	40-100 kHz
Resonant Frequency, Ref V/(m/s)	55 kHz
Resonant Frequency, Ref V/µbar	98 kHz
Directionality	+/-1.5 dB

Environmental

Temperature Range	-35 to 75ºC
Shock Limit	500 g
Completely enclosed crystal for RFI/EMI immunity	

Physical

Dimensions	1.13"OD X 1.6"H 29 mm OD X 40 mm H
Weight	98 grams
Case Material	Stainless Steel (304)
Face Material	Ceramic
Connector	BNC
Connector Locations	Side

Electrical

Gain	40 dB
Power Requirements	20-30 VDC @ 25 mA
Dynamic Range	> 87 dB
Noise Level (RMS RTI)	< 3 µV
Output Drive Impedance	50 Ω
Grounding	Case Grounding, Isolated from mounting surface

ORDERING INFORMATION AND ACCESSORIES

R6I-AST	R6I-AST
Cable (specify length in '-XX' m at end of PN)	1234 - X
Magnetic Hold-Down	MHR6I
Amplifier Subsystems	AE2A, AE5A

Sensors include

NIST Calibration Certificate & Warranty

* AST — Auto Sensor Testing feature allows AE systems to control the sensor as a pulser and a receiver at the same time. It can therefore characterize its own condition as well as send out a simulated acoustic emission wave that other sensors can detect, so the condition of the nearby sensors also can be tested.

WORLDWIDE HEADQUARTERS:
195 Clarksville Rd •
Princeton Jct, NJ 08550 • USA
T: +1.609.716.4000 • F: +1.609.716.0706
E-MAIL: sales.systems@mistrasgroup.com

CANADA	T: +1.403.556.1350	HOLLAND	T: +31.010.245.0325	RUSSIA	T: +7495.789.4549
CHINA	T: +86.10.5877.3631	INDIA	T: +91.22.2586.2444	SCANDINAVIA	T: +46(0)31.252040
FRANCE	T: +331.498.26040	JAPAN	T: +81.33.498.3570	S. AMERICA	T: +55.11.3082.5111
GERMANY	T: +49.040 2000.4025	MALAYSIA	T: +60.9.517.3788	UK	T: +44(0)1954.231.612
GREECE	T: +30.210.2846.801-4	MIDDLE EAST	T: +973.17.729.356		

 #2100-11-124-01 www.mistrasgroup.com

Figure 68 – Product sheet R6I-AST sensor

The Acoustic Emission Company

vallen systeme

AE–Sensor Data Sheet

VS600-Z2

The VS600-Z2 is a passive piezoelectric AE-sensor with integrated cable and full metal housing. Its frequency response is characterized by a peak at 600 kHz where it exhibits a resonance. Its small size makes it especially suited for being mounted on small samples where mounting space is restricted. Additionally it is ideally suited for gluing to the sample because of the full metal housing.

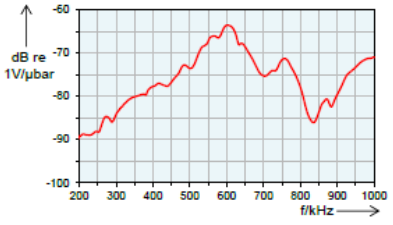

Technical Specification			
Frequency Range (f_{Peak}) [kHz]	400 to 800 (600)	Size (D x H) [mm]	4.75 x 5.3
Capacity [pF]	200 (Incl. Cable)	Weight [g]	20
Integrated Preamplifier	No	Case Material	Stainless Steel (1.4571/ 1.4404)
Operating Temperature [°C]	-40 to +110	Wear Plate	Stainless Steel (1.4571/ 1.4404)
Vibration – Sinus sweep	2 Oct/Min, 5 to 180 Hz, 40 g	Connector	SMA/BNC
Ingress Protection Rating	IP40	Shield Cross-Talk [dB]	< -80

Standards and Directives	
EMC Directive	2014/30/EU
EMC Standards	EN61326-1:2013, EN61326-2-3:2013, EN61000-6-2:2005, EN61000-6-4:2011
Shock and Vibration Stand.	EN60068-2-6:2008
AE Standard	EN13477-1:2013, EN13477-2:2013

Accessories			
Preamplifier	AEP5, AEP3N	Sensor Cable	(Integral)
Mounting Holder			

Think AE - Think Vallen!

Figure 69 – Product sheet VS600-Z2 sensor

APPENDIX 4 – CABLE SPECIMEN

The cable is manufactured by USHA Martin Limited. The cable designation according to the ISO17893:2003(E) standard is as follows: 77-6x36WS-IWRC-1770/1960-zn-sZ. A short description of this designation is given in figure 70.

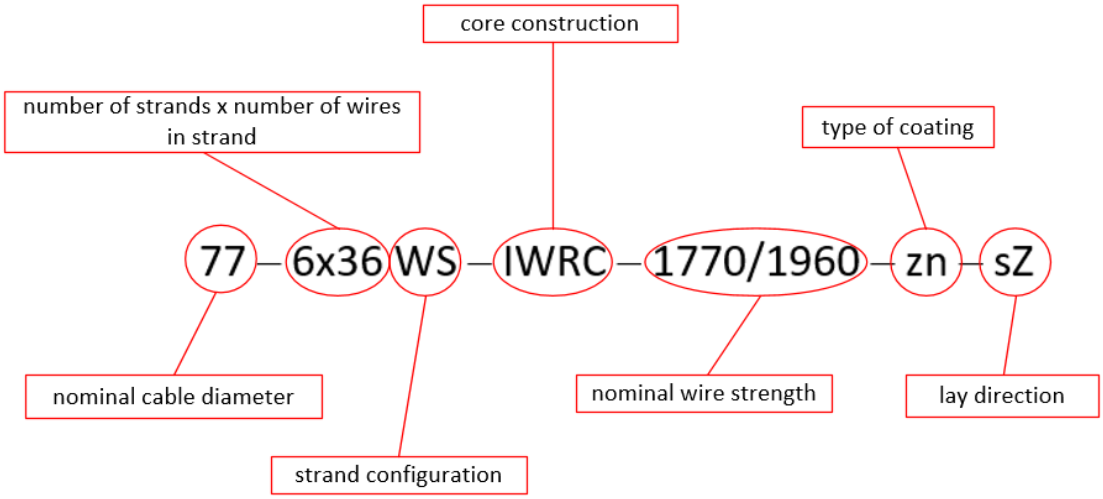

Figure 70 – Cable designation rules

The cable used in this research is further elaborated: This cable has a nominal diameter of 77 mm, it exists of 6 strands of 36 wires each with a Warrington-Seale strand construction and the cable has an Independent Wire Rope Core (IWRC). The nominal wire strength, according to the manufacturer, is a mix of 1770 and 1960 N/mm^2. The wires are zinc coated and the cable has an ordinary right lay direction. In figure 71, the cross section of this cable is represented. The strands exist of four wire layers and a centre wire, all the wire layers exist of different wire diameters. From the centre wire to the outer wire layer the diameters are respectively, 4.81 mm, 3.62 mm, 3.53 mm, 2.73 mm and 4.39 mm. The diameters of the wires in the core is 3 mm for all the wires.

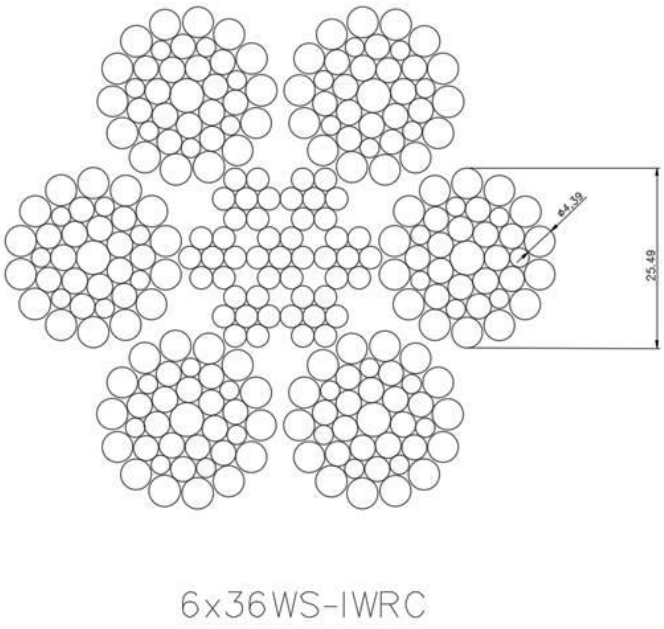

Figure 71 – Cross section of the cable specimen

APPENDIX 5 – RESULTS R3I-AST SENSORS

In figure 72 and 73 the amplitude- and energy-time results are represented for the R3I-AST sensors (sensor 2,6,7 and 10).

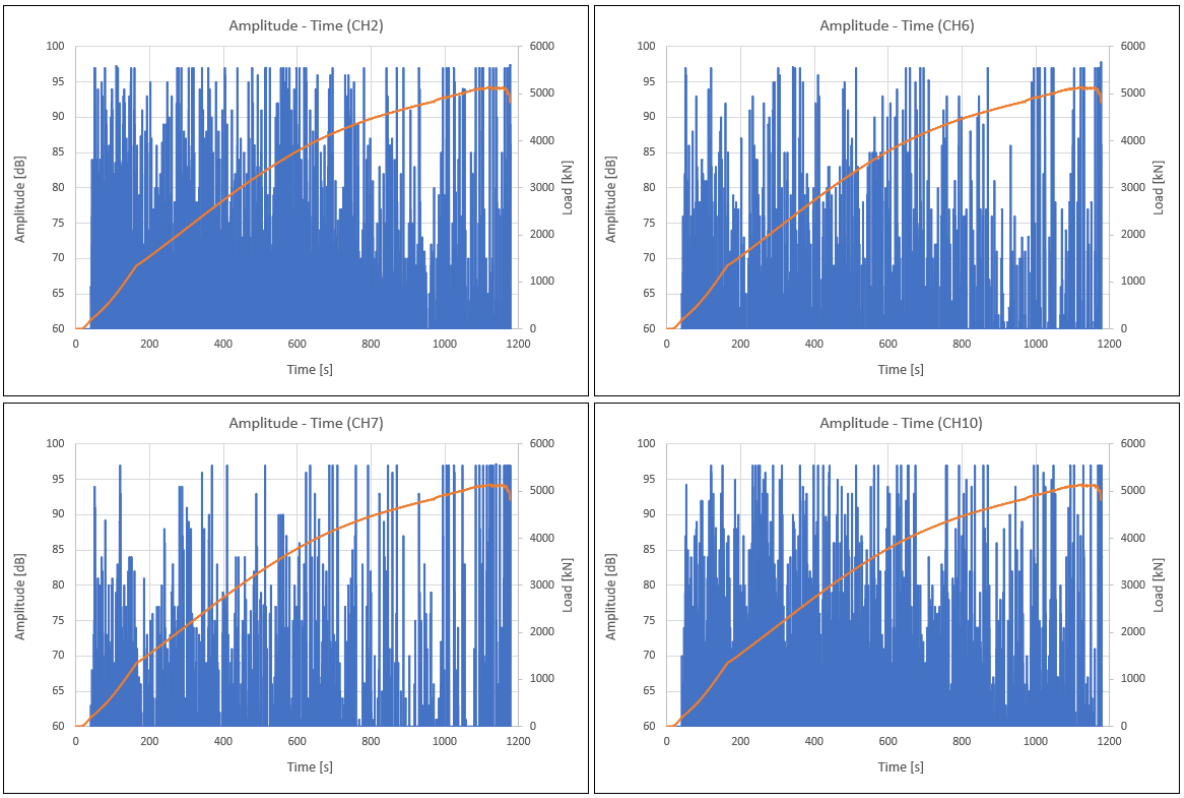

Figure 72 – Amplitude-time for sensors 2,6,7 & 10

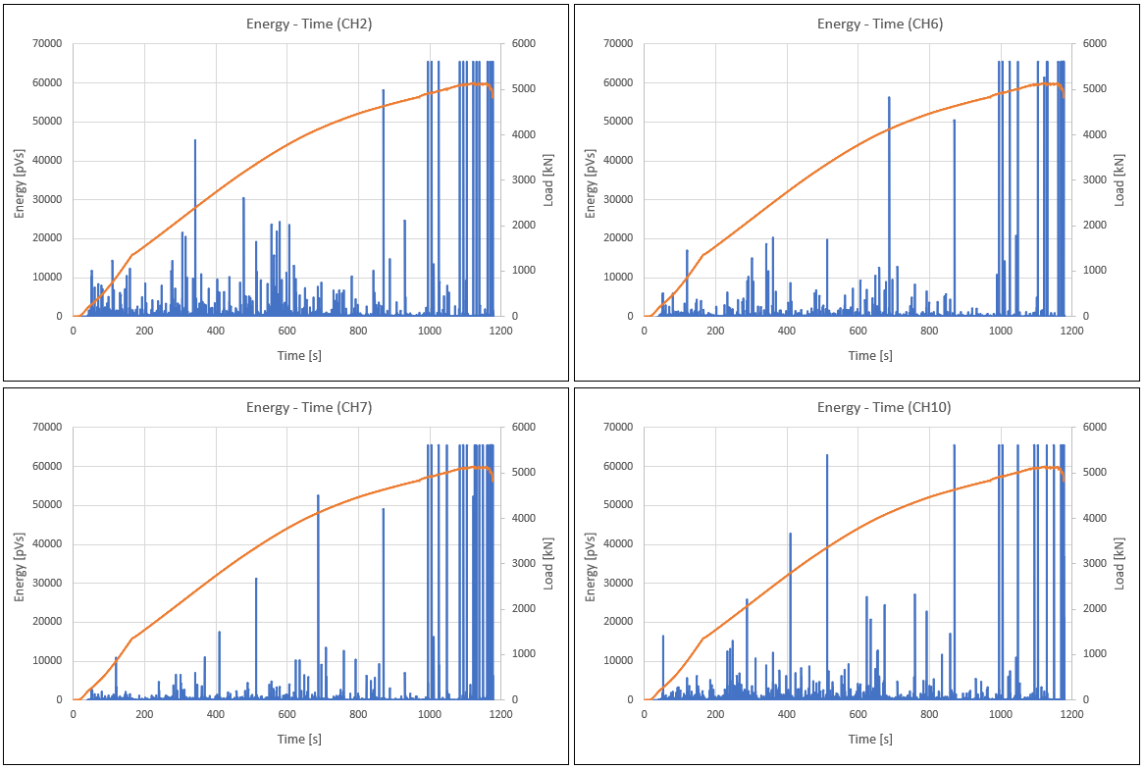

Figure 73 – Energy-time for sensors 2,6,7 & 10